博士論文

Study on highly active covalent organic framework electrocatalysts

based on coordination structure control of metal centers

（金属中心の配位構造制御に基づく高活性な

共有結合性有機構造体電極触媒に関する研究）

岩瀬　和至

Content

Chapter 1

General introduction

1.1 Background of this thesis

With the increase in population of the world and development of industries, energy demand rapidly increases in recent decades. Current energy for industries in our society and our lives are strongly dependent on fossil fuels such as petroleum, coal and natural gas. This situation is very problematic because we are facing on exhaustion of those energy resources and it causes serious climate change and environmental issues on global scale. From these standpoints, many researches have been conducted on developing energy conversion systems which can effectively use sustainable energy sources such as sunlight and wind power. Electrocatalysts are important elements for those systems since they can convert chemical energy and electronic energy to each other.

As for the electrocatalysts which can convert electricity from renewable energy sources into chemical energies and produce value-added products, electrocatalysts which can proceed hydrogen evolution reaction (HER) or carbon dioxide reduction reaction (CO2RR) are widely researched since products of those reactions can be used as fuels or starting materials for various industrial products. For energy conversion devices such as fuel cells, electrocatalysts also play important role. For example, electrochemical oxygen reduction reaction (ORR), hydrogen oxidation reaction (HOR) and organic oxidation reaction (OOR) have attracted considerable attentions as cathode or anode reactions for various types of fuel cells.

For those electrocatalysts, for example, reaction selectivity, product selectivity and reaction over-potential are important. Various types of materials such as bulk metals, alloys, nanoparticles,

organometallic complexes and metal-doped nanostructured inorganic carbon materials have been developed as efficient electrocatalysts. Some of them show unique catalytic activity or reaction selectivity. In next section, the author will give a general introduction of a design principle to synthesize highly active and selective electrocatalysts which possess metal active centers.

1.2 Design principle of electrocatalysts

As described in the previous section, various types of materials were developed as electrocatalysts. Previous theoretical (such as first principle density functional theory [DFT] calculations) and experimental researches suggested that adsorption energy (ΔE_{ads}) of substrate (reactant) and reaction intermediates is an important factor which determine the catalytic activity and reaction selectivity [1−2] in the following reason.
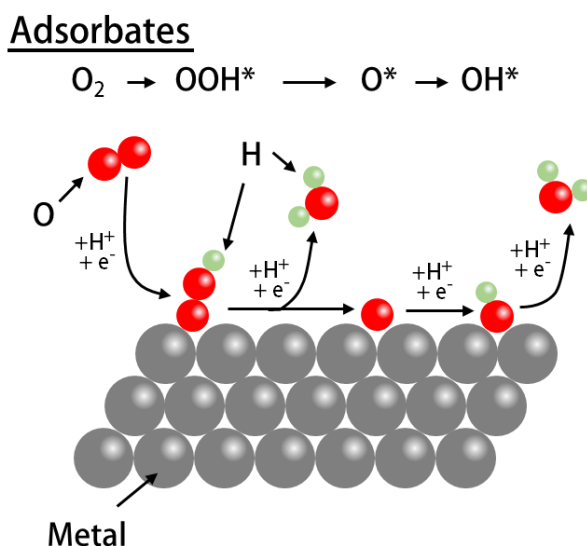
Fig. 1 Schematic illustration of reaction mechanism of oxygen reduction reaction on metal electrodes. * denotes the active site on surface.

Basically, for electrocatalysts with metal active centers, the electrocatalytic reactions proceed with processes of adsorption of substrates (such as molecular oxygen, hydrogen and carbon dioxide) to metal centers, electron (and proton) transfer, and desorption of products from catalytic

centers. For example, for electrochemical oxygen reduction reaction (ORR), molecular oxygen adsorbs on active centers at initial step of the reaction, followed by sequential proton and electron transfers as shown in Fig. 1. In this reaction scheme, O_2 molecule (substrate) are protonated and reduced, then reaction intermediates such as OOH* (* denotes the active sites on the catalysts), O*, and OH* are formed on the catalytic site. Finally, two H_2O molecules are produced as reaction products as shown in the figure. Since most of electrochemical reactions including oxidation and reduction reactions proceed through the above-mentioned process such as adsorption of substrate, ΔE_{ads} of substrates (reactants) and reaction intermediates is one of the important factors which determines the catalytic activity and selectivity for metal containing electrocatalysts.

As described in Sabatier principle [1], ΔE_{ads} of reaction intermediates and (electro)catalytic activities or selectivity are correlated. This principle indicates that ΔE_{ads} has an optimal value for all electrochemical reactions as shown in Fig. 2 and described in below. When ΔE_{ads} of reaction intermediates is too small, the electrochemical reactions (electron transfer) do not proceed because of weak interaction between reactants and catalytic centers (left side of Fig. 2). As ΔE_{ads} of reaction intermediates increases, the reaction rate also gets increases because the electron transfer rate also increases (from left side to center of Fig. 2). In this region, electron transfers (and adsorption of reactants) are still rate determining step. When the ΔE_{ads} of reaction intermediates is close to a specific value, the reaction rate is highest [3−5] (at the middle part of Fig. 2). When the ΔE_{ads} of reaction intermediates is larger than that value, the reaction rate will decrease. In this region, the desorption step is a rate determining step (right side of Fig. 2). As described above and in Fig. 2, ΔE_{ads} and the catalytic activity have a so-called "volcano type" relationship in which the specific value is an optimal value for reaction rate [4]. When ΔE_{ads} are much bigger than the optimal value, substrates or reaction intermediates work as poisoning species of the active centers of electrocatalysts. The above-mentioned reaction mechanism is the reason why many electrocatalytic reactions follow Sabatier principle and

4

volcano-type relation is observed [1,2,6−8]. Therefore, many studies have been conducted on developing electrocatalysts with high activity and selectivity by tuning the ΔE_{ads} of reaction intermediates.
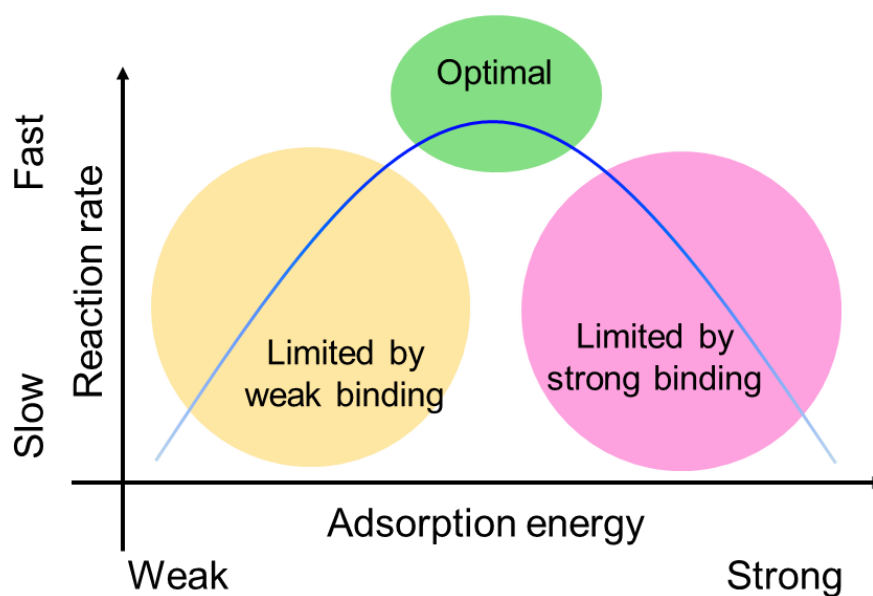
Fig. 2 Schematic illustration of a concept on Sabatier principle [1].

In previous researches, it is suggested that (1) metal species of catalytic centers and (2) coordination and electronic structure of metal centers play important roles to determine the ΔE_{ads} for reaction intermediates (and catalytic activity) of metal containing electrocatalysts.

Metal species (elements) of active centers

One of the important factors which determine ΔE_{ads} of reaction intermediates is metal species (number of d electrons) of active centers. Various previous experimental studies and theoretical

studies by DFT calculations showed that electrocatalytic activities are dependent on the metal species of active centers [9−11].

First principle DFT calculation is widely conducted since this method can clarify the electronic states of metal active centers of catalysts which is important to assess interaction between active centers and reaction intermediates [4,12−13]. It is a useful method for analyses of the reaction mechanism of electrochemical reactions and designing highly active electrocatalysts. For example, F. Calle-Vallejo et al. systematically investigated the ΔE_{ads} of ORR intermediates on various metal atoms with porphyrin like local structure [14]. In this report, authors demonstrated that ΔE_{ads} of ORR intermediates are strongly dependent on d electron number of metal centers (metal species) as shown in Fig. 3. J. K. Nørskov et al. investigated ΔE_{ads} of an ORR intermediate (O atom in this study) on various metal electrodes using DFT calculation and estimated ORR activity on them as shown in Fig. 4 [4]. This result is well consistent with the experimental result that Pt is the best among artificial ORR electrocatalysts. Additionally, O. Diaz-Morales et al. systematically investigated ΔE_{ads} of OER intermediates on Ni based double hydroxide [11]. In this report, authors found that ΔE_{ads} of OER intermediates can be tuned by doping 3d metals such as Fe or Mn into the catalysts. In addition, they also found that ΔE_{ads} of OER intermediates is dependent on doped metal species. As shown above, metal species of active centers in metal containing electrocatalysts is one of the major factors which determine ΔE_{ads} of reaction intermediates. Notably, this dependence of ΔE_{ads} of reaction intermediates on d electron number of metal centers (metal species) is widely observed on various materials such as model structure of molecular catalysts, bulk metal and metal oxide surface for various electrochemical reactions [4,11,15].
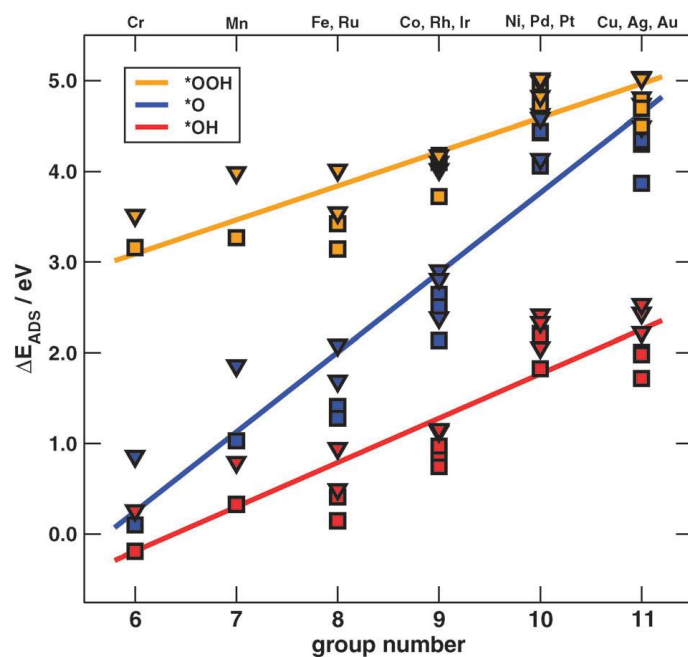
Fig. 3 Trends in adsorption energies of the ORR intermediates in graphitic materials with active sites composed of 4 nitrogen atoms and transition metals, for two types of cells (triangle and square captions). Reprinted with permission from ref. [14]. Copyright 2011, Royal Society of Chemistry.
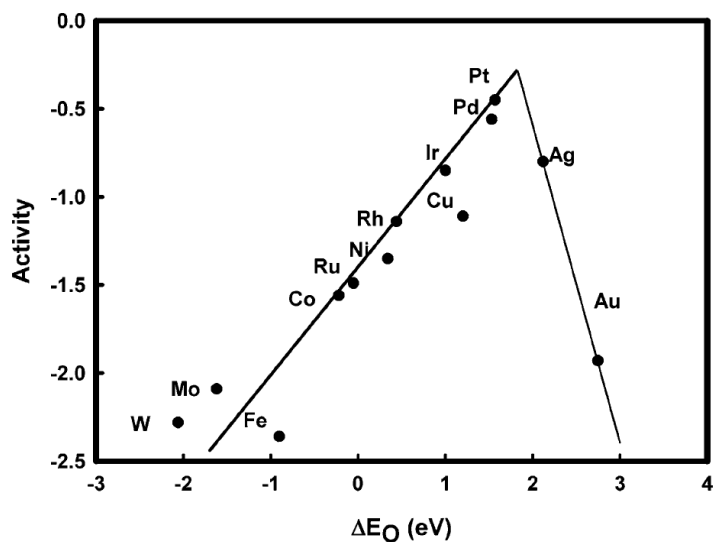
Fig. 4 Trends in oxygen reduction activity plotted as a function of the oxygen binding energy. Reprinted with permission from ref. [4]. Copyright 2004, American Chemical Society.

Coordination structure and electronic structure of metal centers

In addition to the metal species of active centers, coordination structure and electronic structure of metal centers are also essential factors which determine ΔE_{ads} of reaction intermediates and catalytic activity. For organometallic complexes, it is widely known that electronic structure of metal center can be modulated by electron adding/withdrawing properties of organic ligands, resulting in increase/decrease of catalytic activity [16]. Coordination structure and electronic structure of metal centers are also important for inorganic materials. Alloying or doping of hetero-(metal) elements to bulk metal or nanoparticle are representative methods to control them. For example, in the case of Pt based ORR catalysts, it is demonstrated by DFT calculation that d band center of Pt can be tuned by alloying first transition metals to Pt film (Fig. 5), resulting in changes of ΔE_{ads} of ORR intermediates and ORR activity. As shown in this example, many researches demonstrated that alloying method is effective to tune the coordination structure (or composition), electronic structure and electrocatalytic activity of inorganic materials such as metal electrodes, nanoparticles and oxides [6,17−19]. Those previous researches also suggested that coordination structure (neighboring coordinating atoms and geometric structure of metal active centers) is an important factor which determine the ΔE_{ads} and catalytic activity for both of inorganic catalysts and organic molecular catalysts.
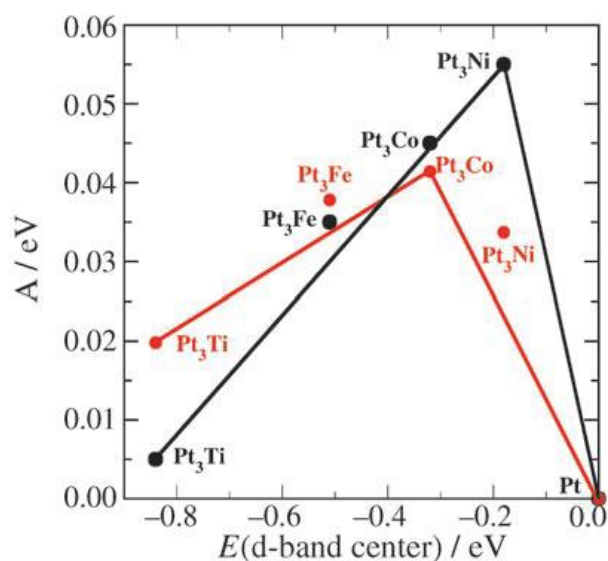
Fig. 5 Activity vs. the experimentally measured d-band center relative to platinum. The activity predicted from DFT simulations is shown in black, and the measured activity is shown in red. Reprinted with permission from ref. [20]. Copyright 2006, WILEY-VCH Verlag GmbH & Co. KGaA, Weinheim.

Coordination number (CN) of metal centers, which is the number of coordinating neighboring atoms, is one element of the coordination structure. CN is proposed as one of the important factors which determine ΔE_{ads}, catalytic activity and reaction selectivity. It is widely known that electrocatalytic activity of metal electrodes or nanoparticles shows surface structure sensitivity. For example, metal surfaces with different crystal plane or metal nanoparticles with different particle size show specific reaction speed or reaction (product) selectivity [12,13,19,21]. Generally, when CN decreases, interaction between metal centers and adsorbates increases because of increase of surface energy of catalysts as shown in Fig. 6. Especially, singly isolated metal centers which have no neighboring same metal species sometimes show completely different catalytic activity and reaction selectivity compared with that of bulk metals or metal nanoparticles [21].
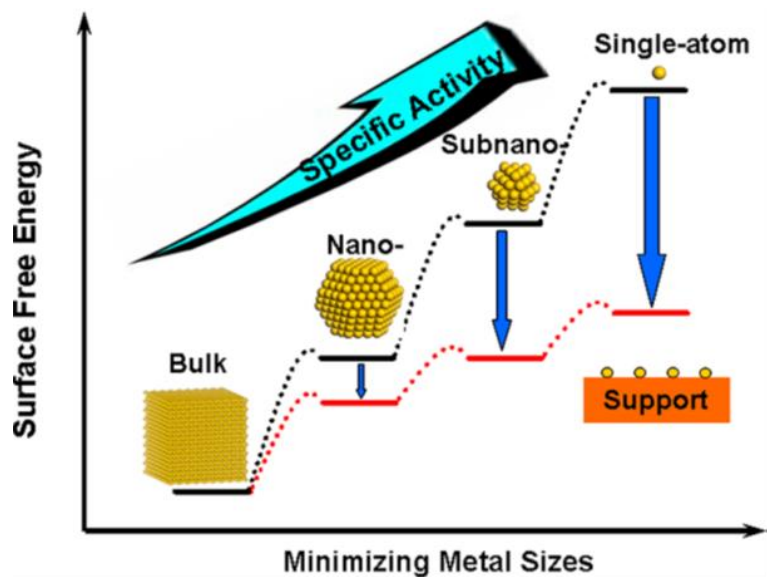
Fig. 6 Schematic illustrate the changes of surface free energy and specific activity per metal atom with metal particle size and the support effects on stabilizing single atoms. Reprinted with permission from ref. [21]. Copyright 2013, American Chemical Society.

Many studies have been conducted on clarifying the relation between catalytic activity and morphology of the catalysts from the view point of the CN of active site on catalytic centers. For example, F. Calle-Vallejo et al. systematically investigated the relation between ΔE_{ads} of ORR intermediates and CN of Pt atoms of catalytic centers (Fig. 7) by using DFT calculation [13]. In this report, authors reported that ΔE_{ads} of ORR intermediates show linear relation to generalized CN (this value takes the number of neighboring atoms of coordinating atom to metal center into account) of Pt center, and predicted ORR activity by DFT calculation. The predicted ORR activity by DFT calculation shows good agreement with experimental results. In addition, Z. Zhao et al. also reported relation between ΔE_{ads} of reaction intermediates of carbon dioxide reduction reaction (CO2RR) and generalized CN on Cu surface [22]. In this report, authors demonstrated that generalized CN shows

linear dependence on ΔE_{ads} of various reaction intermediates of CO2RR such as adsorbed CO*, COOH* and CHO*, and that the over-potential for production of CO2RR products such as CH_4 is dependent on the generalized CN of Cu center (this report shows only results based on the DFT calculation).
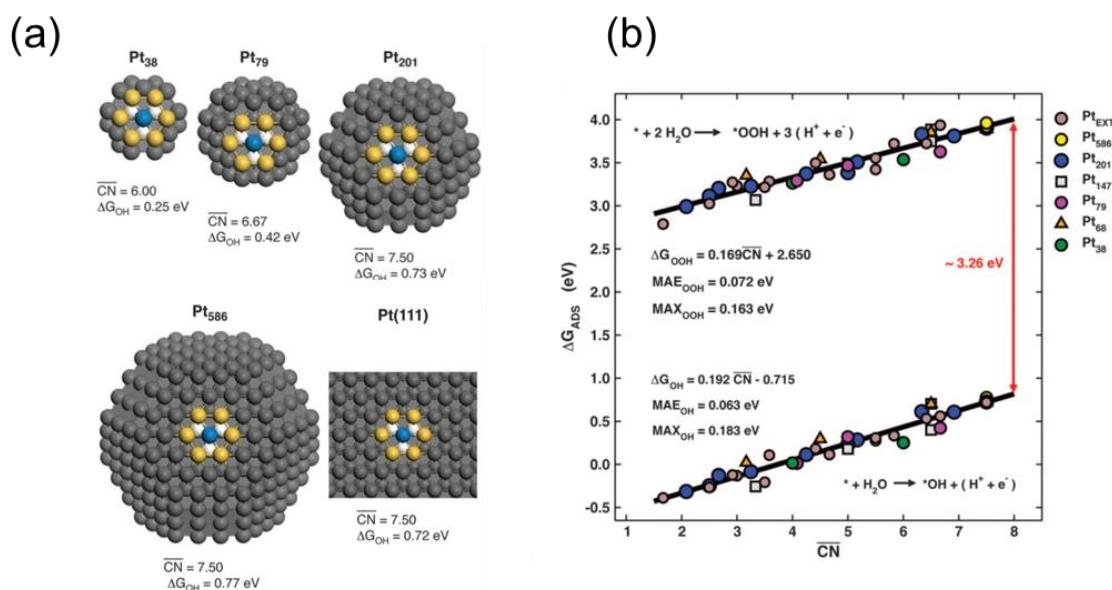
Fig. 7 Adsorption-energy trends (in eV) described by generalized CN ($\overline{CN}$). (A) Schematic illustration of various types of $\overline{CN}$. The differences are due to the second-nearest neighbors. (B) Trends in DG_{OH} and DG_{OOH} described by $\overline{CN}$. The reactions used to calculate the adsorption energies appear as insets. Least-squares fits are provided together with mean and maximum absolute errors (MAE and MAX). Reprinted with permission from ref. [13]. Copyright 2015, American Association for the Advancement of Science.

It has been also proposed that when ΔE_{ads} of one of the reaction intermediates gets larger, ΔE_{ads} of the other reaction intermediates with similar binding mechanism to catalytic centers also gets larger [12,23]. F. Calle-Vallejo et al. systematically investigated the relation between CN of metal centers and ΔE_{ads} of various types of reaction intermediates such as oxygen atom (O) and oxygenated

species (OH, OOH and OCH$_3$) at various metal surfaces with different surface morphology [12]. In this report, authors proposed that all reaction intermediates strongly bind on metal centers with lower CN as mentioned above, and that one of those oxygenated species such as O atoms can be used as an index for evaluation of ΔE_{ads} of other oxygenated species since ΔE_{ads} of each oxygenated species shows linear relation (Fig. 8). Those results also propose that CN of metal centers is one of the important determining factors of ΔE_{ads} and catalytic activity.
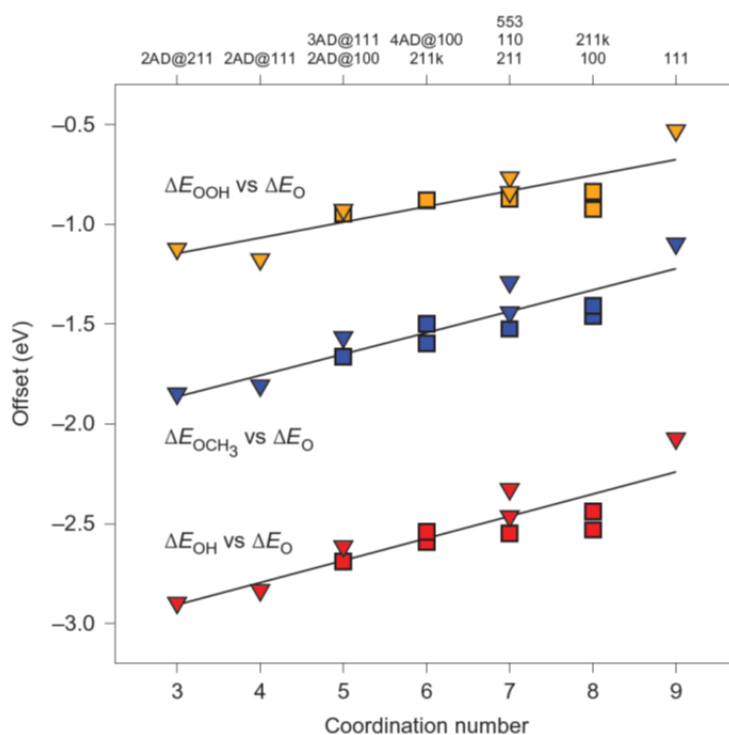
Fig. 8 Structure−energy relations for atomic oxygen and oxygenates. The offsets of the scaling relations between the adsorption energies of *OH versus *O (red), *OOH versus *O (orange) and *OCH3 versus *O (blue), scale in an approximately linear fashion with the coordination number of the adsorption sites. Triangles represent hexagonal-symmetry sites, and squares represent sites with square or mixed hexagonal/square symmetry. Reprinted with permission from ref. [12]. Copyright 2015, Rights Managed by Nature Publishing Group.

Notably, on the basis of those report and Sabatier principle, it is suggested that ΔE_{ads} of all reaction intermediates is close to the optimal value when ΔE_{ads} of one reaction intermediates is close to the optimal value in many cases since ΔE_{ads} of reaction intermediates with similar binding mechanism show linear relations.

Though metal active centers with lower CN, which exist in small nanoparticles, singly isolated metal atoms on catalyst supports and molecular catalysts with open coordination site, show specific catalytic activity and reaction selectivity, they are considered generally unstable and easy to aggregate or change their coordination structure due to their high surface energy (Fig. 6). In previous reports, it is reported that metal centers with unsaturated coordination structure (lower CN) were successfully constructed in metal modified conjugated polymers, and that those metal containing polymers show high catalytic activity or unique reaction selectivity [24,25]. As suggested in these reports, the coordination structure control and construction of metal centers with lower CN (open coordination sites) can be achieved in rigid (inflexible) framework such as conjugated polymer.

1.3 Organic porous materials

Porous materials have attracted a considerable attention because of their high surface area and porosity. For example, inorganic zeolites are widely studied for gas adsorption/separation materials and catalysts [26,27]. Advantages of inorganic porous materials are (ordered) porous structure and higher stability originated from inorganic framework structure. Those materials can be employed under high temperature such as 700 ºC and high-pressure conditions due to their durability to oxidative conditions. However, as those inorganic materials are so stable, introduction of metal center with precisely controlled coordination structure, modification of inside of the pore, changing their composition (substitution of consisting atoms) are difficult. On the basis of this back ground, organic porous materials such as metal organic frameworks (MOFs, those materials are sometimes called as porous coordination polymer [PCP]) and covalent organic frameworks (COFs) are developed as porous materials with various functions [28].

Metal organic framework (MOF)

Metal organic frameworks (MOFs) are organic porous materials consisted with metal ions and organic ligands [29,30]. In MOF structure, metal ions and organic ligands are linked with coordination bonds with each other, and MOFs take an ordered 2D or 3D regular structure. MOFs have attracted a considerable attention because of their high surface area, well defied pore structure and high design flexibility. Various kinds of organic ligands can be used as linkers of MOFs. Since the structure of pores and properties of inside of them such as acidity, hydrophobicity and steric structure can be designed by sophisticated choice of metal ions and ligands, MOFs are widely studied as selective gas adsorption materials. In some cases, MOFs also can be applied as catalysts for gas phase

reactions [31,32] and liquid phase reactions [33].

Some of MOFs are reported as electrocatalysts [34,35]. Most of those MOF-based electrocatalysts so far are consisted with porphyrin units (Fig. 9 shows one example about a carbon dioxide reduction electrocatalyst consisted with MOF) or planar four-coordinate structure [35,36]. There are a few reports on MOF based electrocatalysts which take different coordination structures from porphyrin-like local structure of metal centers or planar four-coordinate structure [34]. Thus, though design flexibility of MOFs as gas or organics adsorption materials is extremely high, the design flexibility of MOFs as electrocatalysts is limited. There are two possible reasons why MOF based electrocatalysts were not developed. First, the coordination bonds which connect organic ligands and metal ions are not stable in electrolytes due to their weak binding strength. Second, the linkage part of metal ions and organic ligands might be weak under electrochemical condition since sometimes redox change of metal centers will change stable coordination structure of them from a view point of ligand field theory. On the basis of this background, in this thesis, the author focused on covalent organic framework as a metal support which can regulate coordination structure of metal centers.
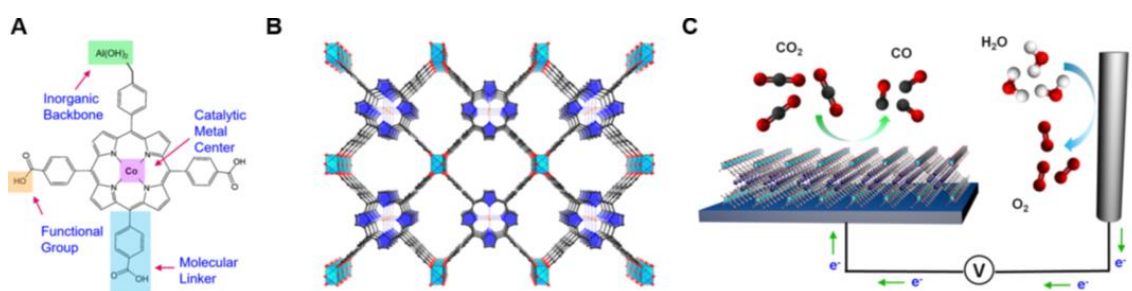
Fig. 9 (A) Developed MOF catalysts in ref. [35]. (B) The organic building units, in the form of cobalt-metalated TCPP, are assembled into a 3D MOF, $Al_2(OH)_2$TCPP-Co with variable inorganic building blocks. (C) Co, orange spheres; O, red spheres; C, black spheres; N, blue spheres; Al, light-blue octahedra; and pyrrole ring, blue. In this structure, each carboxylate from A is bound to the aluminum inorganic backbone. The MOF is integrated with a conductive substrate to achieve a functional CO_2electrochemical reduction system Reprinted with permission from ref. [35]. Copyright 2015, American Chemical Society.

Covalent organic framework (COF)

As MOFs are attractive as gas adsorption materials since they possess well-ordered structure and high design flexibility of inside of the pore (pore size and function groups (side chains) of ligands), development of MOFs with specific functions and related works has been achieved so far. Development of covalent organic frameworks (COFs) is one of the researches inspired by attractive functions of MOFs. COFs are micro or meso porous conjugated polymers consisted with light elements such as carbon (C), nitrogen (N), oxygen (O) and sulfur (S) [37−39]. COF was reported for the first time by A. P. Côté et al. in 2005 [40]. This is the first reported organic framework with high crystallinity, regular porosity with high surface area which is consisted with only covalent bonds. Inspired by this work, many researchers have developed on synthesis of COFs with various functions such as selective gas/metal/organic adsorption, optical response and catalysis. The framework structure of COFs can be modulated by the sophisticated choice of monomers of building blocks as shown in Fig. 10 [39].

Since each building unit of COF is connected with strong covalent bond, most of COFs show higher stability to various solutions such as organic solvent or acidic/alkaline solutions compared with MOFs. Due to their higher stability (insolubility) to the solutions, COFs can be applied as heterogeneous catalysts in solution phase [37,41]. In those reports, functional groups of side chains (e.g. sulfonic groups) or supported metal species can serve as active centers. Especially, COFs can be used as supports of atomically dispersed metal species since they can stabilize metal ions with atomic state through coordination bonds with heteroatoms in COFs. For example, S. Ding et al. synthesized COF-LZU1 and developed Pd loaded COF-LZU1 (Pd/COF-LZU1) as a catalyst for Suzuki-Miyaura coupling reaction (Fig. 11) [42]. In this report, authors demonstrated that Pd ions are highly dispersed on COF and that synthesized Pd/COF-LZU1 showed higher catalytic activity and stability than Pd-

loaded MOF based catalysts reported so far. As this example shows, COFs are attractive as catalyst supports of highly dispersed metal species (single atom) or metal nanoparticles due to its robustness and abundant heteroatoms which can function as metal coordination sites.
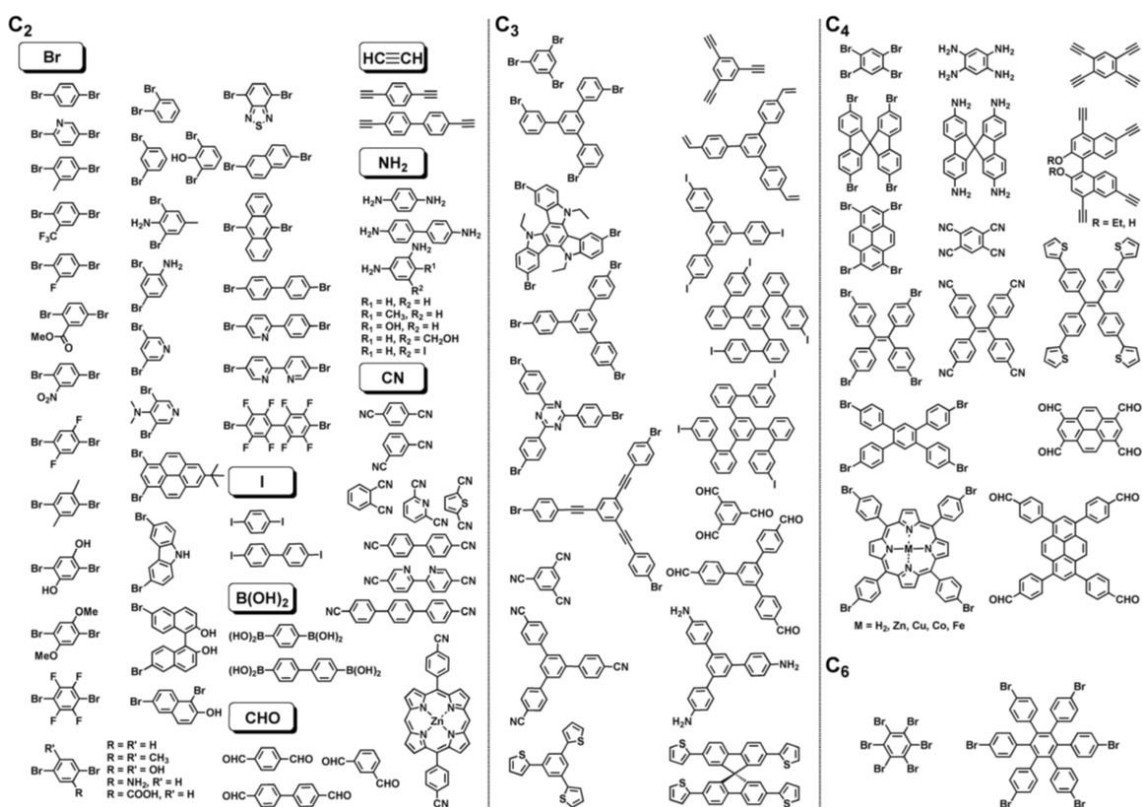

Fig. 10 Schematic representation of the structures of building blocks with different geometries, sizes and reactive groups for the synthesis of conjugated microporous polymer such as COFs. Reprinted with permission from ref. [39]. Copyright 2013, Royal Society of Chemistry.
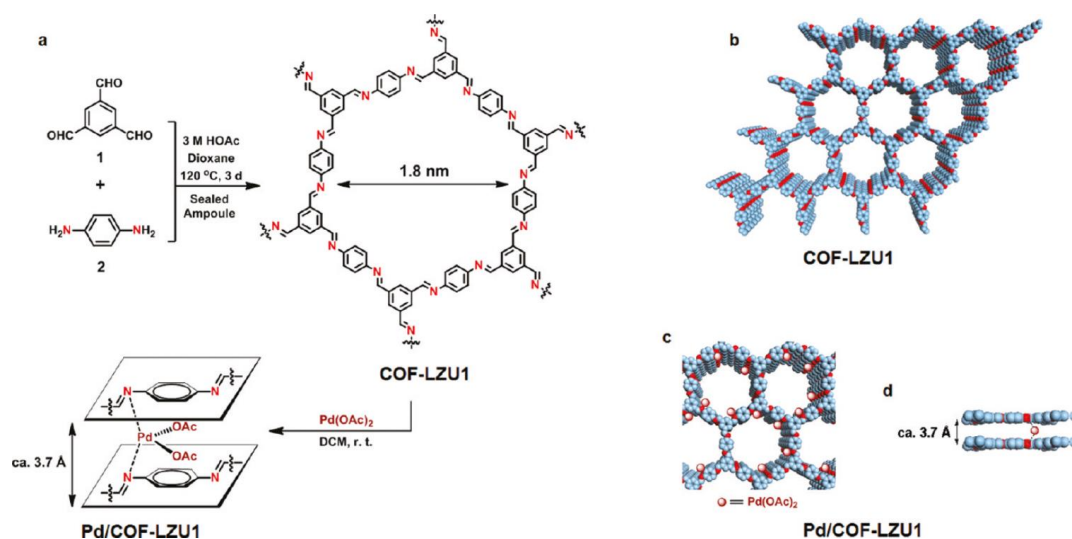
Fig. 11 Construction of COF-LZU1 and Pd/COF-LZU1. (a) Schematic representation for the synthesis of COF-LZU1 and Pd/COF-LZU1 materials. (b) Proposed structures of COF-LZU1 and (c, d) Pd/COF-LZU1, C: blue, N: red, and brown spheres represent the incorporated Pd(OAc)$_2$. H atoms are omitted for clarity. Reprinted with permission from ref. [42]. Copyright 2011, American Chemical Society.

Covalent triazine framework (CTF)

As one kind of COFs, Covalent triazine frameworks (CTFs), which possess 1,3,5-triazine unit as a linker, are also developed [39,43]. CTFs are synthesized mainly by cyclization of nitrile group under molten salt such as ZnCl$_2$. Various types of CTFs can be synthesized by using monomers with nitrile group as a function group in their structure (an example of monomers of CTFs is shown in Fig. 12). Though crystallinity of most of CTFs is lower compared with MOFs and COFs, some of them show certain crystallinity, high surface area and specific gas adsorption properties.

18
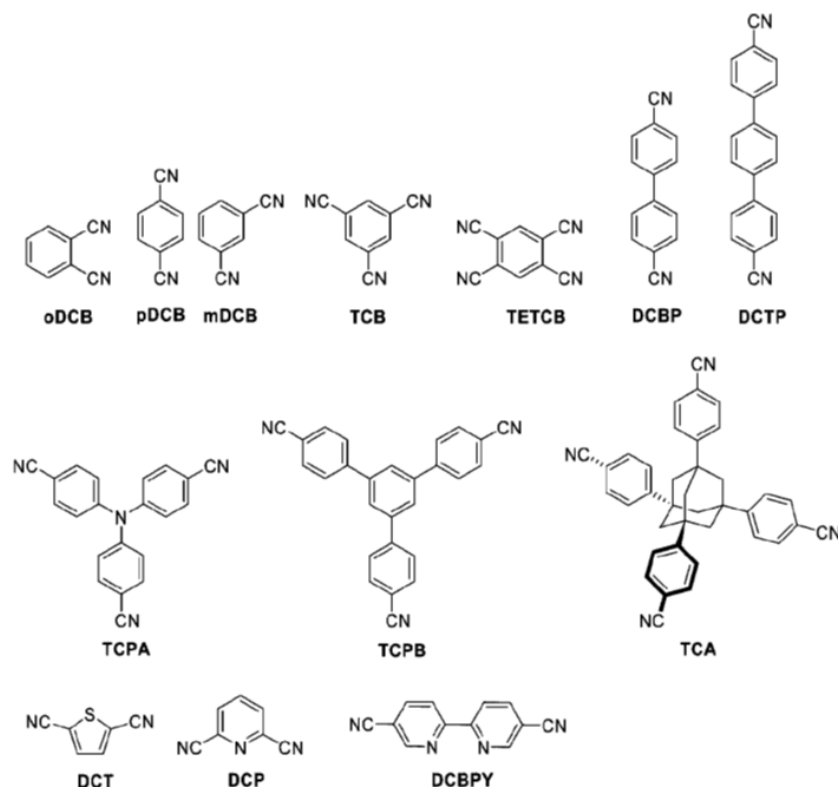
Fig. 12 Representative monomer used for CTF synthesis. Reprinted with permission from ref. [43]. Copyright 2009, American Chemical Society.

One of the advantages of CTFs is high concentration of N atoms with electron lone pair, which can stabilize metal ions through coordination bonds. Thus, CTFs are also attractive as single metal atom loaded catalysts by metal modification. In addition, CTFs which are synthesized through cyclization of nitrile group are expected to show higher robustness since the cyclization of nitrile group is irreversible reaction, which is different from COFs synthesized through reversible condensation reaction such as Schiff base. Actually, some of CTFs show much higher stability to the oxidative conditions compared with other organic materials such as organometallic complexes and MOFs and show thermal stability usually up to 400−500ºC.

Above-mentioned characteristics of CTFs are attractive as heterogenous catalysts with metal

active center. For example, inspired by a partial oxidation catalyst of methane to methanol by R. A. Periana et al. [44], R. Palkovits et al. developed Pt modified CTF (Pt-CTF) as a selective oxidation catalyst of methane to methanol [45] (Fig. 13). Due to higher stability of triazine linker and insoluble nature of CTFs, Pt-CTF showed higher stability and cyclability as a heterogeneous catalyst. In addition, K. Park et al. demonstrated that Ir modified CTF with bipyridine like local structure ([bpyIrCp*Cl]Cl, See Fig. 14b) can function as an efficient heterogeneous catalyst for hydrogenation reaction of carbon dioxide to formate [46]. In this report, authors claimed that high loading amount of Ir atoms and catalytic activity were achieved by using CTFs. Those results experimentally demonstrated that CTFs can work as highly active catalysts by metal loading, and that metal modified CTFs can show higher catalytic activity and stability compared with organometallic complexes in some cases.
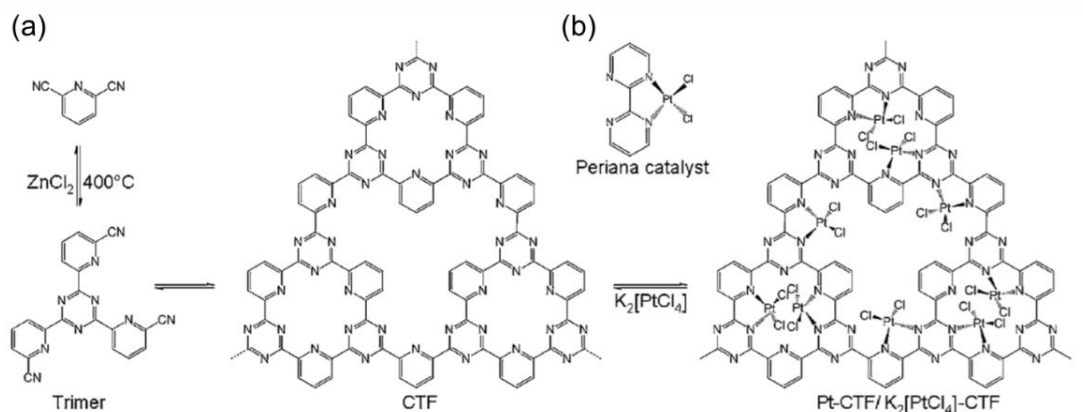
Fig. 13 trimerization of 2,6-dicyanopyridine (DCP) in molten $ZnCl_2$, conversion to a CTF, and subsequent platinum coordination (Pt-CTF); b) Periana's platinum bipyrimidine complex. Reprinted with permission from ref. [45]. Copyright 2009, WILEY-VCH Verlag GmbH & Co. KGaA, Weinheim.
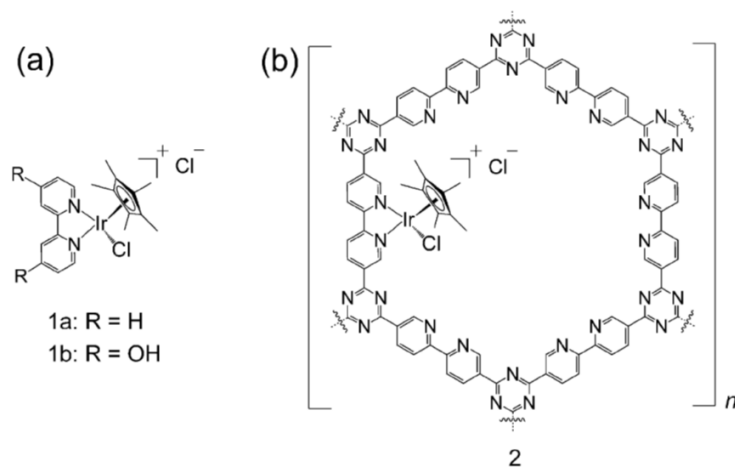
Fig. 14 Structural representation of bipyridine-based (a) homogeneous (organometallic complexes) and (b) heterogeneous (Ir modified CTF) catalysts. Reprinted with permission from ref. [46]. Copyright 2015, WILEY-VCH Verlag GmbH & Co. KGaA, Weinheim.

COF and CTF based electrocatalysts

As mentioned above, CTFs and COFs are attractive as metal loaded catalysts due to its unique physicochemical properties such as porous structure, mechanical and chemical robustness and abundant hetero atoms which can immobilize metal centers. Since covalent bonds are expected to be stable in electrochemical conditions, COFs are also attractive as heterogeneous electrocatalysts. For example, S. Lin et al. demonstrated that Co-COF-366 and Co-COF-367 which possess Co-porphyrin like local structure can function as efficient electrocatalysts for carbon dioxide reduction reaction (See Fig. 15) [47]. In this report, authors claimed that those COFs display higher stability due to cross-linked framework structure. As a metal modified COF based electrocatalyst, H. B. Aiyappa et al, synthesized Co modified bipyridine based COF (Co-TpBpy) with Co-bipyridine like local structure and demonstrated that Co-TpBpy can function as an electrocatalyst for oxygen evolution reaction with high stability [48]. For a CTF based electrocatalyst, K. Kamiya et al. demonstrated that Pt modified

CTF (Pt-CTF) hybridized with electro-conductive carbon nanoparticle (Pt-CTF/CP, molecular structure is essentially same as Pt modified CTF shown in Fig. 13) showed electrocatalytic activity for ORR [49]. In this report, authors demonstrated that CTF which originally shows poor electronic conductivity can function as an electrocatalyst by hybridizing it with electronic conductive carbon nanoparticle, and that Pt-CTF/CP shows high methanol-tolerance which is an unique property as a Pt based catalyst (Fig. 16).
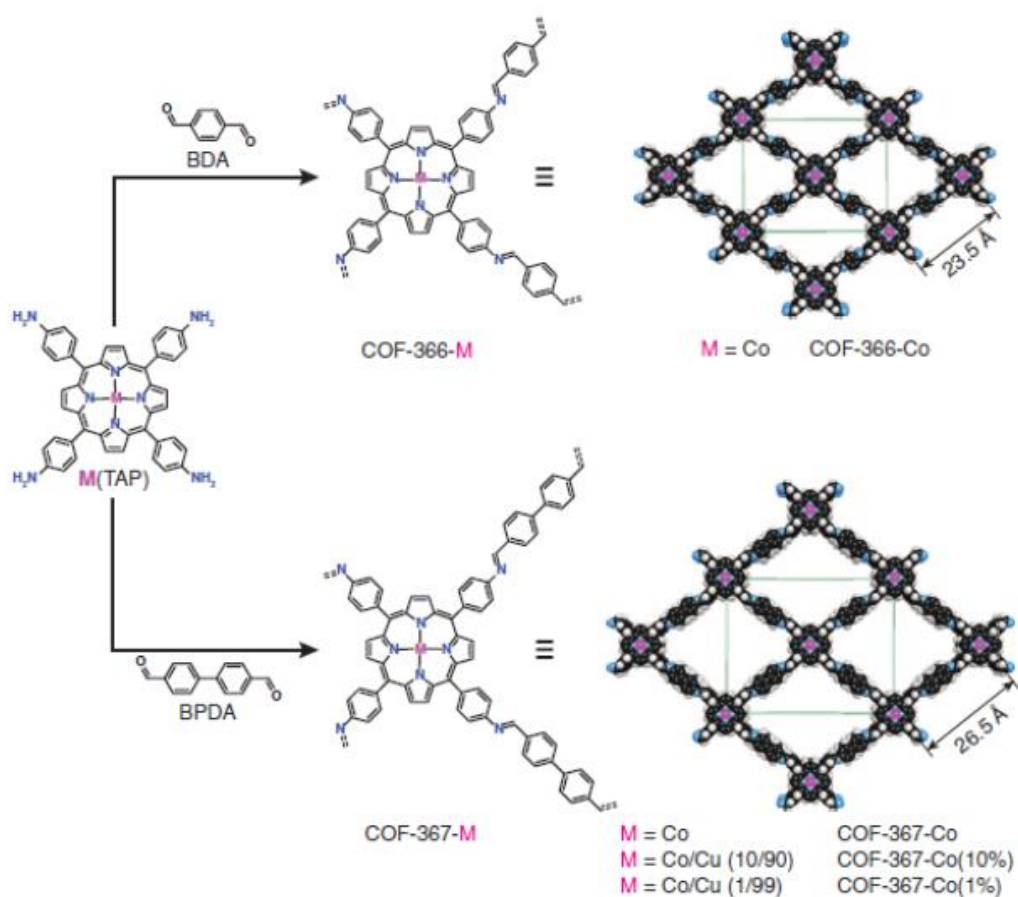
Fig. 15 Design and synthesis of metalloporphyrin-derived 2D covalent organic frameworks. Reprinted with permission from ref. [47]. Copyright 2015, American Association for the Advancement of Science.
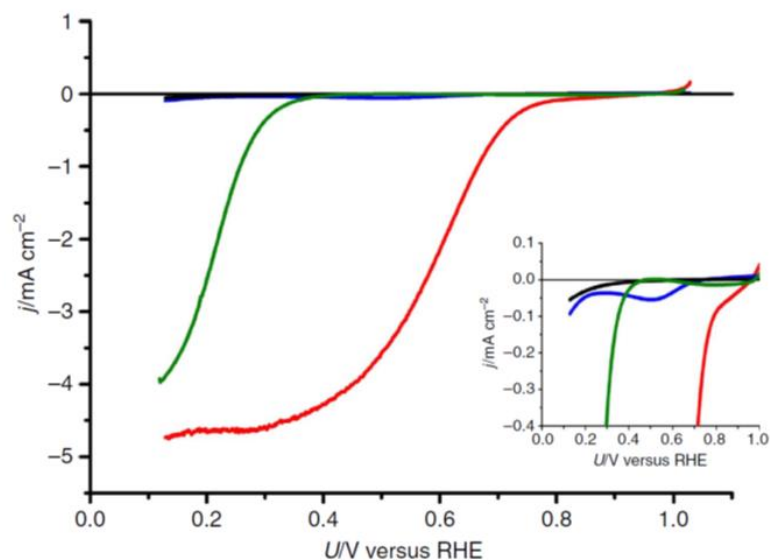
Fig. 16 ORR electrocatalytic activities. *j* versus *U* curves for CTF (black), CTF/CP (green), Pt-CTF (blue) and Pt-CTF/CP (red) in 0.5M H_2SO_4 saturated with dissolved O_2, obtained at a scan rate of 10mVs^{-1}. Rotation rate 1500 rpm. (Inset) Magnified curve. Reprinted from ref. [49] under Creative Commons Attribution 4.0.

Those previous reports about COF-based electrocatalysts demonstrated that COF can function as efficient heterogeneous electrocatalysts for various electrochemical reactions. Notably, those results found that COF is stable under electrochemical conditions in aqueous solutions.

As COFs have high design flexibility since consisting atoms and local structure of COFs can be changed by a sophisticated choice of monomers and synthesis method, it is expected that coordination structure of metal center in metal modified COFs can be controlled by choosing appropriate framework structure of COFs. As explained in this chapter, coordination structure of metal center is one of the essential determining factors of electrocatalytic activity for various electrochemical reactions. Thus, by regulation of coordination structure of metal centers with rigid and inflexible framework of COFs, it is expected that specific electrocatalytic activity and selectivity are achieved by metal modified COF based electrocatalysts.

1.4 Objective and outline of this thesis

The objective of this thesis is development of electrocatalysts with high activity and selectivity based on the coordination structure control of metal centers. COFs are attractive as single metal supports which can function as electrocatalysts since COF can stabilize atomically dispersed metal species through coordination bond with abundant heteroatoms in the framework such as N, S and O. The author hypothesized that coordination structure of metal center modified in framework of COFs can be controlled by framework structure of them. Especially, in this thesis, the author employed CTF, which is a kind of COFs and possesses 1,3,5-triazine as a linkage unit, as metal supports since it contains abundant N which can immobilize metal centers through coordination bonds. The author synthesized first transition metal modified CTFs (M-CTFs) and developed those M-CTFs as electrocatalysts for various reactions.

In chapter 2, Cu modified CTF (Cu-CTF) and Cu modified sulfur-linked CTF (Cu-S-CTF) were developed as non-noble metal electrocatalysts for oxygen reduction reaction (ORR). ORR has attracted a considerable attention because of its importance as a cathode reaction in various types of fuel cells. For ORR, it is well known that ΔE_{ads} of ORR intermediates is an important factor which determine the onset potential (over-potential). ΔE_{ads} of ORR intermediates is dependent on the coordination structure of metal centers. Thus, in this chapter, the author attempted to synthesize Cu based ORR catalysts with high activity by regulation of coordination structure of Cu centers by CTFs.

In chapter 3, the author developed Cu-CTF as a selective electrocatalyst which reduces nitrobenzene to aniline. Conventional carbon-based materials can also proceed nitrobenzene reduction reaction (NBRR) in aqueous solutions, however, the major products of NBRR of them are nitrosobenzene or phenylhydroxylamine, which are the reaction intermediates of aniline generation. Here the author applied Cu-CTF as a nitrobenzene reduction electrocatalyst and investigated the

selectivity of NBRR of Cu-CTF and CTF without Cu modification. In addition, the author also investigated the reaction mechanism of NBRR of Cu-CTF and CTF by using electrochemical characterization.

In chapter 4, metal modified CTFs (M-CTFs, M: Co, Ni, Cu) were developed as electrocatalysts for carbon dioxide reduction reaction (CO2RR). It is well known that ΔE_{ads} of reaction intermediates such as COOH* (*: adsorption site) is an important determining factor of CO2RR activity. In this study, the relation between ΔE_{ads} or catalytic activity on CO2RR and coordination structure was systematically investigated by comparing CO2RR activity of M-CTFs and metal tetraphenylporphyrins (M-TPPs, M : Co, Ni and Cu).

In chapter 5, the researches of above-mentioned M-CTFs are briefly summarized and overviewed. Additionally, possible approaches for further improvement of electrocatalytic activity of COF based electrocatalysts are discussed. The outline of researches of this thesis is written in Fig. 17.
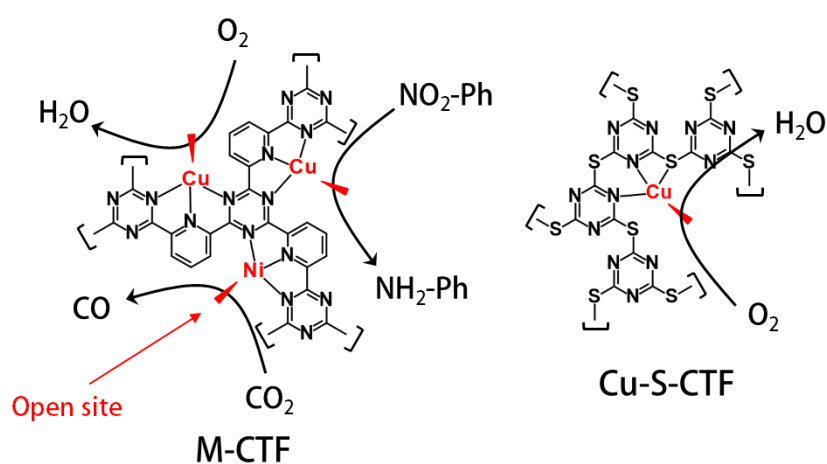

Fig. 17 Outline of this thesis.

References

[1]   A. J. Medford, A. Vojvodic, J. S. Hummelshøj, J. Voss, F. Abild-Pedersen, F. Studt, T. Bligaard, A. Nilsson, J. K. Nørskov, *J. Catal.* **2015**, *328*, 36-42.

[2]   J. H. Montoya, L. C. Seitz, P. Chakthranont, A. Vojvodic, T. F. Jaramillo, J. K. Norskov, *Nat. Mater.* **2016**, *16*, 70-81.

[3]   J. Greeley, T. F. Jaramillo, J. Bonde, I. B. Chorkendorff, J. K. Norskov, *Nat. Mater.* **2006**, *5*, 909-913.

[4]   J. K. Nørskov, J. Rossmeisl, A. Logadottir, L. Lindqvist, J. R. Kitchin, T. Bligaard, H. Jónsson, *J. Phys. Chem. B* **2004**, *108*, 17886-17892.

[5]   C. Kirk, L. D. Chen, S. Siahrostami, M. Karamad, M. Bajdich, J. Voss, J. K. Norskov, K. Chan, *ACS Cent. Sci.* **2017**, *3*, 1286-1293.

[6]   F. Calle-Vallejo, M. T. Koper, *Angew. Chem. Int. Ed.* **2013**, *52*, 7282-7285.

[7]   F. Calle-Vallejo, M. T. M. Koper, *Electrochim. Acta.* **2012**, *84*, 3-11.

[8]   J. K. Norskov, T. Bligaard, J. Rossmeisl, C. H. Christensen, *Nat. Chem.* **2009**, *1*, 37-46.

[9]   H. Alt, *J. Catal.* **1973**, *28*, 8-19.

[10]   K. Hara, A. Kudo, T. Sakata, *J. Electroanal. Chem.* **1995**, *391*, 141-147.

[11]   O. Diaz-Morales, I. Ledezma-Yanez, M. T. M. Koper, F. Calle-Vallejo, *ACS Catal.* **2015**, *5*, 5380-5387.

[12]   F. Calle-Vallejo, D. Loffreda, M. T. Koper, P. Sautet, *Nat. Chem.* **2015**, *7*, 403-410.

[13]   F. Calle-Vallejo, J. Tymoczko, V. Colic, Q. H. Vu, M. D. Pohl, K. Morgenstern, D. Loffreda, P. Sautet, W. Schuhmann, A. S. Bandarenka, *Science* **2015**, *350*, 185-189.

[14]   F. Calle-Vallejo, J. I. Martinez, J. Rossmeisl, *Phys. Chem. Chem. Phys.* **2011**, *13*, 15639-15643.

[15] K. P. Kuhl, T. Hatsukade, E. R. Cave, D. N. Abram, J. Kibsgaard, T. F. Jaramillo, *J. Am. Chem. Soc.* **2014**, *136*, 14107-14113.

[16] M. A. Thorseth, C. E. Tornow, E. C. M. Tse, A. A. Gewirth, *Coord. Chem. Rev.* **2013**, *257*, 130-139.

[17] V. R. Stamenkovic, B. Fowler, B. S. Mun, G. Wang, P. N. Ross, C. A. Lucas, N. M. Markovic, *Science* **2007**, *315*, 493-497.

[18] J. Greeley, I. E. Stephens, A. S. Bondarenko, T. P. Johansson, H. A. Hansen, T. F. Jaramillo, J. Rossmeisl, I. Chorkendorff, J. K. Norskov, *Nat. Chem.* **2009**, *1*, 552-556.

[19] A. S. Bandarenka, M. T. M. Koper, *J. Catal.* **2013**, *308*, 11-24.

[20] V. Stamenkovic, B. S. Mun, K. J. J. Mayrhofer, P. N. Ross, N. M. Markovic, J. Rossmeisl, J. Greeley, J. K. Nørskov, *Angew. Chem.* **2006**, *118*, 2963-2967.

[21] X. F. Yang, A. Wang, B. Qiao, J. Li, J. Liu, T. Zhang, *Acc. Chem. Res.* **2013**, *46*, 1740-1748.

[22] Z. Zhao, Z. Chen, X. Zhang, G. Lu, *J. Phys. Chem. C* **2016**, *120*, 28125-28130.

[23] F. Abild-Pedersen, J. Greeley, F. Studt, J. Rossmeisl, T. R. Munter, P. G. Moses, E. Skulason, T. Bligaard, J. K. Norskov, *Phys. Rev. Lett.* **2007**, *99*, 016105.

[24] K. K. Tanabe, M. S. Ferrandon, N. A. Siladke, S. J. Kraft, G. Zhang, J. Niklas, O. G. Poluektov, S. J. Lopykinski, E. E. Bunel, T. R. Krause, J. T. Miller, A. S. Hock, S. T. Nguyen, *Angew. Chem. Int. Ed.* **2014**, *53*, 12055-12058.

[25] K. K. Tanabe, N. A. Siladke, E. M. Broderick, T. Kobayashi, J. F. Goldston, M. H. Weston, O. K. Farha, J. T. Hupp, M. Pruski, E. A. Mader, M. J. A. Johnson, S. T. Nguyen, *Chem. Sci.* **2013**, *4*.

[26] B. E. Snyder, P. Vanelderen, M. L. Bols, S. D. Hallaert, L. H. Bottger, L. Ungur, K. Pierloot, R. A. Schoonheydt, B. F. Sels, E. I. Solomon, *Nature* **2016**, *536*, 317-321.

[27] S. Grundner, M. A. Markovits, G. Li, M. Tromp, E. A. Pidko, E. J. Hensen, A. Jentys, M.

Sanchez-Sanchez, J. A. Lercher, *Nat. Commun.* **2015**, *6*, 7546.

[28]   A. G. Slater, A. I. Cooper, *Science* **2015**, *348*, aaa8075.

[29]   H. Furukawa, K. E. Cordova, M. O'Keeffe, O. M. Yaghi, *Science* **2013**, *341*, 1230444-1230444.

[30]   S. Kitagawa, R. Kitaura, S. Noro, *Angew. Chem. Int. Ed.* **2004**, *43*, 2334-2375.

[31]   D. J. Xiao, E. D. Bloch, J. A. Mason, W. L. Queen, M. R. Hudson, N. Planas, J. Borycz, A. L. Dzubak, P. Verma, K. Lee, F. Bonino, V. Crocella, J. Yano, S. Bordiga, D. G. Truhlar, L. Gagliardi, C. M. Brown, J. R. Long, *Nat. Chem.* **2014**, *6*, 590-595.

[32]   B. Rungtaweevoranit, J. Baek, J. R. Araujo, B. S. Archanjo, K. M. Choi, O. M. Yaghi, G. A. Somorjai, *Nano. Lett.* **2016**, *16*, 7645-7649.

[33]   H. Fei, M. D. Sampson, Y. Lee, C. P. Kubiak, S. M. Cohen, *Inorg. Chem.* **2015**, *54*, 6821-6828.

[34]   L. Yang, S. Kinoshita, T. Yamada, S. Kanda, H. Kitagawa, M. Tokunaga, T. Ishimoto, T. Ogura, R. Nagumo, A. Miyamoto, M. Koyama, *Angew. Chem. Int. Ed.* **2010**, *49*, 5348-5351.

[35]   N. Kornienko, Y. Zhao, C. S. Kley, C. Zhu, D. Kim, S. Lin, C. J. Chang, O. M. Yaghi, P. Yang, *J. Am. Chem. Soc.* **2015**, *137*, 14129-14135.

[36]   E. M. Miner, S. Gul, N. D. Ricke, E. Pastor, J. Yano, V. K. Yachandra, T. Van Voorhis, M. Dincă, *ACS Catal.* **2017**, *7*, 7726-7731.

[37]   U. Díaz, A. Corma, *Coord. Chem. Rev.* **2016**, *311*, 85-124.

[38]   J. L. Segura, M. J. Mancheno, F. Zamora, *Chem. Soc. Rev.* **2016**, *45*, 5635-5671.

[39]   Y. Xu, S. Jin, H. Xu, A. Nagai, D. Jiang, *Chem. Soc. Rev.* **2013**, *42*, 8012-8031.

[40]   A. P. Cote, A. I. Benin, N. W. Ockwig, M. O'Keeffe, A. J. Matzger, O. M. Yaghi, *Science* **2005**, *310*, 1166-1170.

[41]   Y. Peng, Z. Hu, Y. Gao, D. Yuan, Z. Kang, Y. Qian, N. Yan, D. Zhao, *ChemSusChem* **2015**, *8*,

3208-3212.

[42] S. Y. Ding, J. Gao, Q. Wang, Y. Zhang, W. G. Song, C. Y. Su, W. Wang, *J. Am. Chem. Soc.* **2011**, *133*, 19816-19822.

[43] P. Kuhn, A. Thomas, M. Antonietti, *Macromolecules* **2009**, *42*, 319-326.

[44] R. A. Periana, *Science* **1998**, *280*, 560-564.

[45] R. Palkovits, M. Antonietti, P. Kuhn, A. Thomas, F. Schuth, *Angew. Chem. Int. Ed.* **2009**, *48*, 6909-6912.

[46] K. Park, G. H. Gunasekar, N. Prakash, K. D. Jung, S. Yoon, *ChemSusChem* **2015**, *8*, 3410-3413.

[47] S. Lin, C. S. Diercks, Y. B. Zhang, N. Kornienko, E. M. Nichols, Y. Zhao, A. R. Paris, D. Kim, P. Yang, O. M. Yaghi, C. J. Chang, *Science* **2015**, *349*, 1208-1213.

[48] H. B. Aiyappa, J. Thote, D. B. Shinde, R. Banerjee, S. Kurungot, *Chem. Mater.* **2016**, *28*, 4375-4379.

[49] K. Kamiya, R. Kamai, K. Hashimoto, S. Nakanishi, *Nat. Commun.* **2014**, *5*, 5040.

Chapter 2

Development of copper-based oxygen reduction electrocatalysts based on coordination structure control by covalent triazine framework
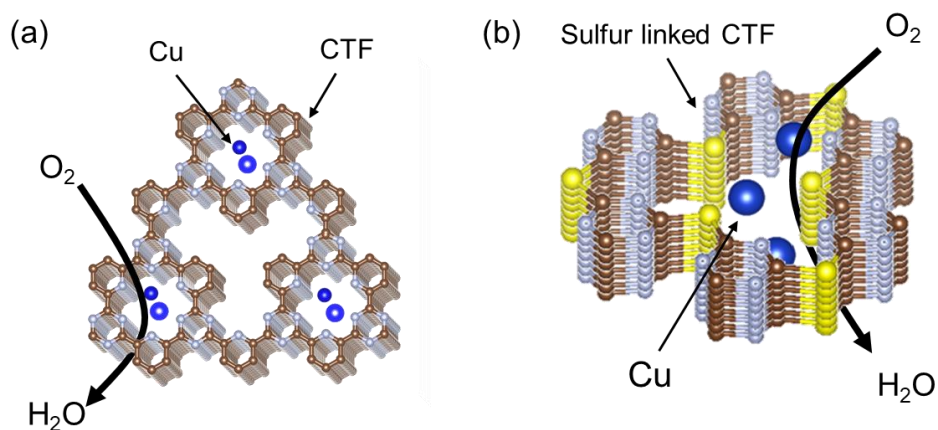
Section 2

Adapted with permission from *Angewandte Chemie International edition,* **2015**, 54, 11068-11072. Copyright 2015, WILEY-VCH Verlag GmbH & Co. KGaA, Weinheim.

Section 3

Adapted with permission from *ChemElectroChem*, **2018**, 5, 805-810. Copyright 2015, WILEY-VCH Verlag GmbH & Co. KGaA, Weinheim.

Electrochemical oxygen reduction reaction (ORR) is important as a cathode reaction of various types of fuel cells. In this chapter, the author attempted to synthesize Cu based efficient ORR catalysts by controlling coordination structure of Cu with covalent triazine frameworks (CTFs). In section 2, the author demonstrated that Cu modified CTF (Cu-CTF) can function as an efficient ORR catalyst in neutral solutions. In section 3, the author successfully increased the ORR activity of Cu-CTF in section 2 by using S linked CTF (S-CTF) as a Cu support.


Figure. Schematic illustration of (a) Cu-CTFs in section 2 and (b) Cu-S-CTF in section 3.

2-1

General introduction of oxygen reduction reaction

Molecular oxygen (O_2) is an ideal electron acceptor since it is harmless, abundant in the air and possesses high redox potential (1.23 V vs. Reversible hydrogen electrode [RHE]). Therefore, the electrochemical oxygen reduction reaction (ORR) has been utilized as a cathode reaction in various types of fuel cells such as polymer electrolyte fuel cell (PEFC). In general, ORR proceeds through 4-electron reduction as shown below:

$$O_2 + 4\ H^+ + 4\ e^- \rightarrow 2\ H_2O\ (E° = 1.23\ V\ vs.\ RHE)$$
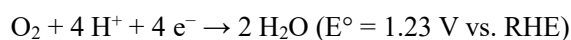
ORR is a bottleneck reaction of fuel cells due to its slow kinetics [1−3]. Currently, platinum (Pt) is used as a practical ORR catalyst since Pt-based catalysts show highest ORR activity among the synthetic ORR catalysts so far. However, the high cost of Pt is a critical problem to widespread dissemination of fuel cells. Therefore, many researches have been directed on developing efficient ORR catalysts (1) with lower Pt content and (2) composed only of abundant elements.

Pt based ORR catalysts

Development of ORR catalysts with lower Pt content is achieved by allying or doping of Pt with abundant elements such as first transition metal or precise size control of Pt nanoparticles [4−9]. This approach is focusing on reducing platinum atoms in catalysts and increasing activity per Pt weight (atom). For example, J. Zang et al. successfully synthesized core-shell nanoparticles with Pt mono

layer (Fig. 1). In this report, authors demonstrated that some of those catalysts show higher onset

potential for ORR than that of pure Pt nanoparticle supported on carbon nanoparticle (Pt/C) [8]. As

one of other researches about Pt-alloy based ORR catalysts, V. Stamenkovic et al. synthesized Pt_3M

(M: Ti, Fe, Co, Ni) alloy film and systematically evaluated ORR activity. In this report, some of Pt-

alloy based electrocatalysts (such as Pt_3Ni or Pt_3Co) show superior ORR activity to that of pure Pt

catalysts. Additionally, first principle density functional theory (DFT) calculations conducted in this

report revealed that electronic structure of Pt and adsorption energy (ΔE_{ads}) of O atom, which is one

of the ORR intermediates, to catalytic surface were slightly tuned by alloying [5] (the Figure is shown

in Fig. 5 in chapter 1). In summary, for Pt based electrocatalysts, the modification of Pt catalysts by

alloying or doping is a promising approach to enhance the onset potential for ORR. Specifically, the

modulation of electronic state and ΔE_{ads} of reaction intermediates to catalytic center are essential to

improve ORR activity.
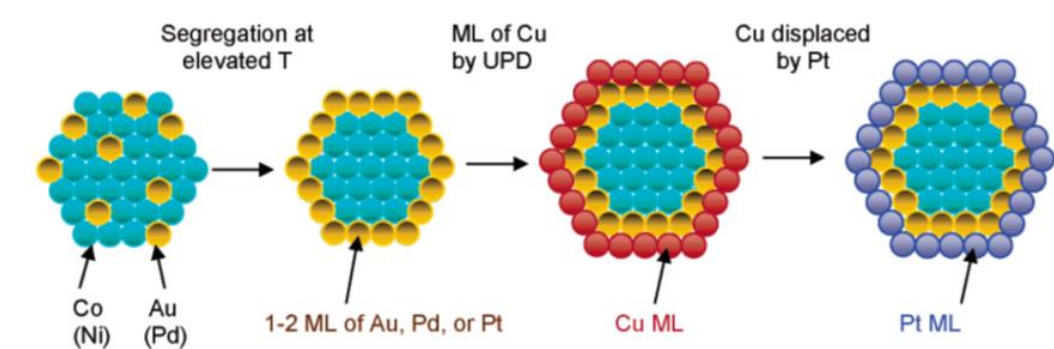
Fig. 1 One of the approaches to synthesize core-shell structure of Pt catalysts. Reprinted with permission from ref. [8]. Copyright 2005, American Chemical Society.

Fe and Co based ORR catalysts

Researches on developing ORR catalysts composed only of abundant elements are also widely conducted. In those researches, first transition metals (such as cobalt [Co], iron [Fe] and copper [Cu]) containing catalysts have attracted a considerable attention because of their high abundance. At least in 1964, it is revealed that Co phthalocyanine catalyzes ORR [10]. Inspired by this work, many researchers have developed metal-N4 macrocyclic compounds (M-N4, M: Co or Fe) as ORR catalysts since they generally show higher catalytic activity (low over-potential) among M-N4 [11−15]. Numerous researchers have intended to improve ORR activity of Co and Fe-N4 by modification of their molecular structure since those organic ligands have high design flexibility [13,16,17]. In those researches, the regulation of electronic structure of metal center with organic ligands is essential for improving ORR activity.

In addition to above-mentioned researches about development of Fe and Co-N4 complexes, development of ORR catalysts has also been achieved by pyrolysis of metal-nitrogen (M-N) containing precursor with electro-conductive carbon substrates. In those researches, Fe or Co-N containing coordination compounds such as M-N4 are mixed with electro-conductive carbon substrates such as graphene or carbon nanoparticle, then the mixtures are pyrolyzed under inert gas (N_2 and Ar) or ammonia (NH_3) atmosphere with high temperature such as 700−1000ºC. Those materials have attracted a considerable attention since some of them show higher ORR activity (lower over-potential) and stability compared with catalysts before heat treatment [3,18−22]. One of the representative synthesis procedures is shown in Fig. 2, which is developed by G. Wu et al [22].

33

(a)

(b)
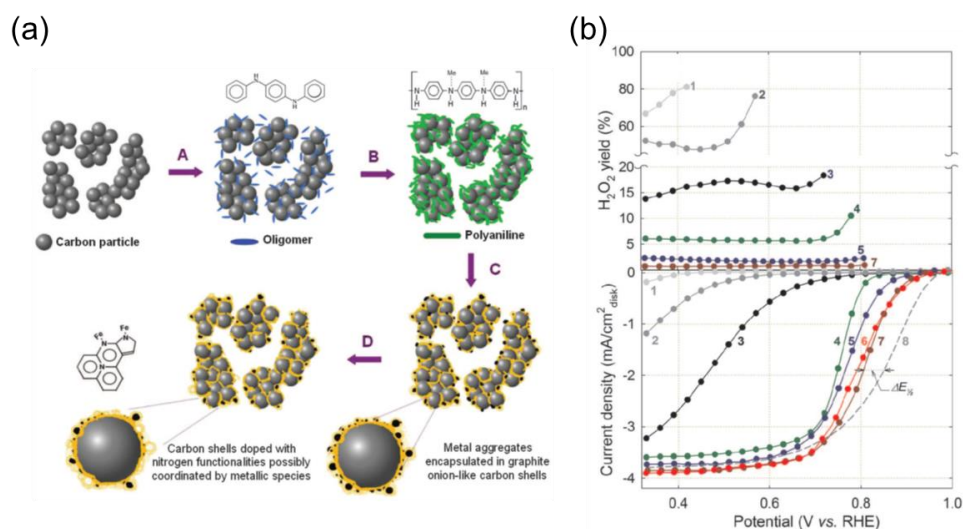
Fig. 2 (a) Schematic procedure of catalyst in ref. [22]. N containing polymer with metal ions were treated in high temperature and catalysts were obtained after acid washed. (b) Steady-state ORR polarization plots (bottom) and H_2O_2 yield plots (top) measured catalysts with different polyaniline (PANI) derived catalysts and reference materials (1, as-received carbon black (Ketjenblack EC- 300J); 2, heat-treated carbon black; 3, heat-treated PANI-C; 4, PANI-Co-C; 5, PANI-FeCo-C(1); 6, PANI-FeCo-C(2); 7, PANIFe- C; 8, E-TEK Pt/C (20 mg Pt cm^{-2}). Electrolyte: O_2-saturated 0.5 M H_2SO_4 [0.1 M HClO4 in experiment involving Pt catalysts (dashed line)]. Reprinted with permission from ref [22]. Copyright 2011, American Association for the Advancement of Science.

As mentioned above, some of those catalysts show relatively higher ORR activity among the first transition metal based ORR catalysts, however, as coordination structure of metal-containing precursors is fully or partially decomposed and aggregation of metal species easily occurs during high temperature heat treatments. Considering that precise control of electronic and coordination structure of active centers is essential for enhancement of ORR activity, further improvement of ORR activity of those pyrolyzed catalysts is very challenging issue.

Cu based ORR catalysts

Among M-N4, Cu-N4 is well known to show very poor (or no) ORR activity unlike above mentioned Fe and Co-N4 [23]. However, Cu based materials are considered as promising ORR catalysts since multi-copper oxidases (MCOs), which contain four Cu ions as active centers, are representative enzymes that catalyze ORR with almost no over-potential [24]. The ORR activity of MCOs is superior to Pt catalysts and the best among the first transition metal-based ORR catalysts [24]. For MCOs, the modulation of the electronic state of the Cu centers through the coordination with amino acid residues is known to be essential for the superior ORR catalytic activity [25–27]. The active centers of MCOs are formed from 3 types of Cu centers (Fig. 3). Type 1 Cu is coordinated by N and S. This Cu site is an entry point of electrons from substrates. Therefore, an important role of this Cu site is determining the redox potential of Cu(II)/Cu(I). Type 2 Cu and type 3 Cu form triangular clusters. These Type 2 and Type 3 Cu are important for activation of O_2 and generation H_2O as a product [25–27].
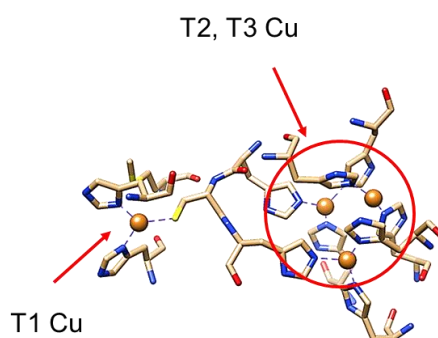
Fig. 3 Structure of MCOs

As mentioned above, electronic and coordination structure modulation of Cu centers in MCOs is important to catalyze ORR with high efficiency. Therefore, many studies have been conducted on developing Cu containing organometallic complexes by mimicking the molecular structure of MCOs [23,28−35]. Fig. 4 shows an example of developed Cu based ORR complexes [23]. Those researches succeeded to modulate the electronic states of Cu centers and improved ORR activity. For example, C. C. L. McCrory et al. demonstrated that Cu-phenanthroline and its derivatives can function as ORR catalysts, and that redox potential of Cu(II)/Cu(I) and ORR activity of them can be tuned by an addition of electron withdrawing/adding function groups to phenanthroline ligands [31]. As typified by this work, many researches have suggested that Cu(I) is active species which proceed ORR. This means that redox potential of Cu center (Cu(II)/Cu(I)) is an essential factor which determine the over-potential (onset potential) for ORR. Additionally, M. S. Thorum et al. reported that onset potential of Cu- 3,5-Diamino-1,2,4-triazole (Cu-Hdatrz) which possesses dinuclear Cu center in its structure was 0.73 V (vs. RHE) [33]. This ORR over-potential of Cu-Hdatrz was relatively lower among synthetic Cu complexes. Authors claimed that distance of Cu centers of Cu-Hdatrz is similar to that of multi Cu centers in MCOs, indicating that modulation of steric structure of Cu centers is also important for higher ORR activity.
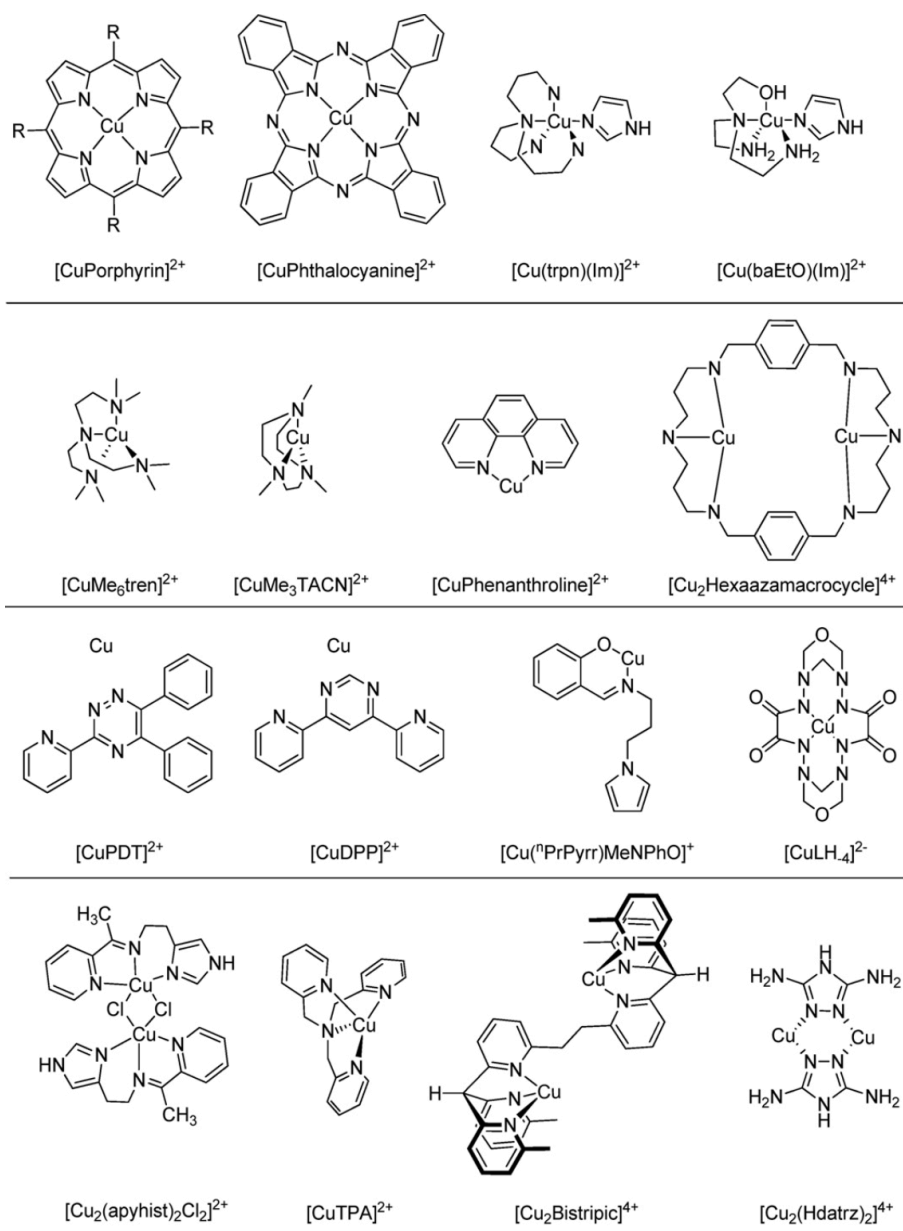
Fig. 4 Diagram of some of the reported Cu ORR catalysts. Reprinted with permission from ref. [23]. Copyright 2013, Elsevier Ltd.

References

[1]   H. A. Gasteiger, S. S. Kocha, B. Sompalli, F. T. Wagner, *Appl. Catal. B: Environ.* **2005**, *56*, 9-35.

[2]   H. A. Gasteiger, J. E. Panels, S. G. Yan, *J. Power Sources* **2004**, *127*, 162-171.

[3]   A. A. Gewirth, J. A. Varnell, A. M. DiAscro, *Chem. Rev.* **2018**, *118*, 2313-2339.

[4]   C. Wang, H. Daimon, T. Onodera, T. Koda, S. Sun, *Angew. Chem. Int. Ed.* **2008**, *47*, 3588-3591.

[5]   V. Stamenkovic, B. S. Mun, K. J. J. Mayrhofer, P. N. Ross, N. M. Markovic, J. Rossmeisl, J. Greeley, J. K. Nørskov, *Angew. Chem.* **2006**, *118*, 2963-2967.

[6]   J. Greeley, I. E. Stephens, A. S. Bondarenko, T. P. Johansson, H. A. Hansen, T. F. Jaramillo, J. Rossmeisl, I. Chorkendorff, J. K. Norskov, *Nat. Chem.* **2009**, *1*, 552-556.

[7]   M. Oezaslan, F. d. r. Hasché, P. Strasser, *J. Electrochem. Soc.* **2012**, *159*.

[8]   J. Zhang, F. H. Lima, M. H. Shao, K. Sasaki, J. X. Wang, J. Hanson, R. R. Adzic, *J. Phys. Chem. B* **2005**, *109*, 22701-22704.

[9]   Y. Bing, H. Liu, L. Zhang, D. Ghosh, J. Zhang, *Chem. Soc. Rev.* **2010**, *39*, 2184-2202.

[10]   R. Jasinski, *Nature* **1964**, *201*, 1212-1213.

[11]   J. H. Zagal, M. Gulppi, M. Isaacs, G. Cardenas-Jiron, M. J. Aguirre, *Electrochim. Acta* **1998**, *44*, 1349-1357.

[12]   J. H. Zagal, M. T. Koper, *Angew. Chem. Int. Ed.* **2016**, *55*, 14510-14521.

[13]   M. Ozer, A. Altindal, A. R. Ozkaya, O. Bekaroglu, *Dalton. Trans.* **2009**, 3175-3181.

[14]   J. Zagal, M. Páez, A. A. Tanaka, J. R. dos Santos, C. A. Linkous, *J. Electroanal. Chem.* **1992**, *339*, 13-30.

[15]   H. Alt, *J. Catal* **1973**, *28*, 8-19.

[16]   P. Vasudevan, Santosh, N. Mann, S. Tyagi, *Transit. Metal. Chem.* **1990**, *15*, 81-90.

[17]   J. Han, Y. J. Sa, Y. Shim, M. Choi, N. Park, S. H. Joo, S. Park, *Angew. Chem. Int. Ed.* **2015**, *54*, 12622-12626.

[18]   J. Masa, W. Xia, M. Muhler, W. Schuhmann, *Angew. Chem. Int. Ed.* **2015**, *54*, 10102-10120.

[19]   R. Zhou, M. Jaroniec, S.-Z. Qiao, *ChemCatChem* **2015**, *7*, 3808-3817.

[20]   Y. Zhao, K. Watanabe, K. Hashimoto, *J. Am. Chem. Soc.* **2012**, *134*, 19528-19531.

[21]   K. Kamiya, K. Hashimoto, S. Nakanishi, *Chem. Commun.* **2012**, *48*, 10213-10215.

[22]   G. Wu, K. L. More, C. M. Johnston, P. Zelenay, *Science* **2011**, *332*, 443-447.

[23]   M. A. Thorseth, C. E. Tornow, E. C. M. Tse, A. A. Gewirth, *Coord. Chem. Rev.* **2013**, *257*, 130-139.

[24]   N. Mano, V. Soukharev, A. Heller, *J. Phys. Chem. B* **2006**, *110*, 11180-11187.

[25]   E. I. Solomon, A. J. Augustine, J. Yoon, *Dalton. Trans.* **2008**, 3921-3932.

[26]   E. I. Solomon, *Inorg. Chem.* **2016**, *55*, 6364-6375.

[27]   E. I. Solomon, D. E. Heppner, E. M. Johnston, J. W. Ginsbach, J. Cirera, M. Qayyum, M. T. Kieber-Emmons, C. H. Kjaergaard, R. G. Hadt, L. Tian, *Chem. Rev.* **2014**, *114*, 3659-3853.

[28]   Y. T. Xi, P. J. Wei, R. C. Wang, J. G. Liu, *Chem. Commun.* **2015**, *51*, 7455-7458.

[29]   M. Asahi, S. Yamazaki, S. Itoh, T. Ioroi, *Dalton. Trans.* **2014**, *43*, 10705-10709.

[30]   S. Gentil, D. Serre, C. Philouze, M. Holzinger, F. Thomas, A. Le Goff, *Angew. Chem. Int. Ed.* **2016**, *55*, 2517-2520.

[31]   C. C. McCrory, X. Ottenwaelder, T. D. Stack, C. E. Chidsey, *J. Phys. Chem. A* **2007**, *111*, 12641-12650.

[32]   V. L. N. Dias, E. N. Fernandes, L. M. S. da Silva, E. P. Marques, J. Zhang, A. L. B. Marques, *J. Power Sources* **2005**, *142*, 10-17.

[33]   M. S. Thorum, J. Yadav, A. A. Gewirth, *Angew. Chem. Int. Ed.* **2009**, *48*, 165-167.

[34]   C. C. McCrory, A. Devadoss, X. Ottenwaelder, R. D. Lowe, T. D. Stack, C. E. Chidsey, *J. Am. Chem. Soc.* **2011**, *133*, 3696-3699.

[35]   M. A. Thorseth, C. S. Letko, E. C. Tse, T. B. Rauchfuss, A. A. Gewirth, *Inorg. Chem.* **2013**, *52*, 628-634.

2-2

Copper-modified covalent triazine frameworks as oxygen reduction electrocatalysts in neutral solutions

Introduction

As mentioned in section 1, oxygen reduction reaction (ORR) has been utilized as a cathode reaction in various types of fuel cells. Although hydrogen–oxygen fuel cells generally operate under acid or alkaline conditions, ORR in neutral solutions has recently attracted increased attention for application in bioelectrochemical systems, such as enzymatic and microbial fuel cells [1−4]. At present, platinum (Pt) is still the most efficient artificial ORR catalyst. It is reported that adsorption energy of ORR intermediates of Pt is close to the top of volcano plot and this is why Pt is the best ORR catalyst [5]. However, as Pt is scarce and expensive, the use of non-noble-metal catalysts operating in neutral solutions is desirable for developing sustainable systems [6−8]. For copper (Cu) based organometallic complexes, it is well known that the modulation of coordination structure of Cu is very important to achieve high ORR activity [9]. In the present work, the author attempted to synthesize a highly active oxygen reduction electrocatalyst by precise control of the coordination structure of Cu by covalent triazine frameworks (CTFs). Specifically, Cu modified covalent triazine framework (Cu-CTF) hybridized with conductive carbon nanoparticle was developed as non-noble metal catalysts for oxygen reduction.

Experimental

(1)   Synthesis procedure

In this study, CTF was prepared by basically the same method as described in previous report [10]. Briefly, a mixture of $ZnCl_2$ (3.41 g, Wako), 2,6-dicyanopyridine (64.5 mg, Koei Kagaku) and electro-conductive carbon nanoparticle (CP, Ketjen Black EC600JD, Lion Corp., 64.5 mg) was vacuum-sealed in a Pyrex glass tube, and then heated at 400 °C for 40 h. The resulting black powder was washed with ultra-pure water (UPW), tetrahydrofuran (THF, Wako) and 1 M HCl (Wako), then dried at 60 °C for overnight and CTF hybridized with carbon nanoparticle (CTF/CP) was obtained. It was then modified with Cu atoms by stirring for 4 h at 60 °C in 1 mM $CuCl_2$ aqueous solution. The resulting Cu-CTF/CP catalyst was washed with UPW to remove unbound Cu atoms. Commercial 20 wt% Pt/C (Platinum on Vulcan XC-72) was obtained from Fuel Cell Earth.

(2)   Electrochemical characterization

The oxygen reduction activity of Cu-CTF was evaluated using a rotating ring disk electrode at room temperature in phosphate, boric acid and acetic acid buffer solutions. The working electrodes were prepared by dispersing 3 mg Cu-CTF/CP or 20 wt% Pt/C in 300 μL ethanol and 20 μL Nafion solution (5 wt% solution; Aldrich) using a homogenizer. The amount of loaded catalyst was controlled to be approximately 0.24 mg cm^{-2}. The electrode forms catalysts layers with thickness of hundreds of μm as shown in a previous report by the author and co-workers [11]. A Pt wire and Ag/AgCl/KCl sat. were used as the counter and reference electrodes, respectively. The number of electrons (n) for the oxygen reduction reaction was calculated using equation (1) [12,13]:

$$n = 4I_d / (I_d + I_r/N) \qquad (1)$$

where N, I_d, and I_r are the collection efficiency, disk current, and ring current, respectively. Here, a

value of 0.48 was used for N.

(3)　　　Physical characterizations

X-ray photoelectron spectroscopy (XPS; Axis Ultra, Kratos Analytical Co.) was conducted

with monochromated Al Kα X-rays. XAFS spectra for Cu-K were recorded on the beamline BL01B1

at SPring-8, which is administered by the Japan Synchrotron Radiation Research Institute (JASRI).

Transmission-yield spectra were acquired using a double-crystal Si (111) monochromator.

Transmission electron microscopy (ARM-200F, JEOL) was used to observe the morphological

structures. Nitrogen adsorption–desorption isotherm measurement was performed on a Micromeritics

3 Flex. The pore size distribution was calculated by nonlocal density functional theory.

Thermogravimetric analyses (TGA-50, Shimadzu) were measured to evaluate the thermal stabilities.

Electron spin resonance was measured by Bruker EMX10/12 at room temperature.

(4)　　　DFT calculations

The density functional theory (DFT) calculations of adsorption energies of oxygen on Cu-

CTF, model of Cu-N4 macrocycle and Pt metal were performed by using OpenMX code [14,15]. The

generalized gradient approximation of the Perdew–Burke–Ernzerhof model (GGA-PBE) was used,

and the kinetic energy cutoff was selected at 120 Ryd. To simplify the DFT calculations, a slab of

single Cu-CTF layer was used as the model structure of Cu-CTF with the coordinatively unsaturated

Cu atoms. One oxygen atom was adsorbed on one Cu site, and the structures were relaxed. For the

Gibbs free energy calculation of ORR intermediates, the zero-point energies and entropy correction

were chosen from previous report [16]. The following equation, computational hydrogen electrode

(CHE) model, was used to model ORR on CTF and metal-N4 macrocycle model when the adsorption

energies of ORR intermediates were calculated:

$$G[H^+ + e^-] = 0.5\ G[H_2] - eU \qquad (4)$$

here, U is the applied over-potential and e is the elementary charge [17].

Results and discussion

CTF/CP and Cu-CTF/CP were synthesized as shown in the experimental section. As no large CTF particles were detected by transmission electron microscopic (TEM) inspection of CTF/CP (Fig. 1), the CTFs appeared to be well mixed with CP. Fig. 2 shows a high-magnification TEM image of Cu-CTF/CP and the corresponding elemental maps (C, N, and Cu) obtained by energy dispersive X-ray (EDX) analysis. High-resolution TEM analysis (Fig. 2a) revealed that no metal nano-particles (> 1 nm) were formed on Cu-CTF/CP. As shown in the EDX maps (Fig. 2b), Cu and N atoms were homogeneously distributed on the CPs. These results demonstrated that the CPs were almost fully covered with CTFs, and that Cu atoms were uniformly impregnated on the CTF.

The author also measured the nitrogen adsorption-desorption isotherms of Cu-CTF/CP to evaluate its porosity and surface area (Fig. 3). Cu-CTF/CP was found to have a hierarchical pore system comprised of micro- and mesopores with pore diameters of 1–2 and 2.5–4 nm, respectively. This pore size distribution was essentially consistent with the reported values of CTFs that were prepared using monomers of 2,6-dicyanopyridine [18,19]. The BET surface area was estimated to be 491 m^2 g^{-1}.
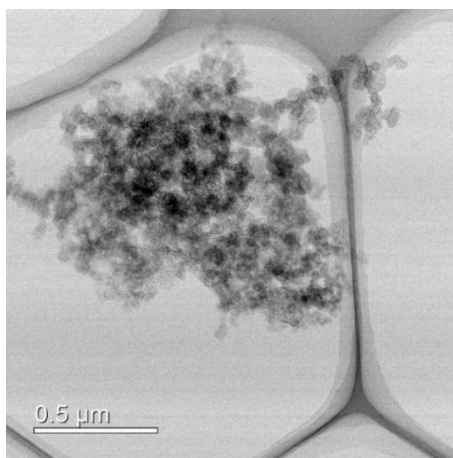
Fig. 1 Representative TEM image of CTF/CP
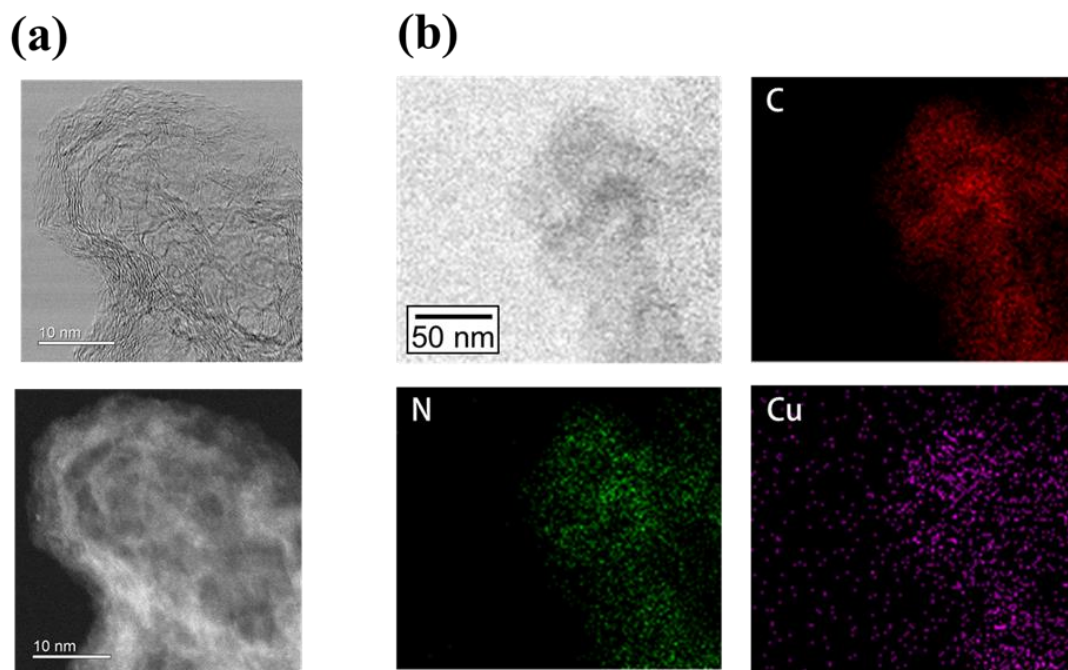
Fig. 2 (a) Representative high-resolution transmission electron microscopy (HR-TEM) image of Cu-CTF (upper) and the corresponding high-angle annular dark-field scanning image (lower). (b) HR-TEM image of Cu-CTF/CP and the corresponding EDX mappings for C, N and Cu atoms.
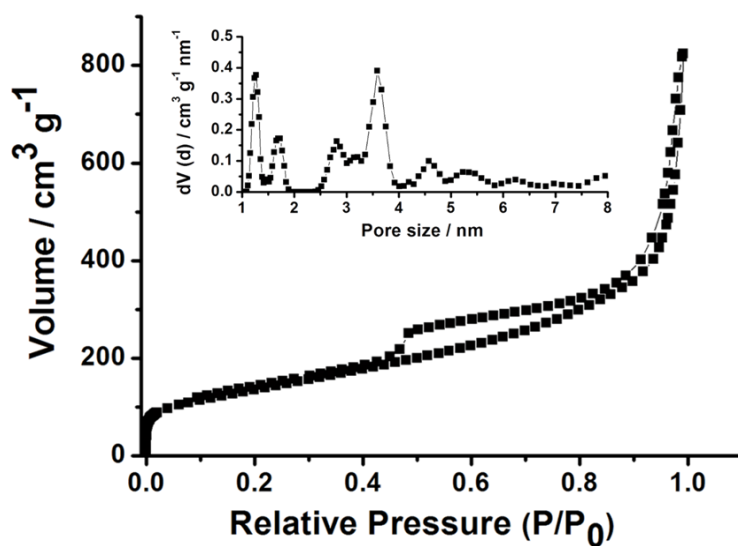

Fig. 3 Nitrogen adsorption–desorption isotherms for Cu-CTF/CP. The inset shows the pore size distribution calculated based on nonlocal density functional theory

Table 1 XPS elemental analyses (at %).

	C	Cu	N	O
CTF	92	-	5.5	3.0
Cu-CTF	92	0.58	5.4	2.4
CP (treated with CuCl$_2$)	97	0.0	-	2.7

The author next performed a detailed characterization of the synthesized Cu-CTF/CP. The surface elemental concentrations of Cu-CTF/CP and CTF/CP, as determined by X-ray photoelectron spectroscopy (XPS), are summarized in Table 1. Cu and N atoms were clearly detected in Cu-CTF/CP, whereas no Cu species were found on CPs that were treated with CuCl$_2$ solution in a similar manner to Cu-CTF/CP (Fig. 4). This result indicated that almost no precipitates of Cu species such as Cu(OH)$_2$, which is formed in alkaline conditions [20,21], was formed on Cu-CTF/CP, and that Cu atoms were anchored on the CTF via coordination with N.
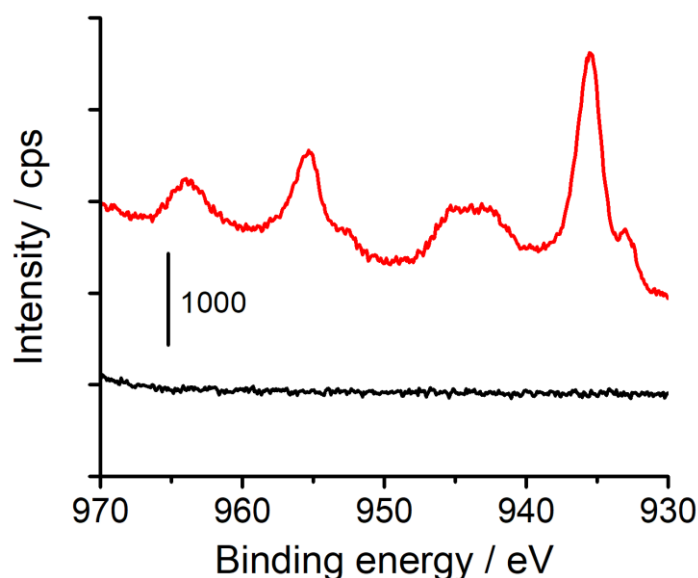
Fig. 4 Cu-2p XPS spectra for Cu-CTF/CP (red) and CP treated with CuCl$_2$ solution (black).

The Cu-N coordination structure in Cu-CTF/CP was directly confirmed by extended X-ray absorption fine structure (EXAFS) analysis. Fourier transformations of k^3-weighted EXAFS oscillations for Cu-CTF/CP are shown in Fig. 5. The EXAFS results before Fourier transformation and inverse FT-EXAFS of Cu-5,10,15,20-tetraphenyl-21H,23H-porphine (Cu-TPP) as a reference and Cu-CTF/CP are shown in Fig. 6. A peak at 0.16 nm, corresponding to Cu-N coordination structures, was clearly observed. However, peaks corresponding to Cu-Cu (0.22 nm) and Cu-O-Cu bonds (0.27 nm) were not detected [22]. The coordination number of the Cu species could also be determined from the EXAFS spectra. The intensity of the Cu-N peak for Cu-CTF at 0.16 nm was approximately two thirds of that for Cu-TPP, suggesting that the first coordination number (CN) for Cu-CTF is smaller than four. The author and co-workers estimated the CN of Cu-CTF as 3.4 by fitting of FT-EXAFS spectra of Cu-CTF/CP in a related work [23]. The author also analyzed the Cu 2p XPS spectrum to obtain information on the electronic state of the Cu atoms in Cu-CTF (Fig. 4). The Cu 2p1/2 peak (955

eV) in the spectrum can be assigned to the Cu (II) valence state, and almost no peaks corresponding to metallic Cu were detected [24−26]. The X-ray absorption near edge structure (XANES) of Cu-K edge also indicated that the Cu(II) valence state is dominant in Cu-CTF (Fig. 7). An electron spin resonance (EPR) measurement of Cu-CTF/CP was also conducted to analyze the coordination structure and counter anion species on Cu-CTF/CP (Fig. 8). However, no strong signal was observed for Cu-CTF/CP, maybe due to the low concentration of Cu ions in Cu-CTF/CP. It is suggested that adsorbed species to Cu in Cu-CTF/CP are weakly binding anion species such as OH^- or H_2O molecules, since no strong signal of Cu-Cl was detected in FT-EXAFS (Fig. 5). Taken together, the TEM, nitrogen isotherms, EXAFS, and XPS results indicate that the Cu atoms in Cu-CTF were individually isolated and have an unsaturated first coordination sphere containing N atoms in the pore of CTF, as shown in Fig. 9.
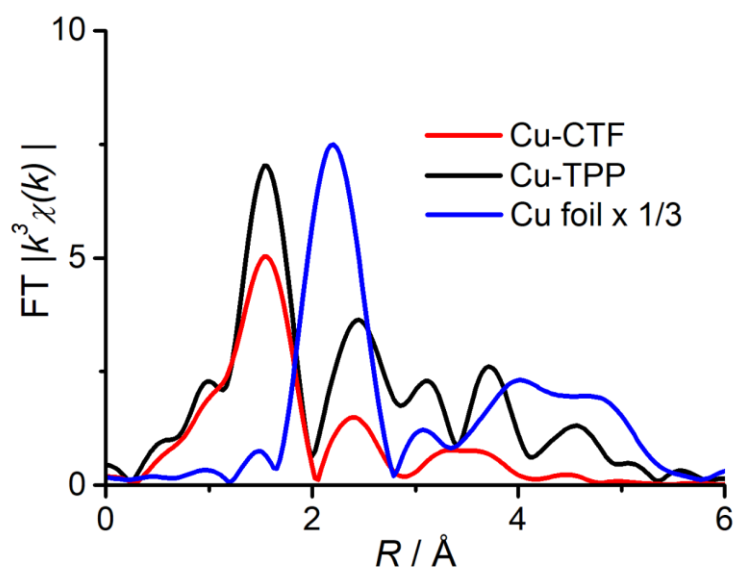

Fig. 5 k^3-weighted Fourier transform of EXAFS spectra of the Cu K edge for Cu-CTF (red), Cu-TPP (black) and Cu metal (blue). The peak intensity for Cu metal is shown at one-third of the measured values for clarity
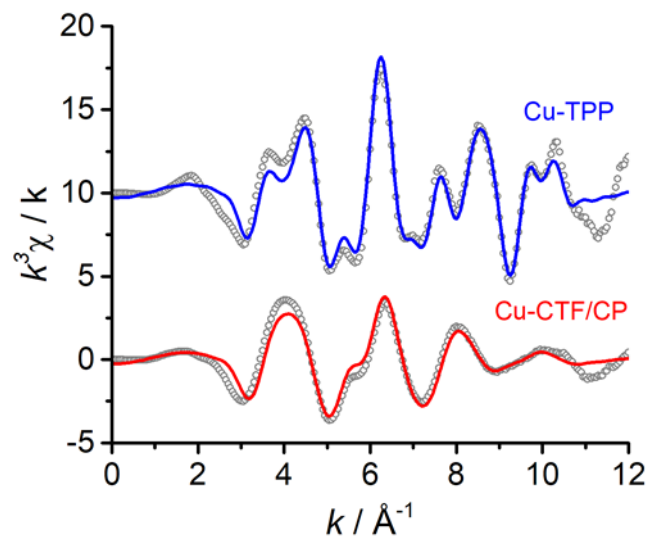
Fig. 6 k^3-weighted EXAFS oscillation (gray dots) for Cu-TPP (upper part) and Cu-CTF/CP (bottom part); solid colored lines show the Inverse Fourier Transform of FT-EXAFS in Fig. 5 for Cu-TPP (blue) and Cu-CTF/CP (red). k: 3–10.5 Å^{-1}, R: 1–6.
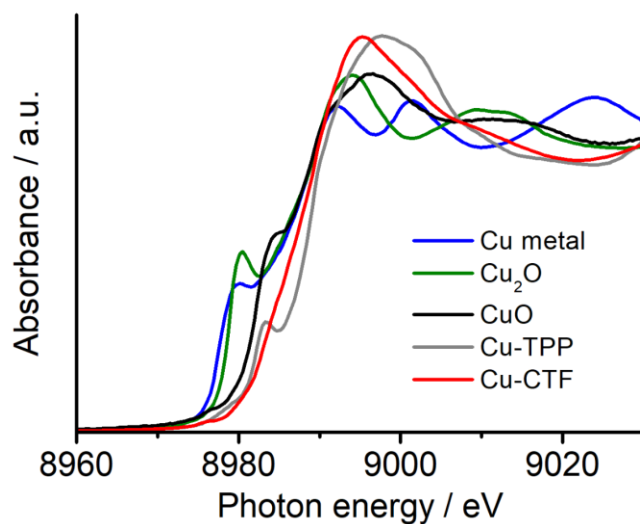
Fig. 7 The Cu-K XANES spectra for Cu (blue), Cu_2O (green), CuO (black), Cu(II)-TPP (gray) and Cu-CTF (red). The absorption edge for Cu-CTF was consistent with that for CuO and Cu(II)-TPP, indicating that the Cu(II) valence state is dominant in Cu-CTF
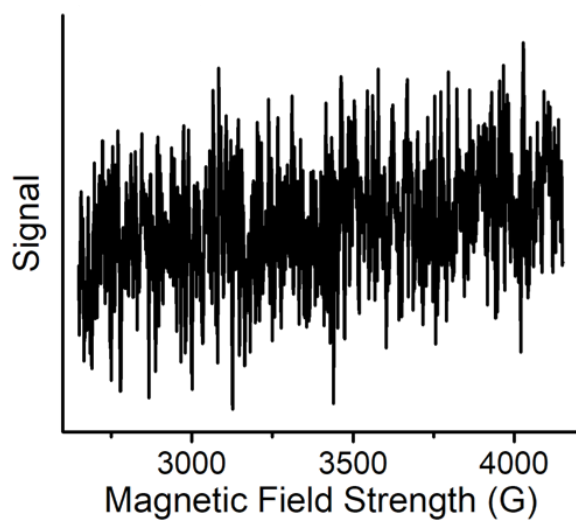
Fig. 8 ESR spectrum (room temperature) for Cu-CTF/CP
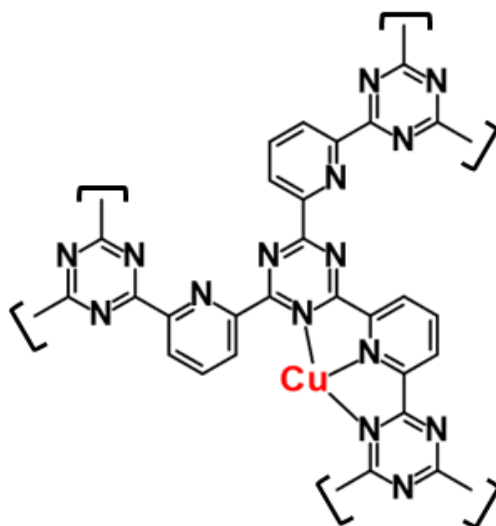
Fig. 9 Schematic illustration of Cu-CTF (weakly adsorbed species in electrolyte, anion species such as OH⁻ and water molecule, and ethanol molecule used for the preparation of electrodes are not shown for clarity).

To examine the electrocatalytic ORR activity of Cu-CTF/CP, current density (j) versus potential (U) curves for Cu-CTF/CP and CTF/CP were measured (Fig. 10). Although no redox peaks for CTF/CP (black curve) were observed in Ar-saturated phosphate buffer solution (PBS), a single pair of redox peaks with a mid-point potential of 0.57 V vs. RHE, which were ascribed to the Cu(II)/Cu(I) redox couple, was detected for Cu-CTF/CP (red curve) (Fig. 10a, also see Fig. 11). When the electrolyte was saturated with dissolved oxygen, a catalytic ORR current (Fig. 10b) and the corresponding ring current assignable to hydrogen peroxide (H_2O_2) oxidation (Fig. 12a) were observed. As shown in Fig. 10b, the ORR onset potential for Cu-CTF/CP was 0.81 V (vs. RHE), a value that is 0.13 V higher than that for CTF/CP, indicating that the Cu in Cu-CTF/CP enhanced the ORR catalytic activity. To the author's knowledge, the ORR onset potential (0.81 V) determined for Cu-CTF is higher than that reported to date for other Cu based electrocatalysts [9,27−31], although the ORR activity is still lower than that of Pt/C (U_{onset} for Pt/C was 1.04 V vs RHE). The electron number for the ORR estimated from the yield of H_2O_2 was in the range of 3.75–3.95 in all examined potential regions (Fig. 12b). It was also confirmed that Cu-CTF showed efficient ORR activity with an onset potential of 0.91 V vs. RHE in alkaline solution (Fig. 13) [9,28].
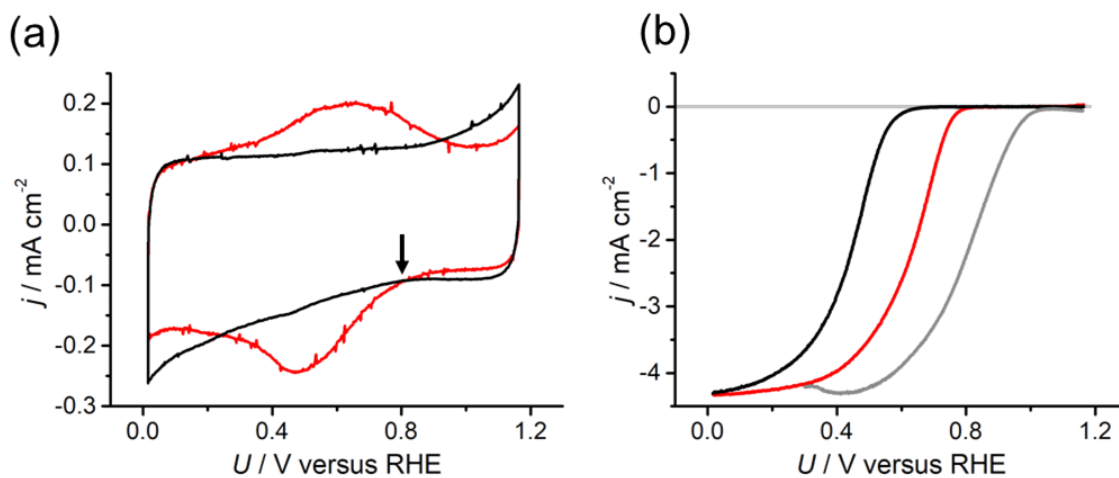
Fig. 10 *j* vs. *U* curves for Cu-CTF/CP (red), CTF/CP (black) and 20 wt% Pt/C (gray) in phosphate buffer solution (pH 7) under (a) argon and (b) oxygen. Scan rate, 10 mV s^{-1}. Rotational speed, 1500 rpm. The arrow indicates the potential at which Cu(II) species are reduced.
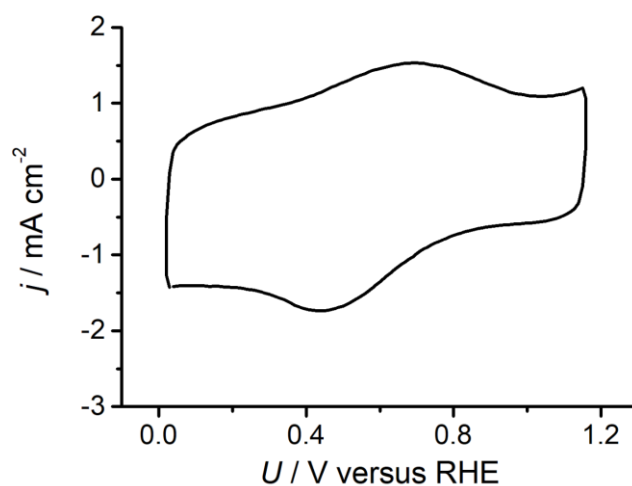
**Fig. 11** *j* vs. *U* curves for Cu-CTF/CP in phosphate buffer solution (pH 7) under argon. Scan rate, 100 mV s^{-1}. Rotational speed, 1500 rpm.

Note : The full-widths-at-half-maximum of the redox peak for Cu-CTF/CP is relatively wide (250–300 mV), which was also observed for the Cu(II)/Cu(I) redox couple of the Cu complexes immobilized onto carbon electrodes [32,33].
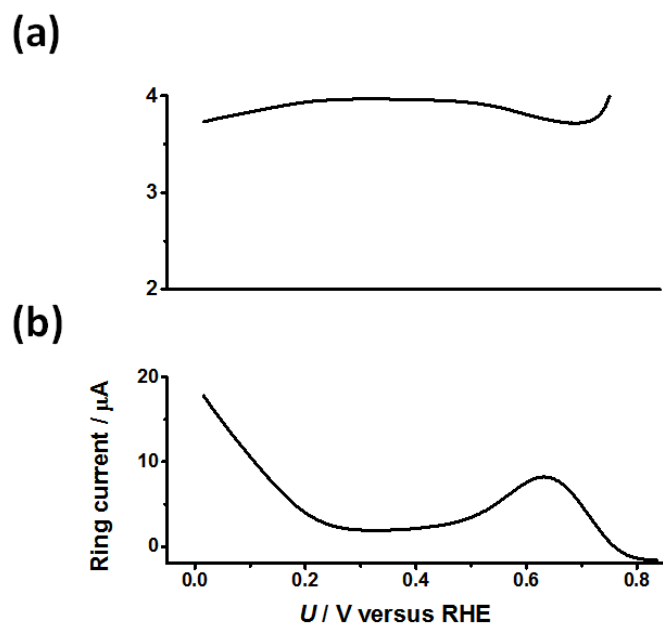
Fig. 12 (a) The ring current and (b) electron number of Cu-CTF/CP in the presence of oxygen. The disk current is shown in Fig. 10. Scan rate, 10 mV s^{-1}. Rotational speed, 1500 rpm.
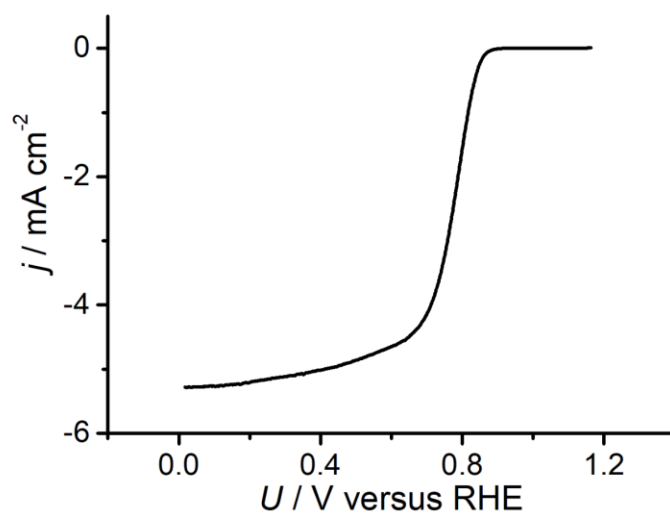
Fig. 13 j vs. U curve for Cu-CTF/CP in 0.1 M NaOH (pH 13) under oxygen saturated condition. Scan rate, 10 mV s^{-1}. Rotational speed, 1500 rpm**.**

Here, the author discusses the properties of the active species for the ORR based on the present electrochemical characterizations. It is important to note that the ORR onset potential (0.81 V, Fig. 10b) at pH 7 was similar to the potential at which Cu(II) is converted to Cu(I) (as indicated by the arrow in Fig. 10a). Therefore, the author compared the Cu(II)/Cu(I) redox potentials with the ORR onset potential at various pH values, as shown in Fig. 14. The ORR onset potential increased linearly by 23.5 mV/pH unit, a finding that is in good agreement with the change of Cu(II)/Cu(I) redox potential (23.4 mV/pH). These results indicate that the ORR was mediated by the Cu(I) species in Cu-CTF/CP. Consistent with this finding, several studies have reported that Cu(I) species readily react with dioxygen to form Cu-dioxygen adducts (i.e., $Cu(I) + O_2 \rightarrow CuO_2$) [30,33−35].
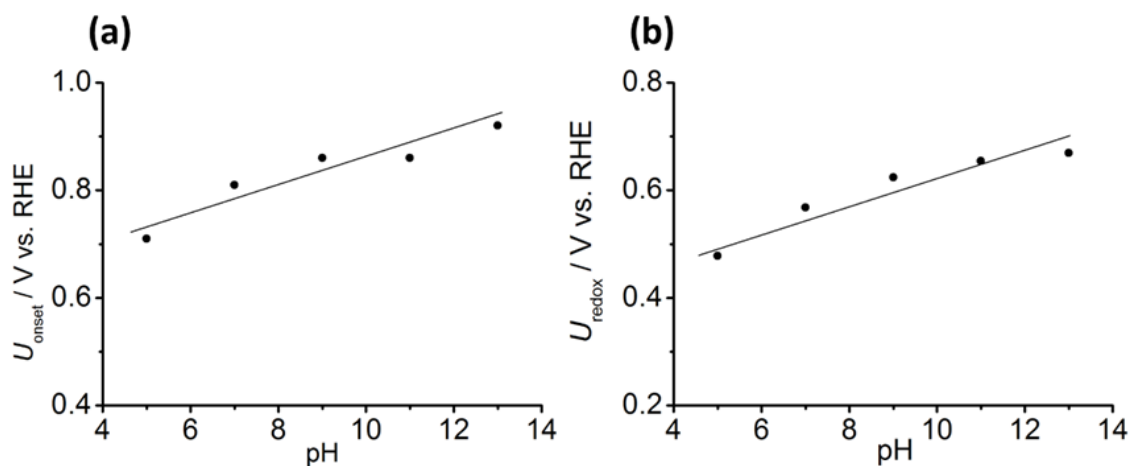

Fig. 14 pH dependence of (a) onset potential of ORR and (b) redox potential of Cu(II)/Cu(I) for Cu-CTF/CP

Let us consider why the Cu-CTF/CP exhibited higher ORR electrocatalytic activity than the other Cu-based catalysts reported to date. First, as described above, Cu(I) species are essential for the ORR. In Cu-CTF/CP, the potential of Cu(II)/Cu(I) (0.57 V vs RHE) is one of the highest reported values among Cu-N based complexes in neutral solutions [9,27,29−31]. Metal cations within the polypeptide structure of enzymes have higher redox potential than those in aqueous solutions, because a cation with a lower valence state is relatively more stable than that with a higher valence state in low dielectric conditions, such as organic frameworks [36−38]. Therefore, the author speculates that the low dielectric environment in the pores of CTF stabilizes Cu(I) species, resulting in a positive shift of the Cu(II)/Cu(I) potential and an increase in the ORR onset potential.

Another possible explanation for the higher ORR activity of Cu-CTF/CP is that the coordinatively unsaturated nature of the Cu centers allows them to strongly interact with molecular oxygen, thereby facilitating the breaking of O-O bonds [9,39]. In general, the interaction of Cu (d10)-based complexes with oxygen molecules is weaker than that of the other 3d metal-based complexes, as oxygen-binding energy depends largely on vacancies in the d-orbitals of the metal center. Consistent with this property, Cu-N4 macrocycles (Cu-porphyrins or Cu-phthalocyanines) show little ORR activity, whereas iron (Fe) and cobalt (Co)-N4 macrocycles function as efficient electrocatalysts [9,40,41]. However, because the coordinatively unsaturated Cu atoms of Cu-CTF/CP were relatively stable, as demonstrated by the EXAFS spectra (Fig. 5), they are expected to have more accessible d-orbitals and less steric hindrance than those in coordinatively saturated Cu-based complexes, such as Cu-N4 macrocycles [40,42−45]. In this section, to confirm this assumption, the author investigated (1) adsorption properties of O_2 molecule, (2) adsorption energy of O atoms and (3) Gibbs free energy change of the formation of ORR intermediates on Cu-CTF using density functional theory (DFT) calculations.

First, the author investigated the adsorption properties of O_2 molecule on Cu-CTF and Cu-

and Fe-N4 macrocycles as reference. Fig. 15a and b show unit cells for M-N4 macrocycles (M: Fe and Cu) and Cu-CTF with coordinatively Cu center used in this study, respectively. Table 2 shows the bond length between metal centers and O_2 molecule (M-O) and O-O distance of O_2 molecule (O-O) after structure optimization of O_2 adsorbed on metal centers. As shown in Table 2, a value of M-O for Cu-N4 macrocycle is much longer than that of Fe-N4 macrocycle and Cu-CTF. In addition, value of O-O for Cu-N4 macrocycle is essentially same value as free O_2 molecule, whereas that for Fe-N4 macrocycle and Cu-CTF is longer than free O_2 molecule. Those results indicated that Fe-N4 macrocycle and Cu-CTF can adsorb and interact with O_2 molecule, and that electron donation from metal centers to O_2 molecule occurs, resulting in longer O-O bond than free O_2 molecule [46]. These results also suggest that Cu-N4 macrocycle cannot adsorb and interact with O_2 molecule as mentioned in previous reports [9]. Fig. 15c and d show the optimized structure of O_2 adsorbed Cu-CTF. As shown in Fig 15c and d, O atom in O_2 molecule is stabilized on the open coordination site, which is not coordinated by N atoms of CTF. This result strongly indicates that first step of O_2 molecule adsorption occurs at open site of Cu atoms for Cu-CTF.
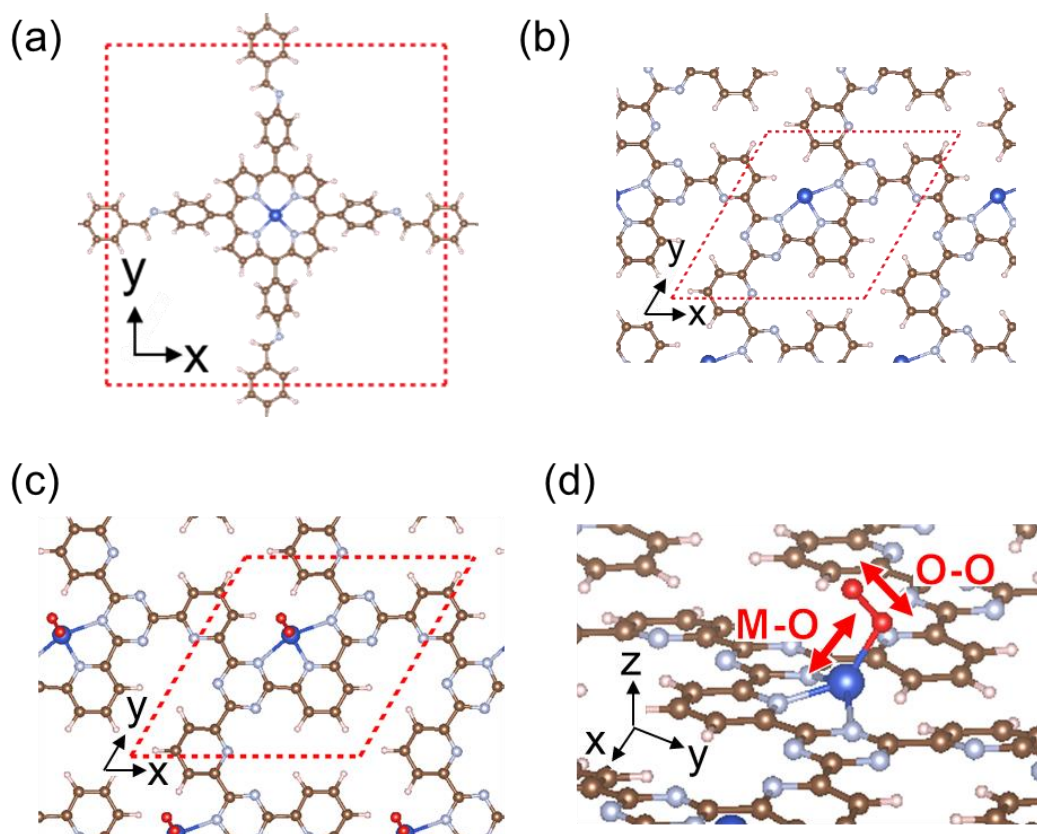
Fig. 15 Unit cell used in this study of DFT calculations for (a) model structure of M-N4 macrocycles (M; Fe, Cu) and (b) Cu-CTF. (c) Top view and (d) slating view of optimized structures of O_2 adsorbed Cu-CTF. Brown: C, pink: H, light blue: N, dark blue: Cu, red: O. The red dashed line shows the unit cell.

Table 2 DFT calculation results of O_2 adsorption on metal centers for M-N4 macrocycles and Cu-CTF. M-O distance represents the bond length of metal active center and adsorbing O atoms in O_2 molecule, and O-O distance represents the bond length between O atom adsorbed on catalysts.

	M-O (Å)	O-O(Å)
Fe-N4 macrocycle	1.73	1.31
Cu-N4 macrocycle	2.69	1.26
Cu-CTF	1.93	1.34
Free O_2 molecule	—	1.27

Second, the adsorption energy of the oxygen atom (ΔE_O) was also calculated. The author calculated ΔE_O as an indicator of binding strength with oxygen species (i.e. dioxygen molecules) using the DFT method [47−51]. On the basis of the Sabatier principle, an optimal ORR electrocatalyst should have moderate binding strength with oxygen species. Using this criterion, Pt metal show an almost ideal adsorption energy [47−51]. A number of researchers have reported that ΔE_O is a suitable indicator of binding strength with oxygen species, such as dioxygen molecules and intermediates of ORR, and is therefore a useful indicator of ORR activity [47−51]. Thus, here the author calculated and compared the ΔE_O on Cu-CTF and Cu-N4 macrocycle, which show very poor ORR activity, with that of Pt (Table 3). The ΔE_O for Cu-CTF was slightly lower (0.2 eV) than that for Pt, suggesting that Cu atoms in Cu-CTF can substantially interact with oxygen species (i.e., oxygen molecules). In contrast, the ΔE_O for Cu-N4 macrocycle was 1.73 eV lower than that for Pt, indicating that the interaction between the Cu atom in Cu-N4 macrocycle and oxygen species is too weak to support ORR. This result shows good agreement with the result obtained in Table 2. The DFT results suggest that the chemical interaction between oxygen molecules and the Cu atoms supported by CTF is sufficiently strong to enhance the ORR activity.

Table 3 The adsorption energies of oxygen atom (ΔE_O) on Cu-CTF, Cu-N4 macrocycle and Pt metal. *a*: The ΔE_O on Pt metal is essentially similar to the reported values [49−51].

|	Cu-CTF	Cu-N4 macrocycle	Pt metal
ΔE_O (eV)	-4.20	-2.67	-4.40^{a}

Third, Gibbs free energy change (ΔG) of formation of ORR intermediates on M-N4 macrocycles (M: Fe and Cu) and Cu-CTF was obtained using DFT calculation (Fig. 16). In this study, O*, OH* and OOH* (* represents the adsorption site on catalysts) were considered as reaction intermediates for ORR [16], and the applied potential was 0.80 V on computational hydrogen electrode model [17]. As shown in Fig. 16, the ΔG of OOH* and O* on Cu-CTF is similar value to that on Fe-N4 macrocycle which shows ORR activity. However, ΔG of ORR intermediates, especially OOH* and O*, on Cu-N4 macrocycle is much higher than those of Fe-N4 macrocycle. On the basis of the DFT calculation results from Table 2, Table 3, Fig. 16 and above-mentioned discussion, it is suggested that open coordination site on Cu which is derived from the coordinatively unsaturated structure of Cu-CTF is essential for O_2 binding and stabilization of ORR intermediates such as OOH* and O* for Cu-CTF. However, ΔG of OH* for Cu-CTF is lower (about 1eV) than that for Fe-N4 macrocycle. This result indicates that tuning ΔG of OH* by further precise control of coordination structure of Cu center can improve the ORR activity of Cu-CTF.
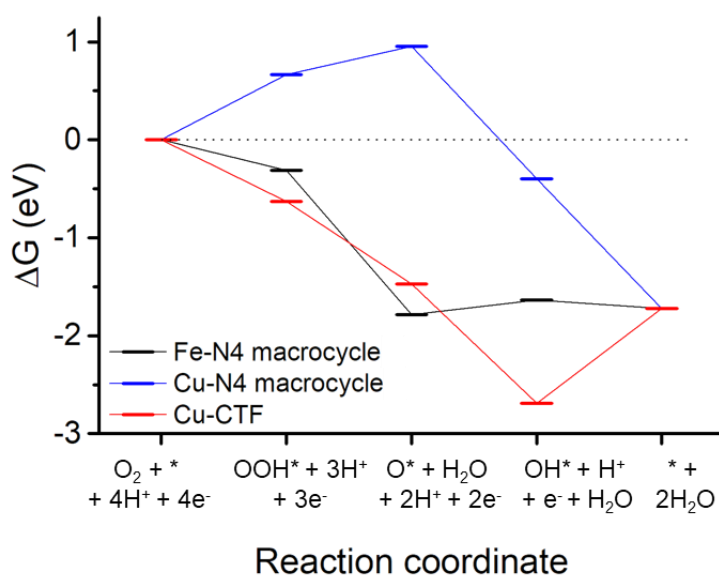
Fig. 16 Free energy diagram of ORR on Fe-N4 macrocycle (black), Cu-N4 macrocycle (blue) and Cu-CTF (red). $U = 0.80$ V. * denote the adsorption site on each catalyst.

In addition, ΔG of the formation of ORR intermediates for Cu–2,4,6-tris(2-piridil)-1,3,5-triazine (Cu-TPT), which is suggested to possess 3-coordinated Cu centers in its structure as shown in Fig. 17a [29], was also calculated. The value of ΔG of formation of ORR intermediates such as OOH* and OH* are comparable to that of Cu-CTF as shown in Fig. 17b. Considering that Cu-TPT shows ORR activity as reported in previous report [29], this result also supports that existence of open coordination site (lower CN of Cu than 4) is essential to catalyze ORR for Cu based molecular catalysts.
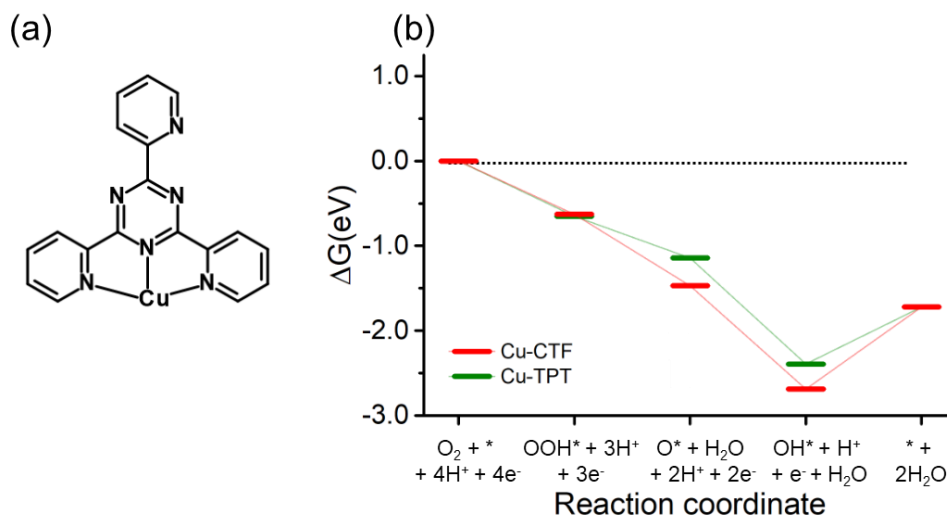

Fig. 17 (a) Molecular structure of Cu-TPT in previous report [29]. (b) Free energy diagram of ORR on Cu-CTF (red, replotted from Fig. 16) and Cu-TPT (green). $U = 0.80$ V. * denote the adsorption site on each catalyst.

In addition to DFT calculation shown above, ligand field theory (LTF) also suggests that open coordination site is essential for Cu based materials to bind O_2 molecule and to function as ORR catalysts. Fig. 18a and b show the representative d electron configuration of Fe and Cu-N4 macrocyclic complexes (M-N4 compounds) such as metal porphyrins [39]. Previous reports suggested that vacant d_z^2 orbital and occupied d_{xz} or d_{yz} orbital are favorable for binding O_2 molecule and electron transfer from metal centers to antibonding π^* orbital of O_2 to weaken O-O bond of O_2 [13,39]. For M-N4, accessible d orbital of the metal center is d_z^2 orbital as shown in Fig. 18c [39]. For Fe-N4 compounds, as d_z^2 orbital is not fully occupied by electrons, adsorption of O_2 to Fe center and π back donation from partially filled Fe d_{yz} and d_{xz} orbitals (Fig. 18a) to antibonding π^* orbital of O_2 are expected to be a favorable process [39]. On the other hand, for Cu-N4 compounds, d_z^2 orbital is fully occupied by electrons, resulting in no adsorption of O_2 molecules as shown in Table 2. However, for Cu center with open coordination site like Cu-CTF, O_2 molecule can interact with Cu $d_{x^2-y^2}$ orbitals which is partially filled by an electron because no ligand exists at this position (Fig. 18d and e). Therefore, the author speculates that O_2 molecule adsorption and π back donation from filled Cu d_{yz} orbital or d_{xy} orbital possibly occur as shown in Fig. 18d and as suggested in previous reports [34,52,53].

Fig. 19 shows schematic images of 5-coordinated Cu centers of (a) square pyramidal configuration and (b) trigonal bipyramidal configuration which can be formed by a structure distortion of square pyramidal configuration. Though both structures possess 5-coordinated Cu centers, the d orbital configuration is different from each other. Cu centers with square pyramidal configuration possess (1) half-filled $d_{x^2-y^2}$ orbital and (2) occupied d_z^2 orbital. Therefore, Cu centers with square pyramidal configuration is expected to possess no ORR activity, same result as Cu-N4 compounds. However, Cu centers with trigonal bipyramidal configuration possess (1) occupied $d_{x^2-y^2}$ orbital and (2) half-filled d_z^2 orbital, which is not occupied by ligands. Therefore, Cu centers with trigonal bipyramidal configuration are also expected to show ORR activity, same as Cu-CTF in this study.

Those results on DFT calculations and knowledge based on the LFT suggest that asymmetric coordination structure of Cu, including existence of open site (unsaturated coordination structure) and coordination structure distortion, is essential for Cu based molecular catalysts to catalyze ORR.
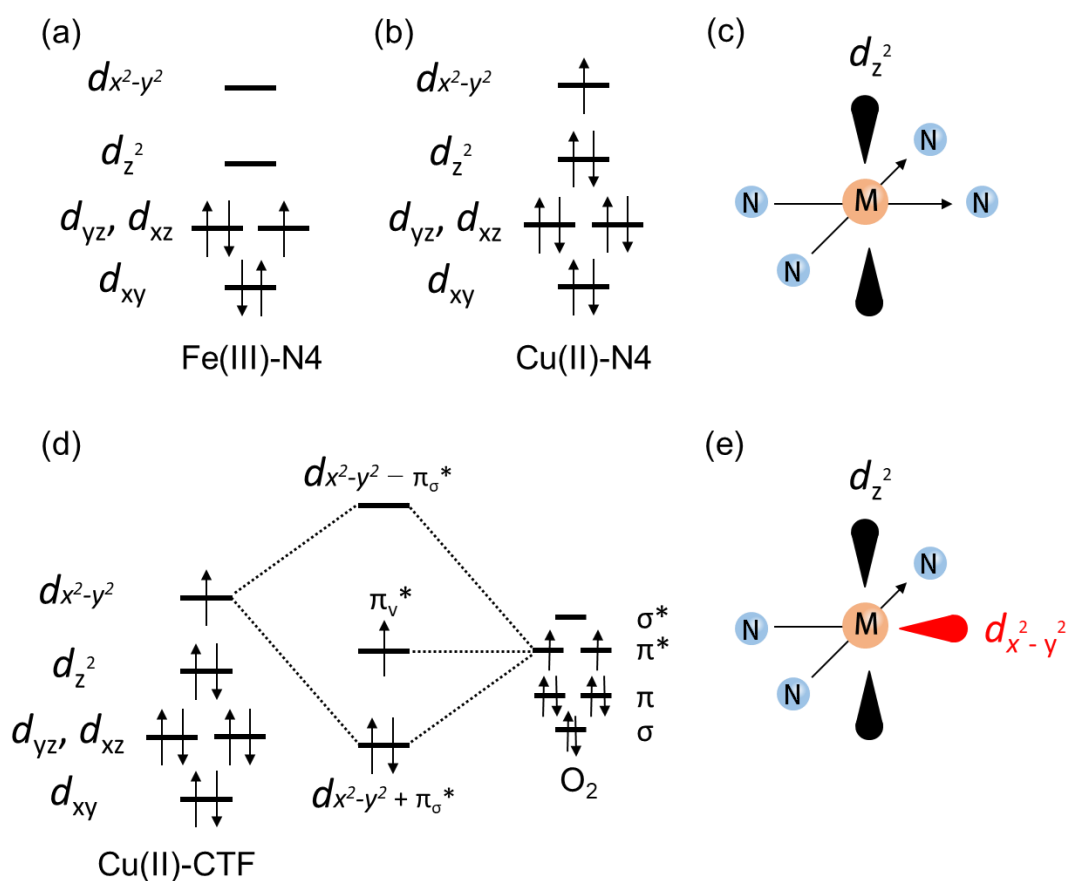

Fig. 18 Representative d-electron configuration of (a) Fe(III)-N4 compounds, (b) Cu(II)-N4 compounds and (d) Cu-CTF and Cu-CTF with molecular O_2 species [34,39,52,53]. Schematic illustration of coordination structure of (c) M-N4 compounds and (e) M-CTF (metal-N3 with open coordination site).
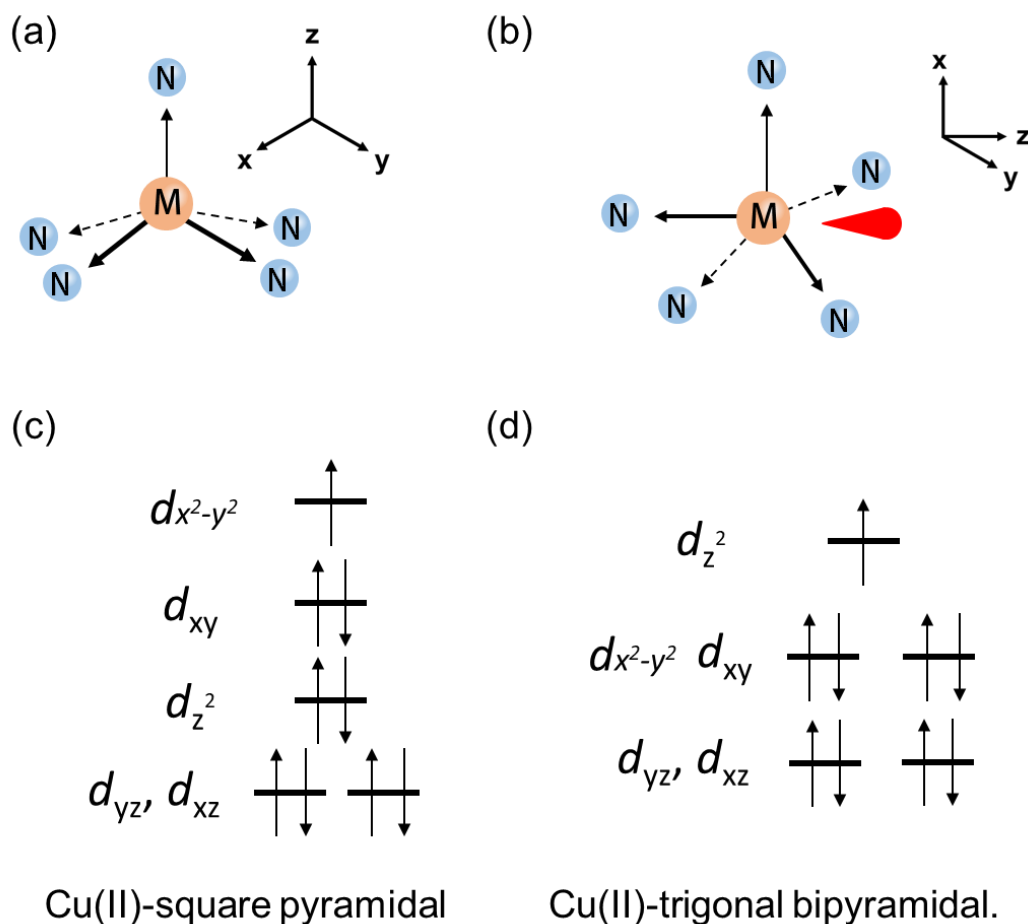
Fig. 19 (Upper figures) Coordination structure of metal ion with (a) square pyramidal configuration and (b) trigonal bipyramidal configuration. (Bottom figures) Representative d-electron configuration of (c) Cu(II)-square pyramidal configuration and (d) Cu(II)-trigonal bipyramidal configuration [34].

Finally, as the stability of electrocatalysts is also an important property, the stability of Cu-CTF/CP during the ORR was evaluated under continuous cycles of cyclic voltammetry (CV). For comparison, a Cu-based organometallic complex, Cu-3,5-diamino-1,2,4-triazole (Cu-Hdatrz) [28], which shows similar ORR onset potential to Cu-CTF/CP, was also tested. As shown in Fig. 20, the current density for Cu-Hdatrz in the kinetic region (0.6 V vs. RHE) decreased by 94% after 1000 CV cycles. In contrast, the current density of Cu-CTF/CP decreased by only 32% after the CV cycling, clearly indicating that Cu-CTF/CP had superior stability to Cu-Hdatrz. The high stability of Cu-CTF/CP can be attributed to its insolubility and resistance to oxidative decomposition. Notably, the

CTF framework is completely insoluble in common solvents, including water, because of its highly

cross-linked structure [54,55], whereas small organic complexes have limited solubility in these

solvents. Therefore, the desorption of the CTF layers from CPs (i.e., electrode) was relatively

suppressed. Furthermore, thermogravimetric analyses (TGA) under air showed that Cu-CTF/CP and

Cu-Hdatrz began to decompose at 478 °C and 420 °C (20% weight loss), respectively, indicating that

CTF-based materials have higher resistance to oxidative decomposition than that of Cu-Hdatrz (Fig.

21). Although the stability of Cu-CTF/CP is still lower than that of Pt/C (Fig. 22), it is expected that

higher stability can be achieved via the fine-tuning of frameworks.
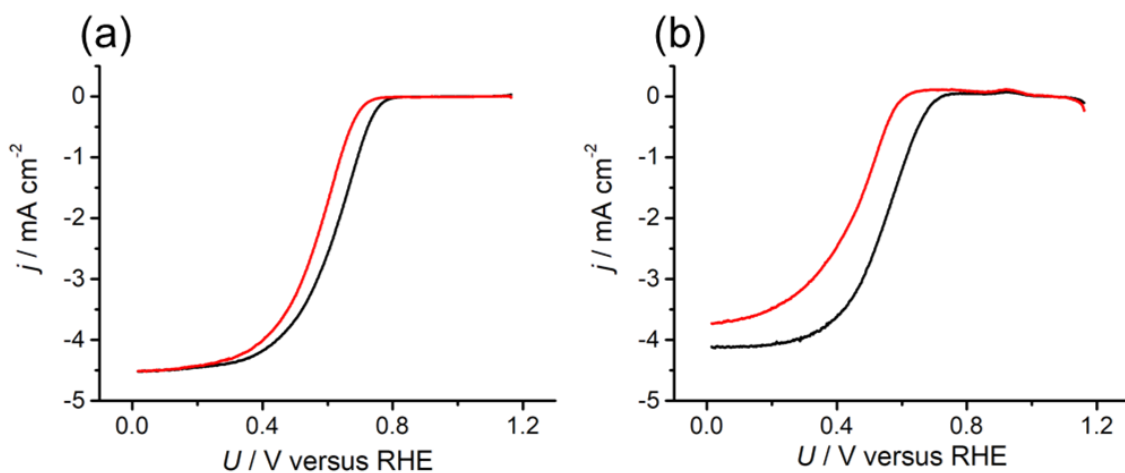
Fig. 20 j vs. U curves for (a) Cu-CTF/CP and (b) Cu-Hdatrz before (black) and after (red) 1000 CV cycles in PBS (pH 7) saturated with dissolved oxygen
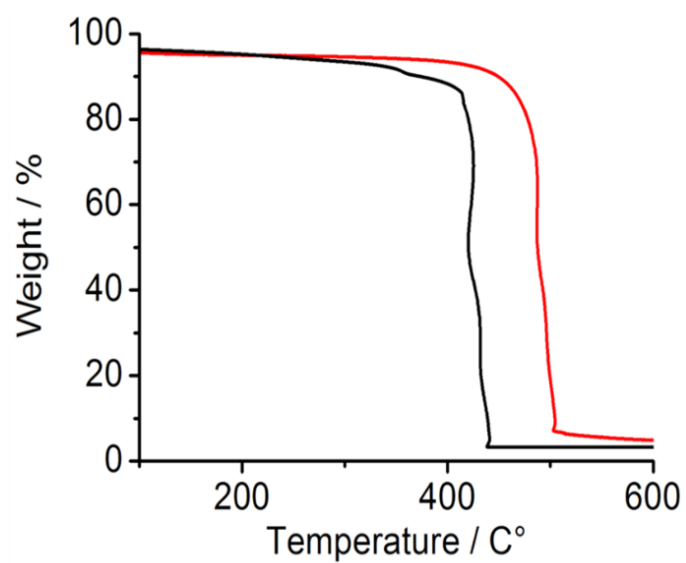
Fig. 21 TGA under air for Cu-CTF (red) and Cu-Hdatrz (black) (Heating rate: 10 ºC min^{-1}, 20% O_2 in N_2)
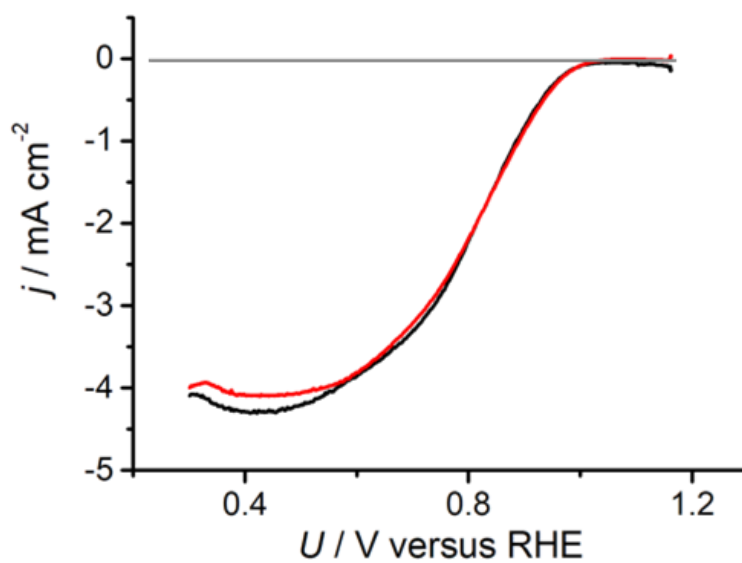
Fig. 22 *j* vs. *U* curves for 20 wt% Pt/C before (black) and after (red) 1000 CV cycles in PBS (pH 7) saturated with dissolved oxygen.

Conclusions

In conclusion, the author successfully modified framework of CTF with Cu atoms and demonstrated that the synthesized material functions as an efficient ORR electrocatalyst in neutral solution. The onset potential of Cu-CTF/CP for the ORR was the highest value among synthetic Cu-based ORR catalysts reported to date. The first principle calculation and theoretical consideration from ligand field theory revealed that unsaturated coordination structure of Cu center in Cu-CTF is responsible for this high ORR activity. In addition, Cu-CTF/CP exhibited higher stability compared to other Cu-based organometallic catalysts due to the rigid cross-linked network of covalent bonds in CTFs. Notably, this is the first report of a non-noble metal-modified CTF functioning as an electrocatalyst.

References

[1]   B. E. Logan, B. Hamelers, R. Rozendal, U. Schröder, J. Keller, S. Freguia, P. Aelterman, W. Verstraete, K. Rabaey, *Environ. Sci. Technol.* **2006**, *40*, 5181-5192.

[2]   A. Heller, *Phys. Chem. Chem. Phys.* **2004**, *6*.

[3]   F. Zhao, R. C. Slade, J. R. Varcoe, *Chem. Soc. Rev.* **2009**, *38*, 1926-1939.

[4]   S. Calabrese Barton, J. Gallaway, P. Atanassov, *Chem. Rev.* **2004**, *104*, 4867-4886.

[5]   J. K. Nørskov, J. Rossmeisl, A. Logadottir, L. Lindqvist, J. R. Kitchin, T. Bligaard, H. Jónsson, *J. Phys. Chem. B* **2004**, *108*, 17886-17892.

[6]   F. Harnisch, U. Schroder, *Chem. Soc. Rev.* **2010**, *39*, 4433-4448.

[7]   L. Birry, P. Mehta, F. Jaouen, J. P. Dodelet, S. R. Guiot, B. Tartakovsky, *Electrochim. Acta* **2011**, *56*, 1505-1511.

[8]   L. Feng, Y. Chen, L. Chen, *ACS Nano* **2011**, *5*, 9611-9618.

[9]   M. A. Thorseth, C. E. Tornow, E. C. M. Tse, A. A. Gewirth, *Coord. Chem. Rev.* **2013**, *257*, 130-139.

[10]   K. Kamiya, R. Kamai, K. Hashimoto, S. Nakanishi, *Nat. Commun.* **2014**, *5,* 5040.

[11]   K. Kamiya, T. Tatebe, S. Yamamura, K. Iwase, T. Harada, S. Nakanishi, *ACS Catal.* **2018**, *8*, 2693-2698.

[12]   R. A. Sidik, A. B. Anderson, N. P. Subramanian, S. P. Kumaraguru, B. N. Popov, *Journal of Physical Chemistry B* **2006**, *110*, 1787-1793.

[13]   K. Kamiya, H. Koshikawa, H. Kiuchi, Y. Harada, M. Oshima, K. Hashimoto, S. Nakanishi, *ChemElectroChem* **2014**, *1*, 877-884.

[14]   T. Ozaki, *Phys. Rev. B* **2003**, *67*.

[15]   T. Ozaki, H. Kino, *Phys. Rev. B* **2004**, *69*.

[16]   F. Calle-Vallejo, J. Tymoczko, V. Colic, Q. H. Vu, M. D. Pohl, K. Morgenstern, D. Loffreda, P. Sautet, W. Schuhmann, A. S. Bandarenka, *Science* **2015**, *350*, 185-189.

[17]   E. Watanabe, J. Rossmeisl, M. E. Björketun, H. Ushiyama, K. Yamashita, *J. Phys. Chem. C* **2016**, *120*, 8096-8103.

[18]   C. E. Chan-Thaw, A. Villa, G. M. Veith, K. Kailasam, L. A. Adamczyk, R. R. Unocic, L. Prati, A. Thomas, *Chem. Asian. J.* **2012**, *7*, 387-393.

[19]   J. Roeser, K. Kailasam, A. Thomas, *ChemSusChem* **2012**, *5*, 1793-1799.

[20]   W. Zhang, X. Wen, S. Yang, Y. Berta, Z. L. Wang, *Adv. Mater.* **2003**, *15*, 822-825.

[21]   J. Yu, J. Ran, *Energy Environ. Sci.* **2011**, *4*.

[22]   H. Irie, K. Kamiya, T. Shibanuma, S. Miura, D. A. Tryk, T. Yokoyama, K. Hashimoto, *J. Phys. Chem. C* **2009**, *113*, 10761-10766.

[23]   T. Yoshioka, K. Iwase, S. Nakanishi, K. Hashimoto, K. Kamiya, *J. Phys. Chem. C* **2016**, *120*, 15729-15734.

[24]   G. G. Jernigan, G. A. Somorjai, *J. Catal.* **1994**, *147*, 567-577.

[25]   J. L. Du, Z. F. Chen, S. R. Ye, B. J. Wiley, T. J. Meyer, *Angew. Chem. Int. Ed.* **2015**, *54*, 2073-2078.

[26]   V. Hayez, A. Franquet, A. Hubin, H. Terryn, *Surf. Interface. Anal.* **2004**, *36*, 876-879.

[27]   M. A. Thorseth, C. S. Letko, E. C. M. Tse, T. B. Rauchfuss, A. A. Gewirth, *Inorg. Chem.* **2013**, *52*, 628-634.

[28]   M. S. Thorum, J. Yadav, A. A. Gewirth, *Angew. Chem. Int. Ed.* **2009**, *48*, 165-167.

[29]   V. L. N. Dias, E. N. Fernandes, L. M. S. da Silva, E. P. Marques, J. J. Zhang, A. L. B. Marques, *J. Power Sources* **2005**, *142*, 10-17.

[30]   C. C. L. McCrory, X. Ottenwaelder, T. D. P. Stack, C. E. D. Chidsey, *J. Phys. Chem. A* **2007**, *111*, 12641-12650.

[31]   K. Slowinski, Z. Kublik, R. Bilewicz, M. Pietraszkiewicz, *J. Chem. Soc. Chem. Commun.* **1994**, 1087-1088.

[32]   M. Kato, K. Kimijima, M. Shibata, H. Notsu, K. Ogino, K. Inokuma, N. Ohta, H. Uehara, Y. Uemura, N. Oyaizu, T. Ohba, S. Takakusagi, K. Asakura, I. Yagi, *Phys. Chem. Chem. Phys.* **2015**, *17*, 8638-8641.

[33]   C. C. McCrory, A. Devadoss, X. Ottenwaelder, R. D. Lowe, T. D. Stack, C. E. Chidsey, *J. Am. Chem. Soc.* **2011**, *133*, 3696-3699.

[34]   E. I. Solomon, D. E. Heppner, E. M. Johnston, J. W. Ginsbach, J. Cirera, M. Qayyum, M. T. Kieber-Emmons, C. H. Kjaergaard, R. G. Hadt, L. Tian, *Chem. Rev.* **2014**, *114*, 3659-3853.

[35]   N. Kitajima, Y. Moro-oka, *Chem. Rev.* **1994**, *94*, 737-757.

[36]   H. B. Gray, B. G. Malmstrom, R. J. P. Williams, *J. Bio. Inorg. Chem.* **2000**, *5*, 551-559.

[37]   A. K. Churg, A. Warshel, *Biochemistry* **1986**, *25*, 1675-1681.

[38]   F. A. Tezcan, J. R. Winkler, H. B. Gray, *J. Am. Chem. Soc.* **1998**, *120*, 13383-13388.

[39]   H. Alt, H. Binder, Sandsted.G, *J. Catal.* **1973**, *28*, 8-19.

[40]   F. Calle-Vallejo, D. Loffreda, M. T. Koper, P. Sautet, *Nat. Chem.* **2015**, *7*, 403-410.

[41]   P. Vasudevan, Santosh, N. Mann, S. Tyagi, *Trans. Met. Chem.* **1990**, *15*, 81-90.

[42]   X. F. Yang, A. Q. Wang, B. T. Qiao, J. Li, J. Y. Liu, T. Zhang, *Acc. Chem. Res.* **2013**, *46*, 1740-1748.

[43]   K. K. Tanabe, M. S. Ferrandon, N. A. Siladke, S. J. Kraft, G. H. Zhang, J. Niklas, O. G. Poluektov, S. J. Lopykinski, E. E. Bunel, T. R. Krause, J. T. Miller, A. S. Hock, S. T. Nguyen, *Angew. Chem. Int. Ed.* **2014**, *53*, 12055-12058.

[44]   K. K. Tanabe, N. A. Siladke, E. M. Broderick, T. Kobayashi, J. F. Goldston, M. H. Weston, O. K. Farha, J. T. Hupp, M. Pruski, E. A. Mader, M. J. A. Johnson, S. T. Nguyen, *Chem. Sci.* **2013**, *4*, 2483-2489.

[45]   J. M. Thomas, R. Raja, D. W. Lewis, *Angew. Chem. Int. Ed.* **2005**, *44*, 6456-6482.

[46]   H. Zhu, S. J. Paddison, T. A. Zawodzinski, *Electrochim. Acta* **2013**, *101*, 293-300.

[47]   F. Calle-Vallejo, M. T. Koper, A. S. Bandarenka, *Chem. Soc. Rev.* **2013**, *42*, 5210-5230.

[48]   J. Greeley, I. E. Stephens, A. S. Bondarenko, T. P. Johansson, H. A. Hansen, T. F. Jaramillo, J. Rossmeisl, I. Chorkendorff, J. K. Norskov, *Nat. Chem.* **2009**, *1*, 552-556.

[49]   A. U. Nilekar, M. Mavrikakis, *Surf. Sci.* **2008**, *602*, L89-L94.

[50]   L. Yang, M. B. Vukmirovic, D. Su, K. Sasaki, J. A. Herron, M. Mavrikakis, S. Liao, R. R. Adzic, *J. Phys. Chem. C* **2013**, *117*, 1748-1753.

[51]   J. Zhang, M. B. Vukmirovic, Y. Xu, M. Mavrikakis, R. R. Adzic, *Angew. Chem. Int. Ed.* **2005**, *44*, 2132-2135.

[52]   N. Ramaswamy, U. Tylus, Q. Jia, S. Mukerjee, *J. Am. Chem. Soc.* **2013**, *135*, 15443-15449.

[53]   E. I. Solomon, J. W. Ginsbach, D. E. Heppner, M. T. Kieber-Emmons, C. H. Kjaergaard, P. J. Smeets, L. Tian, J. S. Woertink, *Faraday Discuss.* **2011**, *148*, 11-39.

[54]   J. Artz, S. Mallmann, R. Palkovits, *ChemSusChem* **2015**, *8*, 672-679.

[55]   X. Zhu, C. Tian, S. M. Mahurin, S. H. Chai, C. Wang, S. Brown, G. M. Veith, H. Luo, H. Liu, S. Dai, *J. Am. Chem. Soc.* **2012**, *134*, 10478-10484

2-3

Enhancement of oxygen reduction reaction activity by copper-modified sulfur-linked covalent triazine frameworks

Introduction

In previous section 2, copper modified covalent triazine framework (Cu-CTF) was developed as an efficient ORR catalyst in neutral solutions. The objective of this section is further improvement of ORR activity of Cu based electrocatalysts. Especially in this section, the author attempted to improve ORR activity by focusing on the redox potential of Cu.

The redox potential of Cu(II/I) (E_{Cu}) is an important factor determining the catalytic activity of Cu-complexes, as the ORR is mediated by Cu(I) species for Cu-CTF/CP in previous section and Cu based ORR complexes in previous reports [1−4]. In addition, it has been reported that the E_{Cu} values of Cu-complexes can be increased by incorporating ligands with stronger electron-withdrawing characteristics, resulting in enhanced ORR catalytic activity [3]. However, unfortunately, the E_{Cu} and ORR catalytic activities of the Cu-complexes developed to date remain insufficient. Although nitrogen (N)-containing molecules have been previously employed as ligands in Cu-complexes intended for the ORR, it is known that replacing these N-ligands with sulfur (S)-ligands increases the E_{Cu} value [5−7], as explained by the hard–soft acid–base (HSAB) theory. However, curiously, there have been no reports describing efficient ORR activity based on Cu-S complexes. Using ligand field theory, the author developed a hypothesis explaining why Cu-complexes having very high E_{Cu} values will not exhibit ORR activity. Cu(I) species generally adopt a closed tetrahedral geometry, whereas Cu(II)

species are most stable in Jahn-Teller distorted octahedral or square planar geometries. In the case of Cu compounds with high E_{Cu} values, such as Cu-S complexes, the autoreduction of Cu(II) to Cu(I) readily occurs [5,8–9] during the synthesis process, resulting in the formation and stabilization of a closed tetrahedral configuration. Unfortunately, this geometry is inactive with regard to the ORR, because the Cu sites are inaccessible to oxygen (O_2) molecules (Fig. 1a) [4,10]. In the present work, the author verified the above hypothesis by evaluating the ORR activity of two Cu-S based complexes: 1,4,8,11-tetrathiacyclotetradecane copper (Cu-ane-S_4) [6,11] and copper dimethyldithiocarbamate (Cu-dmc). The author subsequently attempted to overcome the trade-off between the high redox potential of Cu and a coordination geometry that is ORR-inactive by synthesizing S-linked covalent triazine frameworks (S-CTF) in which both requirements are simultaneously satisfied (Fig. 1b).
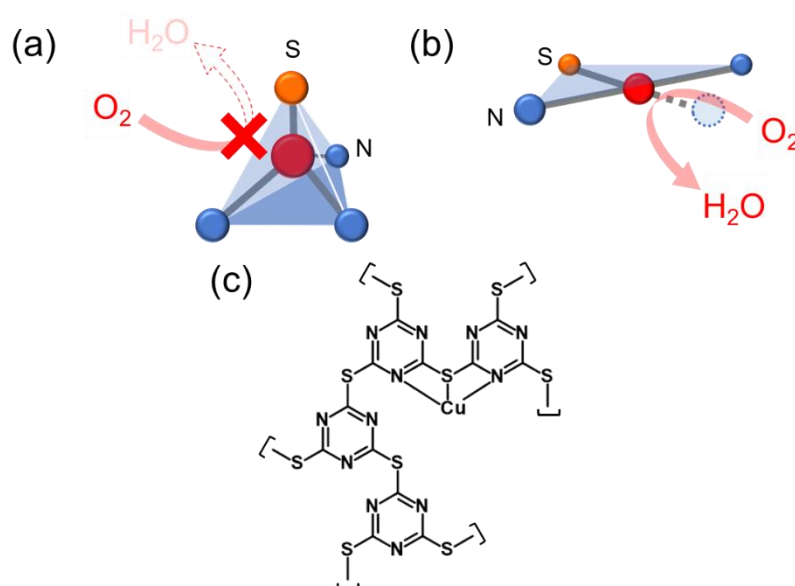
Fig. 1 (a) The closed tetrahedral configuration of a conventional Cu(I) complex, (b) a strategy for the construction of a Cu(I)-modified framework with both high redox potential and oxygen-binding sites in this study, and (c) the structure of the Cu-S-CTF synthesized in the present work (weakly adsorbed species in electrolyte, anion species such as OH⁻ and water molecule, and ethanol molecule used for the preparation of electrodes are not shown for clarity).

Experimental

(1)   Synthesis procedure

S-CTF was synthesized using a modification of a method previously employed to obtain S-linked conjugated polymers [12]. Thiocyanuric acid (TC) was selected as the thiol monomer because it has a relatively high concentration of N and S atoms that are able to immobilize metal centers and donate electrons to Cu. S-CTF was generated by the polymerization of TC and cyanuric chloride (CC) in 1,4-dioxane. Briefly, TC (266 mg, Wako) was dissolved in 1.4-dioxane (60 mL, Wako) maintained at 15 °C, using a magnetic stirrer under a N_2 atmosphere. N,N-diisopropylethylamine (DIPEA, 1.25 mL, TCI) was subsequently added to the solution, followed by the dropwise addition of CC (250 mg, TCI) dissolved in 1,4-dioxane (15 mL). The resulting solution was heated at 85°C for 6 h with magnetic stirring under a continuous flow of N_2.

S-CTF/CP was prepared in a similar manner except for the addition of conductive carbon particles (CPs, 250 mg, Ketjen Black EC600JD, Lion Corp.) prior to the final heating step. The resulting powder was washed with 1.4-dioxane and ethanol, and then dried under vacuum overnight. Samples were impregnated with Cu by dispersion in a $CuCl_2$ solution at 60°C for 4 h, using a method in Section 2 in this Chapter and related reported works [13]. The resulting powder (Cu-S-CTF/CP) was washed with ultrapure water and subsequently dried under vacuum at 200°C for 12 h.

Cu-S complexes on CPs were synthesized by simply adsorbing these complexes onto CPs. In the case of copper dimethyl-dithiocarbamate (Cu-dmc, TCI), the Cu-dmc (18 mg) was dispersed in 5 mL acetone (Wako) containing CPs (80 mg, Lion Corp.) and the resulting dispersion was dried in an oven at 60°C (Cu-dmc/CP). Cu-ane-S_4/CP was prepared by *in situ* synthesis in the presence of CPs. In this procedure, an excess of 1,4,8,11-tetrathiacyclotetradecane (44.8 mg, ane-S_4, TCI) was dissolved in 10 mL of acetone and 980 μL of a 0.8 mM methanol solution of $CuClO_4 \cdot 2H_2O$ (Sigma) was added

to the solution to prepare Cu-ane-S$_4$. Following this, CPs (100 mg) were added to the solution and dispersed using ultrasonication. The mixture was subsequently dried in a furnace at 60 °C to obtain Cu-ane-S$_4$/CP powder.

(2)　　Electrochemical characterization

A rotating disk electrode system was used to evaluate the oxygen reduction activity of samples at room temperature in a 0.1 M phosphate buffer solution (PBS) at pH 7 (scan rate = 10 mV s^{-1}, rotational rate = 1500 rpm). The catalyst ink was prepared by the same method of Section 2. Then, the author applied this ink to a glassy carbon electrode to fabricate a working electrode. The catalyst loading on the electrode was approximately 0.24 mg cm^{-2}. A titanium wire and Ag/AgCl/KCl (sat.) were used as the counter and reference electrodes, respectively. The quantity of electrons (n) involved in the oxygen reduction reaction was calculated using the equation:

$$n = 4I_d / (I_d + I_r/N) \ (1)$$

in which N, I_d and I_r are the collection efficiency, disk current and ring current, respectively. A value of 0.48 was used for N, in keeping with a previous work [14].

(3)　　Physical characterizations

X-ray photoelectron spectroscopy (XPS; Axis Ultra, Kratos Analytical Co.) was conducted using monochromatic Al Kα X-rays. Transmission electron microscopy (TEM; ARM-200F, JEOL) was used to observe morphological structures. Solid-state CP/MAS ^{13}C NMR and FT-IR spectra were acquired using a JNM-ECA500 500 MHz spectrometer (JEOL) and a Cary 600 series spectrometer (Agilent Technologies), respectively. High-resolution transmission electron microscopy (TEM) and energy-dispersive X-ray (EDX) analysis were performed using a spherical aberration-corrected TEM system (JEOL ARM-200F). A powder X-ray diffraction (XRD) pattern was recorded on a PANalytical

X'Pert PRO diffractometer with Cu Kα radiation. The N$_2$ adsorption-desorption isotherm was obtained by a Micromeritics 3 Flex at 77K.

(4)   X-ray absorption spectroscopy (XAS) analysis

Cu K edge X-ray absorption fine structure (XAFS) spectra were acquired using the BL01B1 beamline at SPring-8 at the Japan Synchrotron Radiation Research Institute (JASRI), employing a double-crystal Si (111) monochromator to obtain XAS data. During XAFS analyses, the energy levels were calibrated by setting the first peak maximum in the Cu foil spectrum equal to 8980.3 eV. All X-ray adsorption near-edge structure (XANES) and Extended X-ray absorption fine structure (EXAFS) spectra were analyzed using the ATHENA software package (further details concerning XAS are provided below) [15]. The peak maxima of reference samples [16] were compared with results in this work by replotting the literature data using the spectrum of Cu foil as a standard.

(5)   *In situ* XAFS analysis

The electrode used for *in situ* XAFS measurements was prepared by modifying carbon paper (Panasonic Corp.) with the same catalyst ink used for the electrochemical characterization. The electrochemical cells and the experimental *in situ* XAFS set up were the same as previously reported [17], and involved using a carbon paper electrode. All experimental trials were conducted in a PBS (pH 7) under an argon (Ar) atmosphere, while applying a constant potential to the system. *In situ* XAFS data were also acquired at the SPring-8 BL01B1 beamline, using a 19-element germanium solid-state detector (SSD) in the fluorescent mode at room temperature.

Results and Discussion

Initially, the E_{Cu} values and ORR activities of these Cu-S complexes were investigated in argon (Ar)-purged or O_2-saturated phosphate buffer solution (PBS; pH 7), respectively. Cu-S complexes in this study were hybridized with carbon nanoparticle (CPs; Ketjen Black EC600JD, detail see Experimental Section). The cyclic voltammetry (CV) plots acquired in an Ar-purged PBS are shown in Fig. 2, and the redox potentials of the Cu-S complexes synthesized in this report are summarized along with the potentials reported for Cu-N complexes in Table 1. These results confirm that the E_{Cu} values of the Cu-S complexes (Cu-ane-S_4/CP: 0.88 V, Cu-dmc/CP: 0.92 V, on the RHE scale) were 300–500 mV higher than those of conventional Cu-N complexes [1−4]. The ORR activities of these Cu-S compounds are presented in Fig. 3. The ORR onset potentials of these complexes (0.58 V and 0.62 V for Cu-ane-S_4/CP and Cu-dmc/CP, respectively) were similar to that of bare CPs (0.62 V), indicating that the Cu-S complexes had almost no ORR activity.
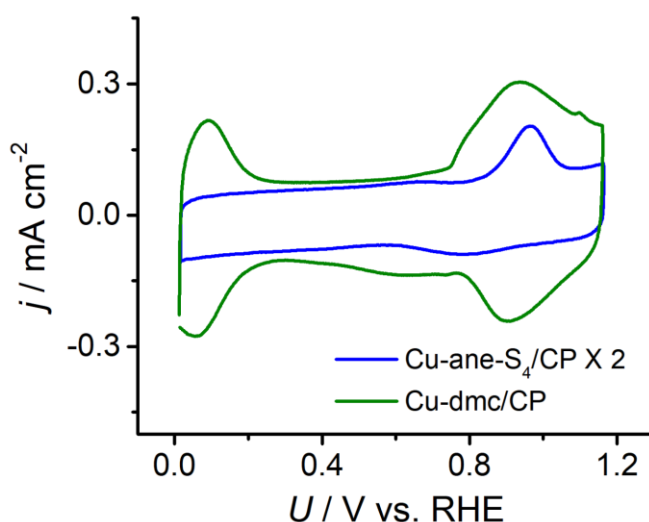
Fig. 2 *j-U* curves under argon for Cu-ane-S4/CP (blue), Cu-dmc/CP (green) in phosphate buffer solution (pH 7). Scan rate=10 mV s^{-1}. Rotational speed=1500 rpm.

Table 1 E_{Cu} and U_{onset} values of Cu-S compounds as obtained in the present study and as reported for conventional Cu-N complexes in neutral solutions. All values are on the RHE scale.

	Cu(II/I)	U_{Onset}	References
[Cu(baEtO)(Im)](ClO$_4$)$_2$ (pH 7)	0.42	0.57	Ref. [18]
[Cu(TPA)](ClO$_4$)$_2$ (pH 7)	0.23	0.69	Ref. [19]
[Cu(PMEA)](ClO$_4$)$_2$ (pH 7)	0.37	0.69	Ref. [4]
[Cu(PMAP)](ClO$_4$)$_2$ (pH 7)	0.42	0.69	Ref. [19]
[Cu(TEPA)](ClO$_4$)$_2$ (pH 7)	0.52	0.69	Ref. [4]
Cu with hexaaza-xylyl macrocycle (pH 7.3)	0.58	0.68	Ref. [20]
Cu-CTF/CP	0.57	0.81	Section 2 in this Chapter
Cu^{II}-tmpa	0.27	0.61	Ref. [21]
Cu^{II}-bmpa	0.36	0.61	Ref. [21]
Cu^{II}-tepa	0.78	0.61	Ref. [21]
Cu-S-CTF/CP	0.82	0.88	This study
S-CTF/CP	-	0.55	This study
Cu-ane-S$_4$/CP	0.88	0.58	This study
Cu-dmc/CP	0.92	0.62	This study
CP	-	0.62	This study
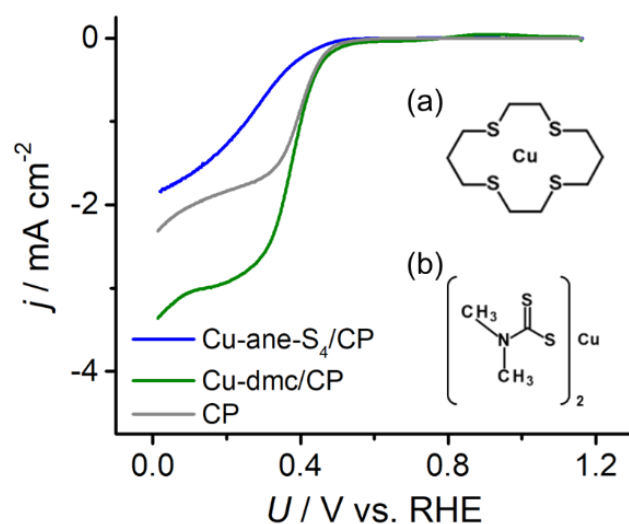
Fig. 3 Current density (j) versus potential (U) curves obtained under O_2 for Cu-ane-S_4/CP (blue), Cu-dmc/CP (green) and CPs (gray) in a PBS (pH 7). Scan rate=10 mV s^{-1}, rotational rate=1500 rpm. Insets show the structural formula of (a) Cu-ane-S4 and (b) Cu-dmc.

The electronic states of the Cu centers in the Cu-S compounds were also examined using X-ray techniques and electrochemical characterization. X-ray photoelectron spectroscopy (XPS) narrow scans in the Cu 2p region and X-ray adsorption near-edge structure (XANES) spectral analysis were used to determine the oxidation states of the Cu atoms. The Cu 2p$_{3/2}$ XPS peaks generated by both complexes at 933.3 eV can be assigned to the Cu(0) or Cu(I) oxidation states [22] (Fig. 4). The Cu K-edge XANES spectra for Cu metal, Cu$_2$O, CuO and the as-prepared Cu-S compounds are shown in Fig. 5. Here, the absorption edges of the Cu-S compounds at 8982 eV match that of the Cu$_2$O. Taken together, the XANES and XPS results indicate that the Cu(I) oxidation state was dominant in the as-prepared Cu-S compounds.
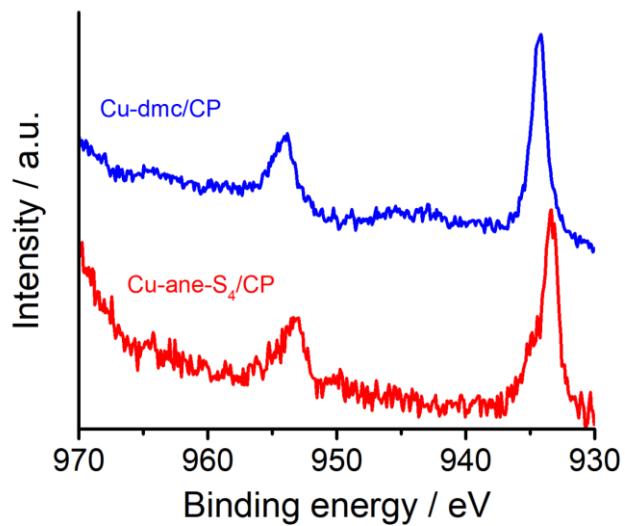
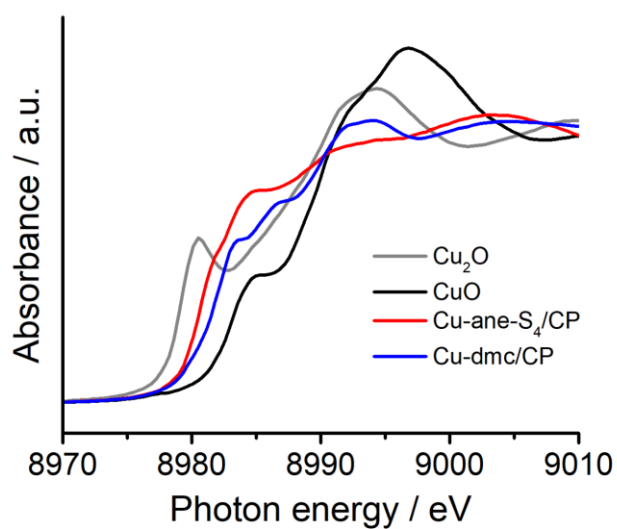**Fig. 4** The Cu 2p XPS spectra of the Cu-S complexes.

Fig. 5 The XANES spectra of Cu-ane-S$_4$/CP (red) and Cu-dmc/CP (blue)

The author subsequently attempted to identify the coordination geometry required for ORR activity, based on considering the O_2 binding at metal sites. Solomon et al. previously demonstrated the relationship between the peak maximum position in the K edge XANES spectrum of Cu(I) and the coordination geometry [16,23]. Fig. 6a shows the Cu K edge XANES spectra of the synthesized Cu-S compounds. The Cu-ane-S_4/CP, which is reported to have a distorted tetrahedral configuration [6,11] generated a peak maximum at 8984.5 eV with an amplitude of 0.77, while the Cu-dme/CP peak maximum appeared at 8983.6 with an amplitude of 0.60. The coordination geometries of these Cu-S compounds were elucidated by plotting peak heights and positions in the Cu K edge XANES spectra along with reference data from a previous report [16], as shown in Fig. 6b and Table 2. These results clearly indicate that the coordination geometries of the synthesized Cu-S complexes resemble a distorted four-coordinated tetrahedral structure. Therefore, it was verified that Cu-complexes having high redox potentials tend to form closed tetrahedral configurations and exhibit no ORR catalytic activity due to a lack of O_2 binding sites.

Having demonstrated the existence of a problematic trade-off relationship between a high redox potential and oxygen-binding ability, the author next attempted to overcome this issue. The author focused on S-linked covalent triazine frameworks (S-CTFs) as supports for Cu sites, because these were considered to represent promising candidates satisfying both requirements. CTFs, which are cross-linked conjugated polymers, possess abundant heteroatoms with lone electron pairs [12,24–29]. Thus, various metals can be loaded onto CTFs via coordination bonds with these heteroatoms, which include N, O and S [28–33]. In addition, because the rigid framework of a CTF is likely to be maintained following modification with metals or changes in the redox state of the metal, they are may stabilize Cu(I) sites having an open coordination state and thus promote oxygen binding (Fig. 1c).
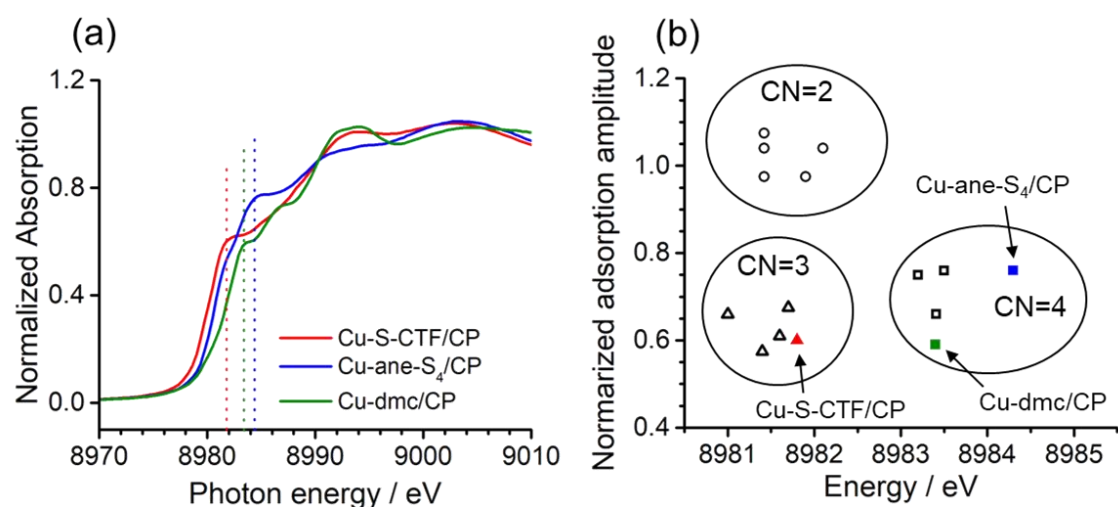
Fig. 6 (a) XANES spectra of Cu-S-CTF/CP (red), Cu-and-S$_4$/CP (blue) and Cu-dmc/CP (green), in which vertical colored lines indicate the energy values for the peak maxima, and (b) a graphic summary of the peak top maxima of the Cu(I) compounds synthesized in this study (Cu-S-CTF/CP [red], Cu-ane-S$_4$/CP [blue] and Cu-dmc/CP [green]) as well as data from the literature [16]. Empty symbols indicate literature data and circles, triangles and squares indicate two-, three- and four-coordinated Cu(I) complexes, respectively. CN = coordination number.

Table 2 Reference peak maxima positions and maxima for the Cu-S complexes in the present study.

|	Energy (eV)	Normalized adsorption amplitude	
CN = 2	8981.5 ~ 8981.9	0.98 ~ 1.04	Ref. [16]
CN = 3	8981.0 ~ 8981.7	0.58 ~ 0.68	Ref. [16]
CN = 4	8983.2 ~ 8983.5	0.66 ~ 0.76	Ref. [16]
Cu-S-CTF/CP	8981.8	0.60	This work
Cu-ane-S$_4$/CP	8984.3	0.76	This work
Cu-dmc/CP	8983.4	0.59	This work

A S-linked CTF with CPs (S-CTF/CP) was polymerized by the nucleophilic substitution of cyanuric chloride (CC) with thiocyanuric acid (TC) on electroconductive CPs in the similar manner in Section 2 in this chapter and previous reports [13,34,35], using a previously reported method with minor modifications [12] (for details see Scheme 1, Figs. 7–10 and their captions). The resulting polymer was impregnated with $CuCl_2$ in an aqueous solution which is the same method as the previous section to obtain Cu-modified S-CTF/CP (Cu-S-CTF/CP, BET surface area was 188.4 m^2/g as shown in Fig. 11). High-resolution transmission electron microscopy (TEM) analyses demonstrated the absence of metal nanoparticles (>1 nm) on the Cu-S-CTF/CP (Fig. 12a). In addition, the energy dispersive X-ray (EDX) maps show that the S, N and Cu atoms were homogeneously distributed throughout the sample (Fig. 12b). Observations using TEM (Fig. 12), XPS and ICP-AES analyses (Table 3) confirmed that the CPs were almost completely covered with the S-CTF, and that the Cu atoms were well-dispersed throughout the S-CTF/CP. The author also confirmed that the Cu centers in the Cu-S-CTF were in the Cu(I) state, based on XPS (Fig. 13a) and XANES spectra (Fig. 13b).
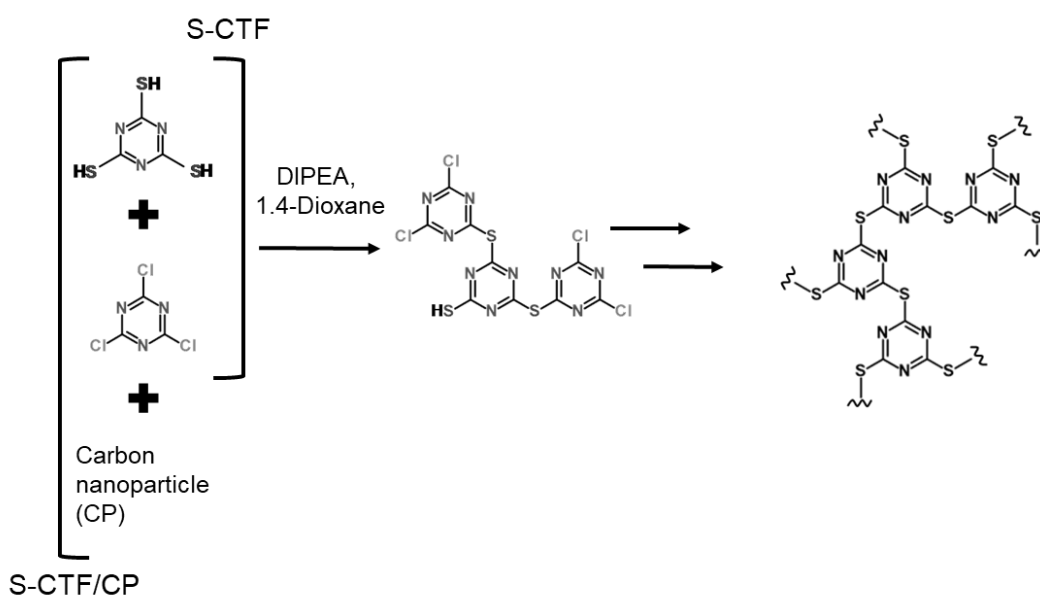
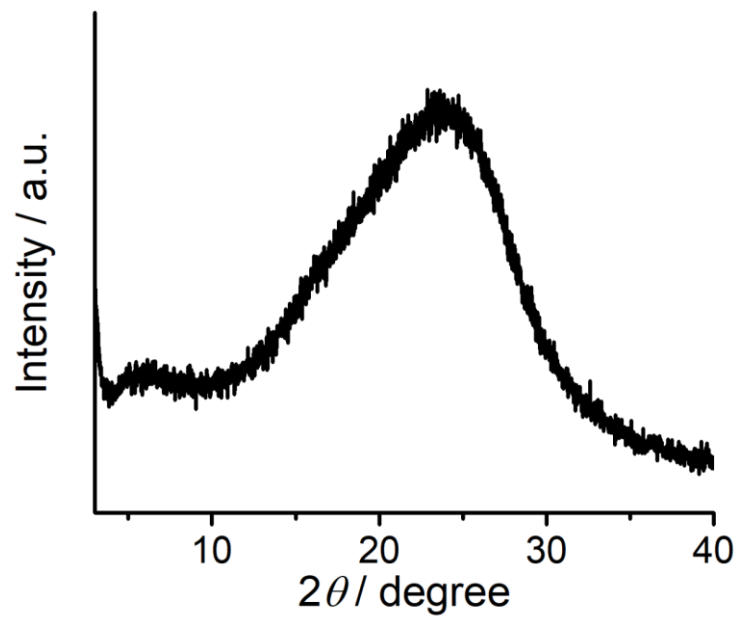**Scheme 1** Procedure for the synthesis of S-CTF and S-CTF/CP.
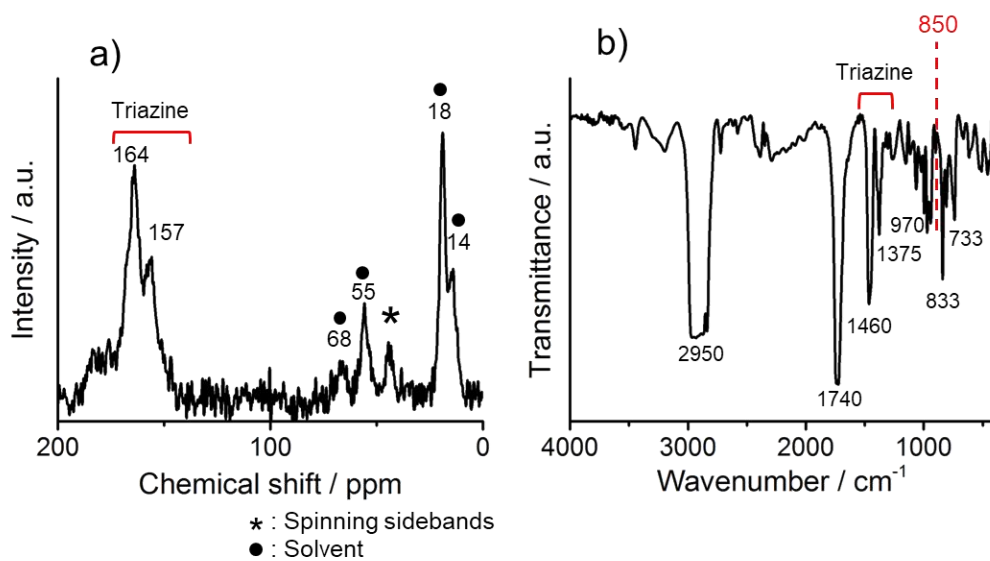
Fig. 7 (a) Solid-state ^{13}C-NMR CP/MAS spectrum and (b) FT-IR spectrum of S-CTF.
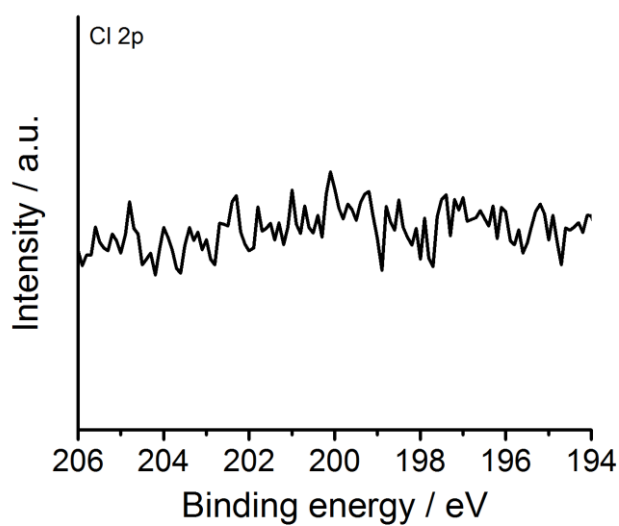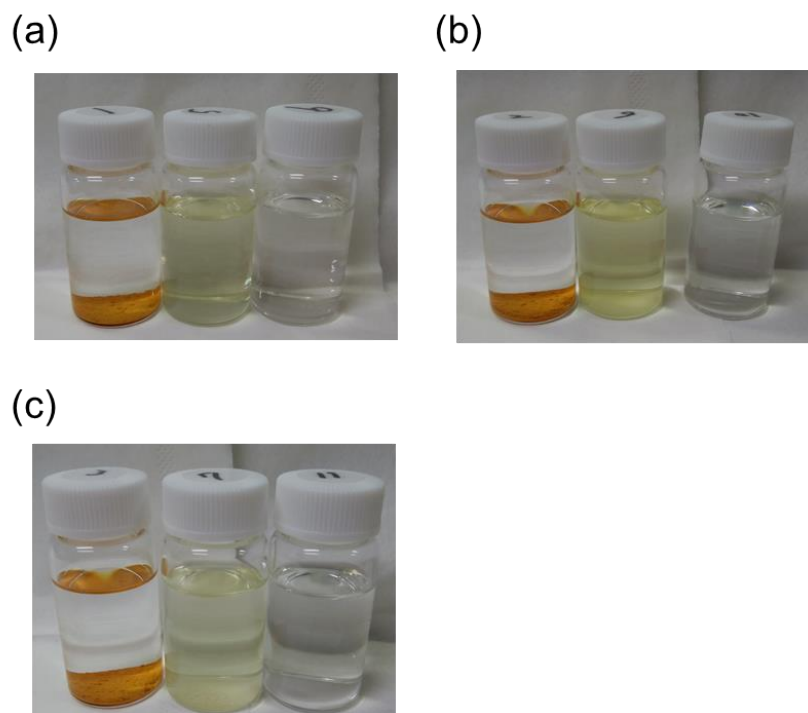

Fig. 8 The Cl 2p XPS spectrum of S-CTF.

Fig. 9 XRD pattern of S-CTF

Fig. 10 Solubility test of S-CTF and monomers in organic solutions ((a) 1.4-dioxane, (b) acetone and (c) ethanol, immersion time;43 h). S-CTF (orange sample at the left) was insoluble in these organic solvents, whereas TCA (yellow solution at the center) and CC (transparent solution at the right) were soluble to these solvents.

Note:

The S-CTF polymer framework (without CPs) was characterized using solid-state ^{13}C NMR, FT-IR and XPS. In the CP-MAS ^{13}C NMR spectrum of S-CTF, the main peak corresponding to the triazine rings appears at 164 ppm (Fig. 7a). In addition, the shoulder at 157 ppm is assigned to the terminal carbons of triazine rings attached to OH or SH groups. These results show that the triazine rings were maintained intact during the polymerization reaction. The FT-IR spectrum (Fig. 7b) exhibits several strong bands between 1200 and 1600 cm^{-1} that are attributed to the heterocyclic CN ring [12]. However, a C-Cl stretching peak is not present at 850 cm^{-1} [12]. Furthermore, the XPS spectrum does not contain a Cl 2p peak at 198 eV after polymerization (Fig. 8), indicating that Cl did not maintain in the S-CTF. The author confirmed that S-CTF was not dissolved in any organic solvents including 1,4-dioxane, acetone and ethanol (Fig. 10), whereas the monomers were easily soluble in these solvents. Taken together, these results indicate that no decomposition of triazine rings occurred and that polymerization of S-CTF proceeded through the nucleophilic substitution of all three chlorine atoms on the CC by the CTF thiol groups, as illustrated in Scheme 1. An X-ray diffraction patter of S-CTF showed one broad peak, suggesting that S-CTF has low crystallinity (Fig. 9).
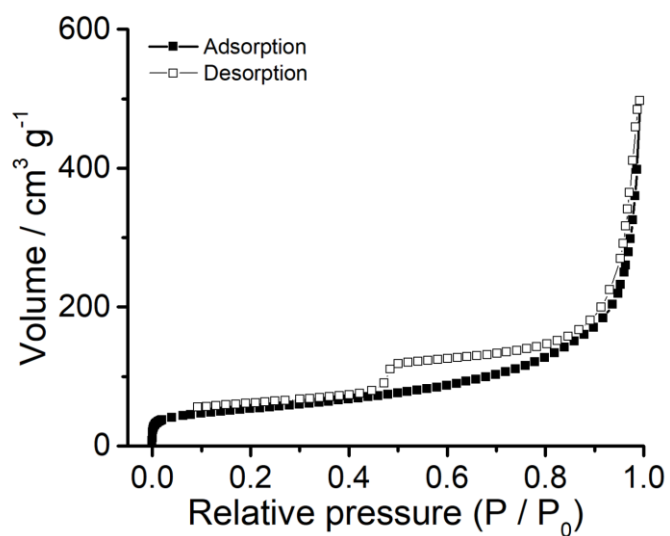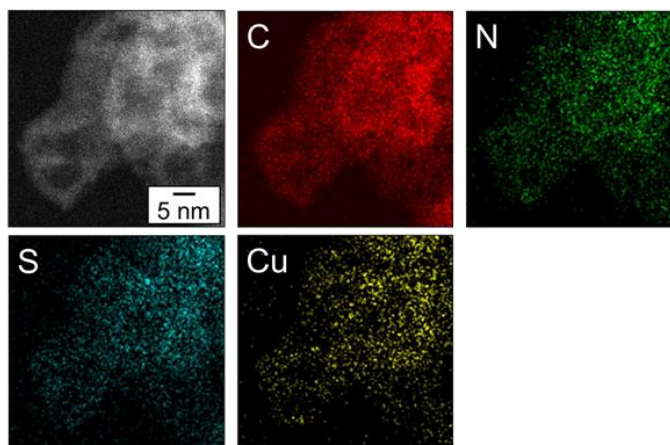
Fig. 11 Nitrogen adsorption-desorption isotherms for Cu-S-CTF/CP. Closed marks show adsorption line and open marks show desorption (BET surface area: 188.4 m^2/g).

a) BF-STEM and HAADF-STEM
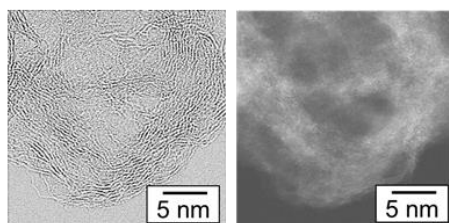
b) EDX

Fig. 12 (a) Bright-field scanning TEM (BF-STEM) and high-angle annular dark field scanning TEM (HAADF-STEM) images and (b) EDX maps of Cu-S-CTF/CP.

**Table 3** Elemental analyses of Cu-S-CTF/CP and S-CTF/CP.

	Cu-S-CTF/CP	S-CTF/CP
N/C (XPS)	0.148	0.123
S/C (XPS)	0.026	0.025

|	Weight %	
Cu (ICP)	6.25	-

Note:

Cu, S and N atoms were clearly detected in the Cu-S-CTF/CP, although no Cu species were found on bare CPs modified with a $CuCl_2$ solution in a similar manner to the Cu-S-CTF/CP as shown in Section 2 in this chapter. The author also checked the Cu content of Cu-S-CTF/CP and precursor $CuCl_2$ solution and confirmed that not all Cu ions in Cu solution were coordinated by S-CTF/CP, suggesting that S-CTF cannot coordinate Cu ions any more.
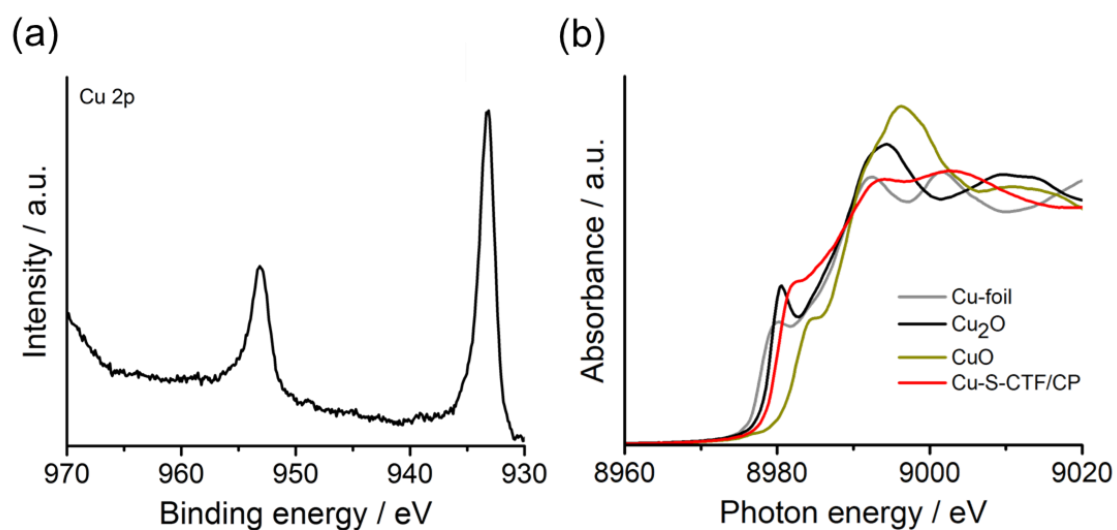

Fig. 13 (a) The Cu 2p XPS spectrum of Cu-S-CTF/CP and (b) XANES spectra of Cu-foil, Cu_2O, CuO and Cu-S-CTF/CP.

The author first evaluated the E_{Cu} potential of the Cu-S-CTF/CP using CV, and Fig. 14a shows the *j-U* curves obtained from Cu-S-CTF/CP and S-CTF/CP in an Ar-purged PBS (pH 7). Although no redox peaks were generated by the S-CTF/CP, a single pair of redox peaks with a mid-point potential of 0.82 V was obtained from the Cu-S-CTF/CP. Electrochemical *in situ* X-ray absorption fine structure (XAFS) measurements demonstrated that these peaks can be ascribed to the Cu(II)/Cu(I) redox couple (Fig. 15 and its footnote). The Cu(II)/Cu(I) potential for Cu-S-CTF/CP was found to be much higher than values reported for several organometallic Cu-N complexes in neutral solution (Table 1), similar to the results for synthetic and previously reported Cu-S complexes.
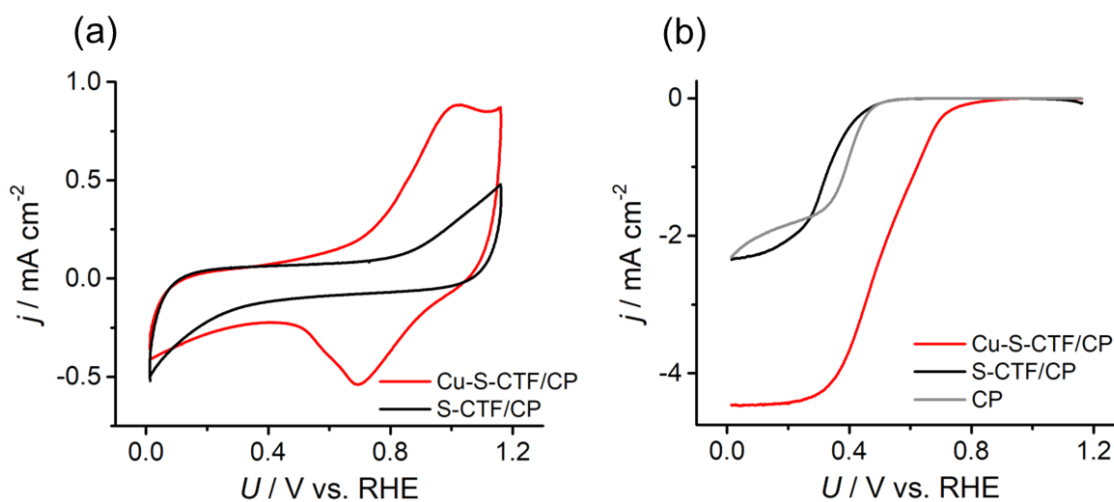
Fig. 14 *j - U* curves under argon (a) and oxygen (b) in phosphate buffer solution (pH 7) for Cu-S-CTF/CP (red), S-CTF/CP (black) and bare CP (gray). Scan rate = 10 mV s^{-1}. Rotational speed = 1500 rpm.
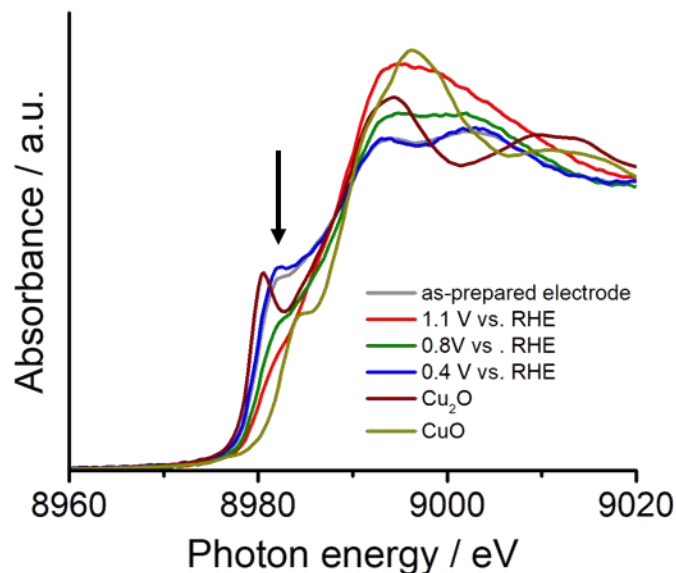
**Fig. 15** In-situ XANES spectra of Cu-S-CTF/CP

Note:

In-situ XANES spectra of the as-prepared electrode (an electrode without an applied potential, gray), electrode at 1.1 V vs. RHE (higher potential than a couple of redox peaks of the CVs in Fig. 14a, red), 0.8 V vs. RHE (middle point of the redox peaks, green) and 0.4 V vs. RHE (lower potential than a couple of the redox peaks, blue). For the as-prepared electrode and electrode measured at 0.4 V, a characteristic peak top was observed around 8982 eV (black arrow). These two spectra were similar to that of Cu_2O, indicating that Cu species exist as Cu(I) in a lower potential region than the redox peaks. The height of the peak top of Cu(I) was reduced as the applied potential increased. The XANES spectra of Cu-S-CTF/CP shifted to a higher energy region as the applied potential increased. At 1.1 V vs. RHE, which is a higher value than the redox peaks of Cu-S-CTF/CP, the characteristic peak of Cu(I) disappeared. These results indicated that the Cu(I) species in Cu-S-CTF/CP were oxidized to Cu(II) in response to the applied potential, which is consistent with the observed redox behavior of Cu species in the CVs (Fig. 14a). Therefore, the result shown in this figure confirm that the pair of redox peaks in Fig. 14 correspond to the redox couple of Cu(II)/Cu(I).

90

The coordination geometry of the Cu center in Cu-S-CTF/CP was also investigated, to determine the presence of oxygen-binding sites, using XAFS. Cu K edge Extended X-ray absorption fine structure (EXAFS) analysis was initially carried out to determine neighboring atoms in the Cu-S-CTF/CP. The Fourier transformations of k^3-weighted EXAFS oscillations for Cu-S-CTF/CP are shown in Fig. 16. The EXAFS results before Fourier transformation (FT) and Inverse FT-EXAFS of Cu-TPP and Cu-S-CTF/CP are shown in Fig. 17. The Cu-N peak of Cu-TPP and the Cu-S peak of Cu-ane-S_4/CP were located at 1.6 and 1.9 Å, respectively (Fig. 18). In the case of the Cu-S-CTF/CP, a peak was also observed at 1.6 Å and was much broader than the Cu-N and Cu-S peaks. Considering the molecular structure of S-CTF, the broader peak generated by the Cu-S-CTF/CP at 1.6 Å is likely assignable to an overlap of the Cu-N and Cu-S peaks. In contrast, peaks corresponding to Cu-Cu bonds (2.2 Å) and Cu-O-Cu bonds (2.7 Å) [36] were not detected. Taken together, the TEM, EXAFS and electrochemical characterization (i.e. high redox potential) data indicate that the Cu ions in Cu-S-CTF/CP were individually isolated and had a first coordination sphere containing S and N atoms (Fig. 1c). The coordination geometry of Cu-S-CTF/CP was also assessed, using XANES data. The Cu-S-CTF/CP produced peak maxima at lower energy values than those generated by synthesized four-coordinated tetrahedral complexes (Fig. 6a). In particular, the Cu-S-CTF/CP showed a peak maximum at 8982.1 eV together with an amplitude of 0.61. This result clearly indicates that the coordination geometry of this compound resembles a distorted three-coordinated structure (Fig. 6b).
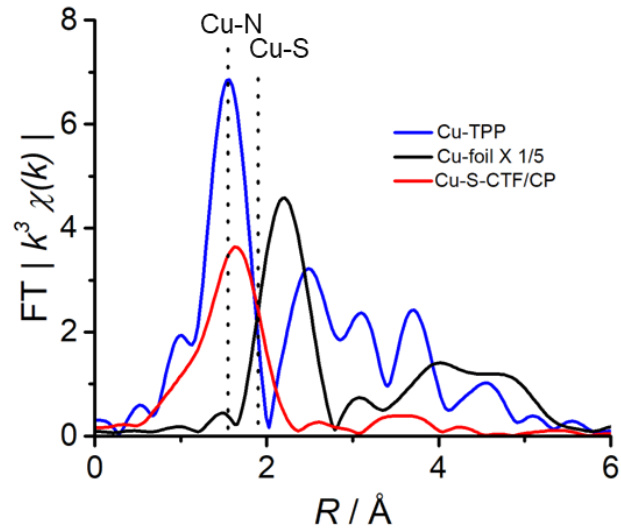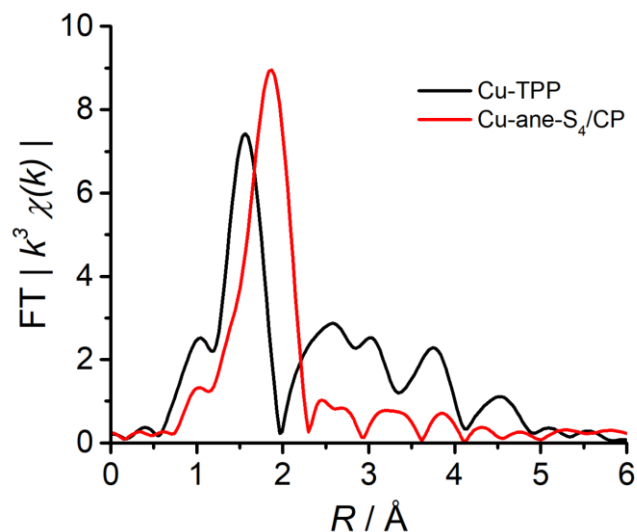
Fig. 16 Fourier transform of EXAFS of Cu-TPP, Cu-foil and Cu-S-CTF/CP
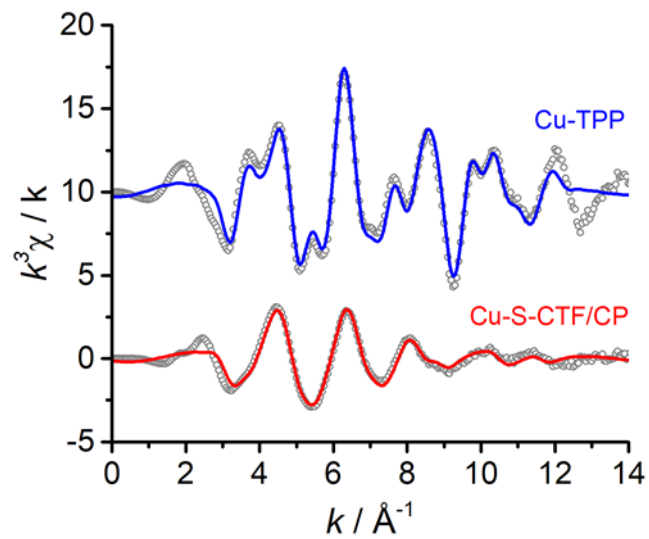
Fig. 17 k^3-weighted EXAFS oscillation (gray dots) for Cu-TPP (upper part) and Cu-S-CTF/CP (bottom part); solid colored lines show the Inverse Fourier Transform of FT-EXAFS result in Fig. 16 for Cu-TPP (blue) and Cu-S-CTF/CP (red). k: 3–12 Å^{-1}, R: 1–6.

Fig. 18 The k^3-weighted Fourier transforms of the Cu K-edge EXAFS spectra for Cu-TPP and Cu-ane-S_4/CP.

Because it was confirmed that the Cu center in Cu-S-CTF possesses both a high redox potential and oxygen-binding sites, the author subsequently evaluated and compared the electrocatalytic ORR activities of Cu-S-CTF/CP and S-CTF/CP (Fig. 14b). In the presence of O_2, the Cu-S-CTF/CP clearly generated an ORR current from 0.88 V, whereas the ORR onset potential for the S-CTF/CP was 0.55 V. In addition, the ORR current was generated close to the potential at which Cu(II) is reduced to Cu(I), indicating that the Cu(I) species in the Cu-S-CTF/CP mediated the ORR. Notably, the ORR activity of the Cu-S-CTF/CP (E_{onset} = 0.88 V) was over 70 mV higher than that of several recently-reported Cu-based ORR catalysts [4], including Cu-3,5-diamino-1,2,4-triazole [37], Cu-tris(2-pyridyl-methyl) amine [19] and Cu-N-doped graphene [38]. Notably, this ORR over-potentials is lower than Cu-CTF in section 2 in this chapter. The amperometric responses of the Pt ring electrodes in the rotating ring-disk electrodes (RRDE) system were also monitored to detect peroxide species formed at the disk electrode. The reaction electron number was close to four in each potential

region examined, demonstrating that the majority of O_2 molecules were reduced to water (Fig. 19). As for the stability test, the slight decrease of the ORR activity was observed after 500 and 3000 CV cycles (for detail, see Fig. 20). In addition, the onset potential for ORR on Cu-S-CTF/CP is 0.41 V and 0.89 V vs. RHE in acidic and alkaline conditions, respectively (Fig. 21). The pH dependence of the ORR activity for a catalyst developed in this study is basically consistent with the reported trend for Cu based ORR electrocatalysts [4]. As variable types of CTFs can be synthesized, further enhancement of ORR activity and stability can be accomplished by the sophisticated choice of monomers and synthesis method.
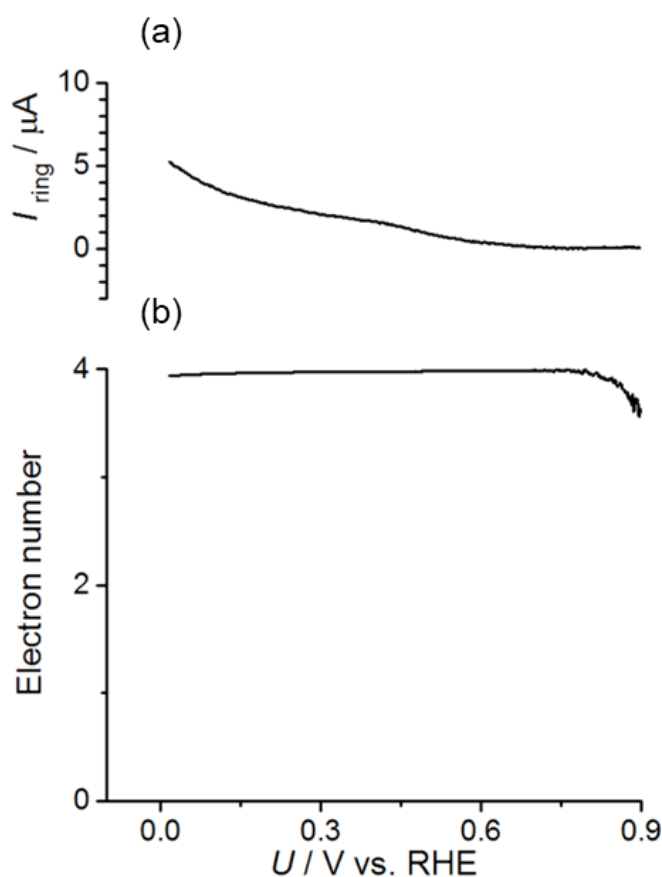
Fig. 19 Rotating ring-disk electrodes (RRDE) data for Cu-S-CTF/CP: (a) the ring current and (b) the electron quantity for Cu-S-CTF/CP in the presence of oxygen (the disk current is shown in Fig. 14b). Scan rate = 10 mV s^{-1}, rotational rate = 1500 rpm.
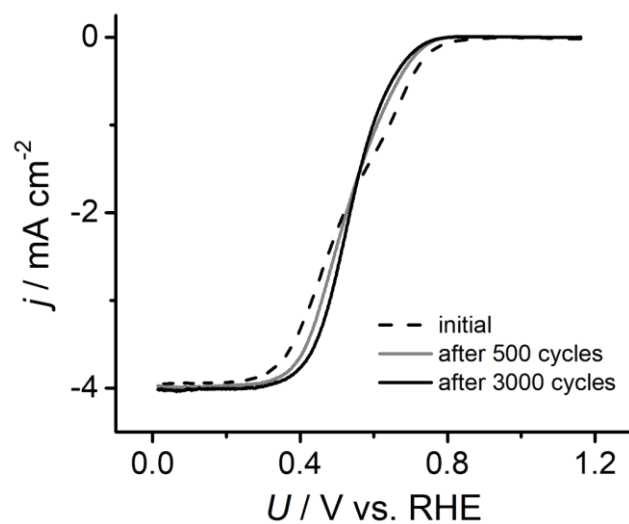
Fig. 20 *j* vs. *U* curves plots of Cu-S-CTF/CP for initial (black dotted line), after 500 CV cycles (gray line) and 3000 CV cycles (black solid line) saturated with dissolved oxygen.
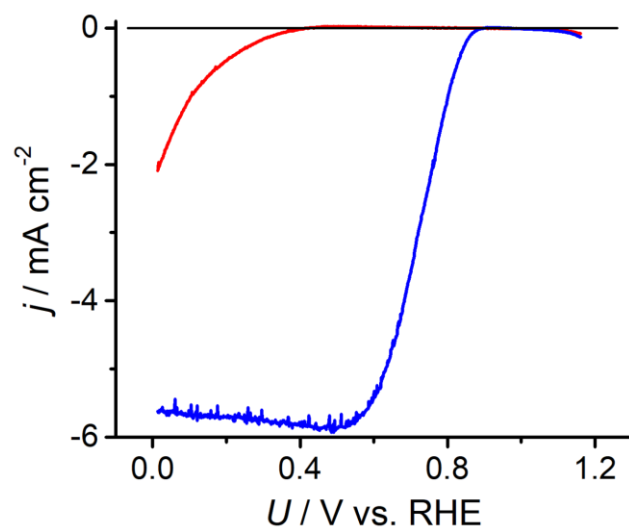
Fig. 21 *j* vs. *U* curves for Cu-S-CTF/CP in oxygen saturated 0.1 M KOH (pH 13, blue) and 0.1 M HClO$_4$ (pH 1 red). Scan rate, 10 mV s^{-1}. Rotational speed, 1500 rpm.

Conclusions

In conclusion, this work has demonstrated that there is a problematic trade-off relationship between high redox potential and suitable oxygen-binding ability in Cu-based ORR electrocatalysts. In particular, based on the HSAB theory, Cu atoms coordinated with S exhibit high redox potential and exist as Cu(I) due to autoreduction. However, Cu(I) atoms prefer a closed tetrahedral configuration, which lacks oxygen adsorption sites and thus shows little ORR activity. To break this trade-off based on the redox potential dependency of the coordination geometry of Cu sites, the author newly synthesized a Cu-modified S-linked conjugated polymer. The onset potential of this Cu-S-CTF for the ORR was found to be the highest yet reported for a synthetic Cu-based ORR catalyst. The rigid cross-linked network of the S-CTF maintained the oxygen adsorption sites and ORR activity of the Cu sites, such that the Cu atoms continued to exhibit high redox potential and remained in the Cu(I) oxidation state. Using this novel synthesis approach, the author was able to independently modulate the electronic properties and coordination geometry of Cu atoms using a S-linked conjugated polymer to increase the redox potential and number of oxygen binding sites of the resulting electrocatalyst. The author anticipates that this metal-modified CTF approach has the potential to serve as a novel platform for heterogeneous coordination compounds and will allow for the modulation of the electronic properties and coordination geometries of metal catalytic centers.

References

[1]   V. L. N. Dias, E. N. Fernandes, L. M. S. da Silva, E. P. Marques, J. J. Zhang, A. L. B. Marques, *J. Power Sources* **2005**, *142*, 10-17.

[2]   M. A. Thorseth, C. S. Letko, E. C. M. Tse, T. B. Rauchfuss, A. A. Gewirth, *Inorg. Chem.* **2013**, *52*, 628-634.

[3]   C. C. L. McCrory, X. Ottenwaelder, T. D. P. Stack, C. E. D. Chidsey, *J. Phys. Chem. A* **2007**, *111*, 12641-12650.

[4]   M. A. Thorseth, C. E. Tornow, E. C. M. Tse, A. A. Gewirth, *Coord. Chem. Rev.* **2013**, *257*, 130-139.

[5]   M. R. Malachowski, M. Adams, N. Elia, A. L. Rheingold, R. S. Kelly, *J. Chem. Soc. Dalton Trans.* **1999**, 2177-2182.

[6]   M. M. Bernardo, M. J. Heeg, R. R. Schroeder, L. A. Ochrymowycz, D. B. Rorabacher, *Inorg. Chem.* **1992**, *31*, 191-198.

[7]   U. Sakaguchi, A. W. Addison, *J. Chem. Soc. Dalton Trans.* **1979**, 600-608.

[8]   T. Sakurai, K. Kataoka, *Cell. Mol. Life Sci.* **2007**, *64*, 2642-2656.

[9]   S. Kitagawa, M. Munakata, A. Higashie, *Inor. Chim. A-Art. Lett.* **1984**, *84*, 79-84.

[10]   J. J. Zhang, F. C. Anson, *J. Electroanal. Chem.* **1993**, *348*, 81-97.

[11]   E. R. Dockal, L. L. Diaddario, M. D. Glick, D. B. Rorabacher, *J. Am. Chem. Soc.* **1977**, *99*, 4530-4532.

[12]   H. A. Patel, F. Karadas, J. Byun, J. Park, E. Deniz, A. Canlier, Y. Jung, M. Atilhan, C. T. Yavuz, *Adv. Funct. Mater.* **2013**, *23*, 2270-2276.

[13]   T. Yoshioka, K. Iwase, S. Nakanishi, K. Hashimoto, K. Kamiya, *J. Phys. Che. C* **2016**, *120*, 15729-15734.

[14]   K. Kamiya, H. Koshikawa, H. Kiuchi, Y. Harada, M. Oshima, K. Hashimoto, S. Nakanishi, *Chemelectrochem* **2014**, *1*, 877-884.

[15]   B. Ravel, M. Newville, *J. Synchrotron Radiat.* **2005**, *12*, 537-541.

[16]   L. S. Kau, D. J. Spirasolomon, J. E. Pennerhahn, K. O. Hodgson, E. I. Solomon, *J. Am. Chem. Soc.* **1987**, *109*, 6433-6442.

[17]   M. Kato, K. Kimijima, M. Shibata, H. Notsu, K. Ogino, K. Inokuma, N. Ohta, H. Uehara, Y. Uemura, N. Oyaizu, T. Ohba, S. Takakusagi, K. Asakura, I. Yagi, *Phys. Chem. Chem. Phys.* **2015**, *17*, 8638-8641.

[18]   M. Wang, X. Xu, J. Gao, N. Jia, Y. Cheng, *Russ. J. Electrochem.* **2006**, *42*, 878-881.

[19]   M. A. Thorseth, C. S. Letko, T. B. Rauchfuss, A. A. Gewirth, *Inorg. Chem.* **2011**, *50*, 6158-6162.

[20]   K. Slowinski, Z. Kublik, R. Bilewicz, M. Pietraszkiewicz, *J. Chem. Soc. Chem. Commun.* **1994**, 1087-1088.

[21]   M. Asahi, S. Yamazaki, S. Itoh, T. Ioroi, *Dalton Trans.* **2014**, *43*, 10705-10709.

[22]   J. P. Espinos, J. Morales, A. Barranco, A. Caballero, J. P. Holgado, A. R. Gonzalez-Elipe, *J. Phys. Chem. B* **2002**, *106*, 6921-6929.

[23]   R. E. Cowley, J. Cirera, M. F. Qayyum, D. Rokhsana, B. Hedman, K. O. Hodgson, D. M. Dooley, E. I. Solomon, *J. Am. Chem. Soc.* **2016**, *138*, 13219-13229.

[24]   X. Feng, X. S. Ding, D. L. Jiang, *Chem. Soc. Rev.* **2012**, *41*, 6010-6022.

[25]   P. Kuhn, M. Antonietti, A. Thomas, *Angew. Chem. Int. Ed.* **2008**, *47*, 3450-3453.

[26]   K. Sakaushi, M. Antonietti, *Bull. Chem. Soc. Jpn.* **2015**, *88*, 386-398.

[27]   A. Karmakar, A. Kumar, A. K. Chaudhari, P. Samanta, A. V. Desai, R. Krishna, S. K. Ghosh, *Chem. Eur. J.* **2016**, *22*, 4931-4937.

[28]   S. Rajendiran, K. Park, K. Lee, S. Yoon, *Inorg. Chem.* **2017**, *56*, 7270-7277.

[29]   L. Hao, S. S. Zhang, R. J. Liu, J. Ning, G. J. Zhang, L. J. Zhi, *Adv. Mater.* **2015**, *27*, 3190-3195.

[30]   J. Artz, S. Mallmann, R. Palkovits, *ChemSusChem* **2015**, *8*, 672-679.

[31]   C. E. Chan-Thaw, A. Villa, D. Wang, V. Dal Santo, A. O. Biroli, G. M. Veith, A. Thomas, L. Prati, *Chemcatchem* **2015**, *7*, 2149-2154.

[32]   R. Palkovits, M. Antonietti, P. Kuhn, A. Thomas, F. Schuth, *Angew. Chem. Int. Ed.* **2009**, *48*, 6909-6912.

[33]   J. Roeser, K. Kailasam, A. Thomas, *ChemSusChem* **2012**, *5*, 1793-1799.

[34]   R. Kamai, K. Kamiya, K. Hashimoto, S. Nakanishi, *Angew. Chem. Int. Ed.* **2016**, *55*, 13184-13188.

[35]   K. Kamiya, R. Kamai, K. Hashimoto, S. Nakanishi, *Nat. Commun.* **2014**, *5*, 5040.

[36]   H. Irie, K. Kamiya, T. Shibanuma, S. Miura, D. A. Tryk, T. Yokoyama, K. Hashimoto, *J. Phys. Chem. C* **2009**, *113*, 10761-10766.

[37]   M. S. Thorum, J. Yadav, A. A. Gewirth, *Angew. Chem. Int. Ed.* **2009**, *48*, 165-167.

[38]   H. Koshikawa, S. Nakanishi, K. Hashimoto, K. Kamiya, *Electrochim. Acta* **2015**, *180*, 173-177.

Chapter 3

Copper-modified covalent triazine frameworks as electrocatalysts for reduction of nitrobenzene to aniline in aqueous solutions

In chapter 2, it is demonstrated that Cu modified covalent triazine framework (Cu-CTF) can function as a non-noble metal electrocatalyst for oxygen reduction reaction. In this chapter, Cu-CTF was developed as a selective electrocatalyst of nitrobenzene reduction to aniline in neutral aqueous solutions. Notably, a faradaic efficiency reached up to 65% at −0.6V versus Ag/AgCl. Electrochemical characterization indicated that the organic framework part of Cu-CTF reduced nitrobenzene to phenylhydroxylamine, followed by the reduction of phenylhydroxylamine to aniline at single Cu sites. This is the first example of a cooperative electrocatalytic reaction at metal centers and at the framework with a metal-modified CTF.
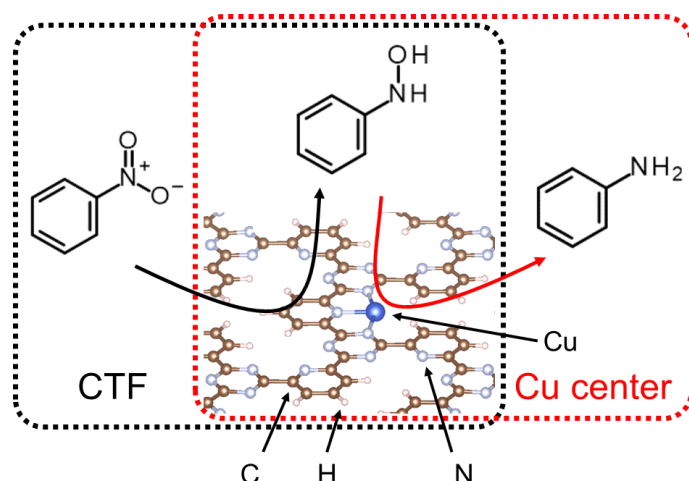
Figure. Schematic illustration of reaction mechanism of nitrobenzene reduction to aniline using Cu modified CTF in this study

Introduction

Nitrobenzene (NB) is an industrial raw material for the manufacturing of aniline (AN), which is a key intermediate in the synthesis of dyes, pharmaceuticals and agrochemicals. In the current industry, zero-valent iron or tin is used as the reducing agent for the conversion of NB to AN [1–4]. However, a large amount of metal oxide residue is formed as a by-product in this reaction. Although non-metal reagents such as hydrogen [5−8] or hydrazine [9−13] are alternative candidates to reduce NB, they are highly toxic or flammable. One promising approach to synthesize AN is the electrochemical reduction of NB because the process does not require toxic or flammable reagents and produces no by-products.

The electrochemical NB reduction reaction (NBRR) in aqueous solution proceeds through a stepwise mechanism and generates AN or azobenzene via nitrosobenzene (NSB) and phenylhydroxylamine (PHA) [14−18], as shown in Fig. 1a. However, no electrode material has been reported to efficiently reduce NB to AN in aqueous solutions. For example, chemically-functionalized multi-wall carbon nanotubes (MWNTs) modified electrodes reduced NB and its derivatives from approximately −0.15 V vs. SCE in acidic solutions, but the major final product was PHA [19]. In addition, Wang *et al.* reported that the faradaic efficiencies of AN and NSB by the NBRR on a carbon cloth was ca. 26% and 74%, respectively [20]. The author assumed that these carbon-based materials could not strongly adsorb reduction substrates such as PHA or NSB, and thus AN production has not been achieved due to the weak adsorption of intermediates. The author has established a working hypothesis that the construction of active centers doped into a carbon-based framework capable of strongly adsorbing these reaction intermediates is required for the complete reduction of NB to AN.

As shown in Chapter 2, Chapter 4 in this thesis and other related work, it is demonstrated that metal-modified covalent triazine frameworks (M-CTFs) [21−23] can serve as a platform for

heterogeneous electrocatalysts [24–28]. The author and co-workers have previously reported copper-modified CTF (Cu-CTF, Fig 1b) as an electrocatalyst for the nitrate reduction reaction (NRR) [27]. The single Cu centers in the Cu-CTF strongly bind nitric oxide (NO), which is one of the reaction intermediates of the NRR, and further reduction of NO to nitrous oxide (N_2O) proceeded. Thus, the author assume that Cu-CTFs could strongly bind the intermediates generated for the NBRR, such as NSB or PHA, and further reduce those compounds to AN (reaction (d) in Fig. 1a). In addition, although the CTF served as a mere support for single metal centers in the previous work [24−28], the CTF is expected to function as a site for the reduction of NB to NSB in the NBRR. Here, the author applies Cu-CTF hybridized with conductive carbon nanoparticle (Cu-CTF/CP) as electrocatalysts for the NBRR in neutral aqueous solutions and demonstrate that the Cu sites and CTF cooperatively reduce NB to AN. In previous reports, it is shown that formation of azoxybenzene (AOB) from a condensation reaction of NSB and PHA (reaction [g] in Fig. 1a), AOB reduction to azobenzene (reaction [h] in Fig. 1a) and Bamberger rearrangement of PHA to form p-aminophenol (reaction [f] in Fig. 1a) occur under organic electrolyte such as ethanol or acidic solution conditions [15,17−19]. Therefore, in this study, the electrocatalytic activity on Cu-CTF/CP and CTF/CP (without Cu) was evaluated under phosphate buffer solution in neutral pH.
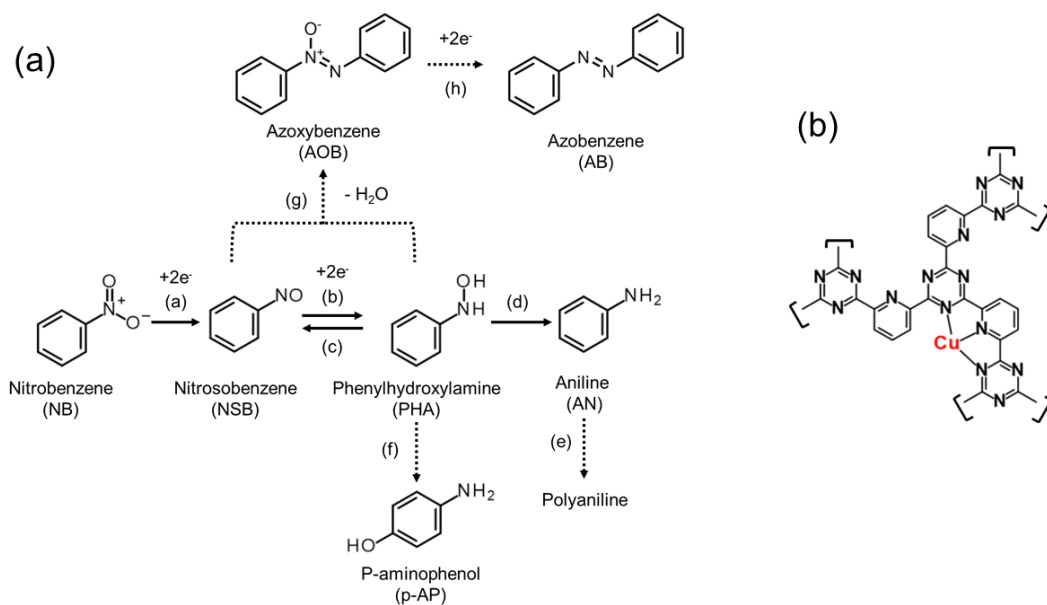
Fig. 1 (a) Reaction path for the reduction of NB to AN. (b) Schematic illustration of the Cu-CTF molecular structure (weakly adsorbed species in electrolyte, anion species such as OH⁻ and water molecule, and ethanol molecule used for the preparation of electrodes are not shown for clarity).

Experimental

(1)   Synthesis procedure

In this study, Cu-CTF hybridized with electro-conductive carbon nanoparticle (Cu-CTF/CP) was prepared following the method as described in Chapter 2 and related works [27].

(2)   Electrochemical characterization

For electrochemical measurements, a catalyst ink was prepared by dispersing 3 mg of Cu-CTF/CP or CTF/CP (without Cu) in 525 uL of ethanol (Wako) and 28.4 uL of 5 wt% Nafion solution (Aldrich). The catalyst ink was dropped on a glassy carbon electrode to prepare a working electrode (ca. 0.071 cm^2). The amount of catalyst loading was controlled to be ca. 0.38 mg cm^{-2}. All electrochemical experiments were performed using a three-electrode system at room temperature with 0.1 M phosphate buffer solutions (PBS) at pH 7. A titanium wire and Ag/AgCl/KCl (sat.) were used as the counter and reference electrodes, respectively. All electrolytes were deaerated by purging with argon (Ar) prior to the experiments. The scan rate of the potential sweep for cyclic voltammetry (CV) was 50 mV s^{-1}. Note that the 5th CV cycle is displayed for all the CV results. Double-chamber electrochemical cells, where the chambers were separated by a Nafion membrane (Aldrich), were used for quantitative analysis of the constant potential. For the constant potential experiments. a 45 mL quantity of the catalyst ink was dropped onto a glassy carbon plate (1.13 cm^2) for a preparation of a working electrode, which was then left to dry in air at room temperature. Reaction products in liquid phases after long-term electrolysis with the double-chamber electrochemical cells were quantitatively analyzed using high-performance liquid chromatography (HPLC; L-2130, Hitachi) with an inert sustain C18 column (GL Science Inc.) and a UV/visible detector (L-2455, Hitachi). Solutions for HPLC consisted of 50% methanol (HPLC grade, Wako) and 50% deionized water as a mobile phase

(1 mL min^{-1}). All chemicals were used as-received without purification.

Results and discussion

The detail characterization of CTF/CP and Cu-CTF/CP was conducted in Chapter 2 in this thesis and related previous reports [25,27]. Briefly, the Cu atoms (0.5 at%) in Cu-CTF/CP were singly isolated and coordinated with N atoms of the framework, and the Cu(II) valence state was dominant [27].

Changes in current density (j) at different potentials (U) from −0.95 to 0.44 V (vs. Ag/AgCl) were examined using CV for CTF/CP and Cu-CTF/CP in 0.1 M PBS both in the presence and absence of 5 mM NB (red and black curves in Fig. 2, respectively). In the presence of NB, the increase in the reduction current started from ca. −0.4 V (vs. Ag/AgCl), and the cathodic peak (peak A) was observed at −0.7 V for both electrodes. This cathodic current was not observed in the absence of NB, and thus it was attributed to the reduction of NB. The onset potential (−0.4 V) and the value of the cathodic current (peak A) for Cu-CTF/CP were almost identical to those for CTF/CP, which indicates that the main active sites for the reduction of NB is the framework itself. In addition to peak A, a single pair of redox peaks with a mid-point potential around 0.0 V (peak pair B) appeared for CTF/CP by the addition of NB (Fig. 2a), whereas it was certainly suppressed for Cu-CTF/CP (Fig. 2b). Carbon-based electrodes are known to convert NB to PHA [19,20]; therefore, the peak pair B was assigned to the NSB/PHA redox couple (reaction [b] and [c] in Fig. 1a).

To confirm the assignment to the NSB/PHA redox couple, CVs were measured in the presence of 0.4 mM PHA on CTF/CP (Fig. 3). As expected, only one redox peak pair coincided with peak pair B in the CV with 5 mM NB (Fig. 2a). These results clearly indicate that peak pair B is a redox peak of NSB/PHA (reactions [b] and [c] in Fig. 1a) and that CTF/CP generated PHA (or NSB) by the NBRR.
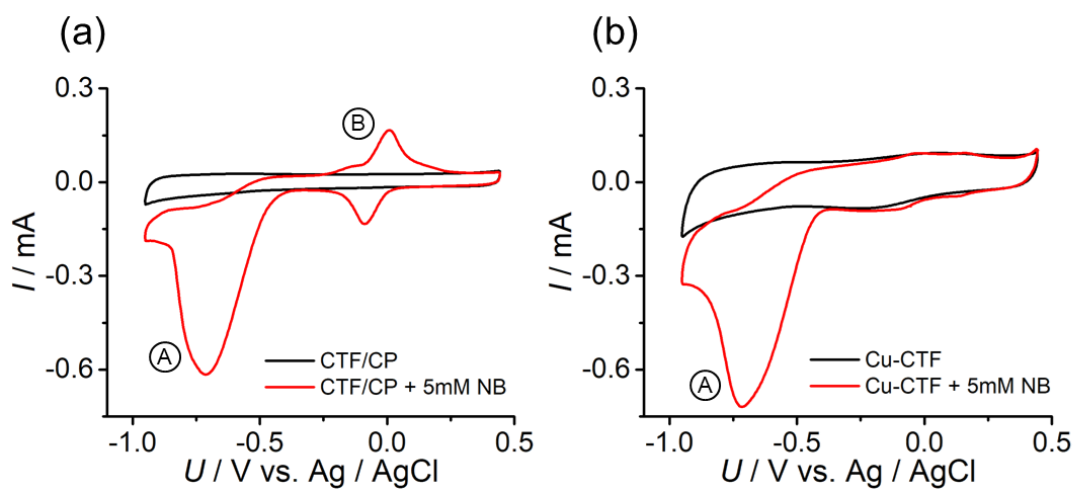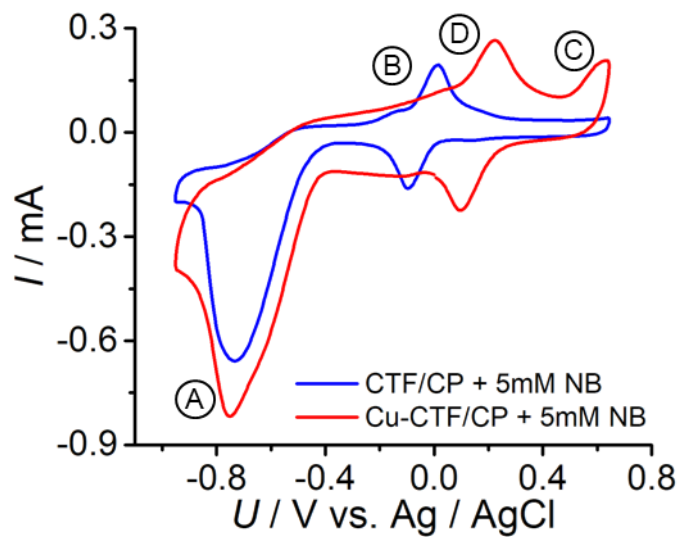
Fig. 2 *j-U* curves under argon for (a) CTF/CP and (b) Cu-CTF/CP. Black and red lines represent CV measurements conducted in the absence and presence of 5 mM NB, respectively
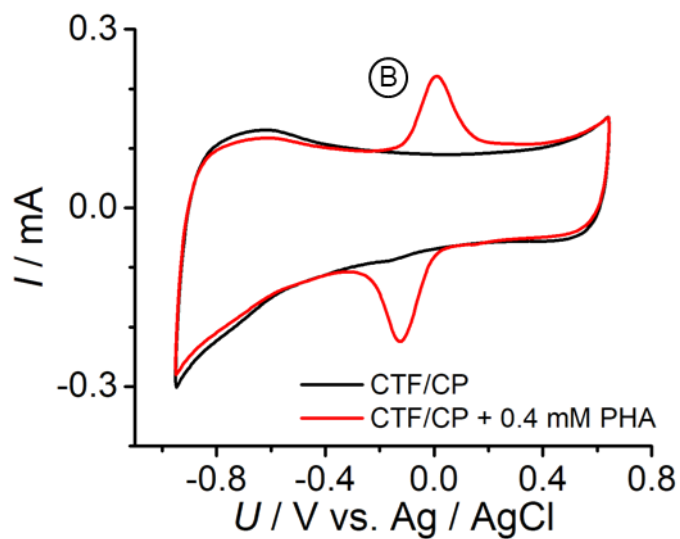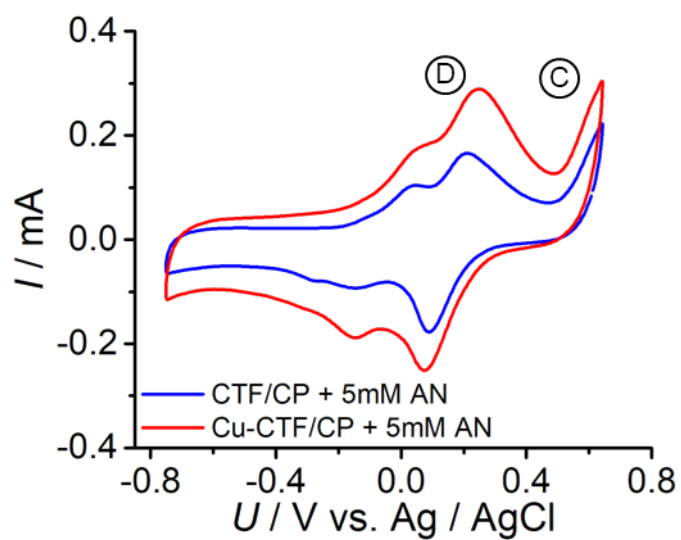

Fig. 3 *j-U* curves under argon for CTF/CP. Black and red lines represent the CV measurements conducted in the absence and presence of 0.4 mM PHA, respectively.

CV measurements were then performed with a more positive potential (−0.95 to 0.64 V) to confirm the production of AN on Cu-CTF/CP because AN can be easily oxidized to poly-ANs in the positive potential region [29]. Fig. 4 shows that although no other peaks were observed apart from peak A and the peak pair B for CTF (blue line), an anodic peak (peak C) and one pair of redox peaks at mid-point of 0.2 V (peak pair D) appeared for Cu-CTF (red line). The same peak C and peak pair D were also observed in CVs measured in the presence of 5 mM of AN (Fig. 5) over both of CTF/CP and Cu-CTF/CP, which indicates that peak C and the peak pair D can be assigned to the oxidation of AN to poly-AN (reaction [e] in Fig. 1a) and the redox couple of poly-AN, respectively [29]. The author also measured the CV of Cu-CTF/CP with 0.4 mM PHA (Fig. 6). In addition to peaks B, C and D, the new cathodic peak E was observed. This peak E was likely assigned to the oxidation of PHA to AN at the Cu sites. In addition, the author observed a single pair of redox peaks with a mid-point potential of −0.05 V in the CV of Cu-CTF without PHA (black line in Fig. 6), which were assignable to the Cu(II)/Cu(I) redox couple [28]. The potential of peak E was basically similar to that at which Cu(II) is converted into Cu(I). Therefore, the author assumed that the reduction of PHA to AN was mediated by the Cu(I) species. Taken together, these CV results (Figs. 2–5) indicate that the CTF framework reduces NB to PHA, followed by the electrocatalytic reduction of PHA to AN by the single Cu sites.
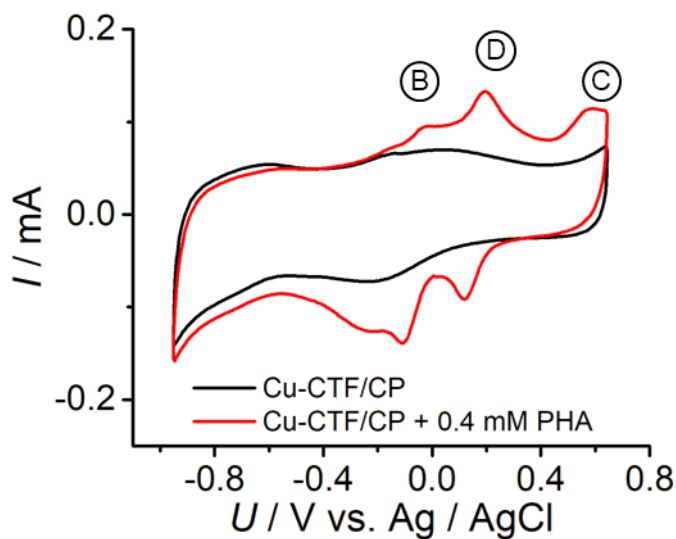
**Fig. 4** Wide range *j-U* curves under argon for Cu-CTF/CP (red) and CTF/CP (blue) in the presence of 5 mM NB.

Fig. 5 Wide range *j-U* curves under argon for Cu-CTF/CP (red) and CTF/CP (blue) in the presence of 5 mM AN

Fig. 6 *j-U* curves under argon for Cu-CTF/CP. Black lines and red lines represent the CV measurements conducted in the absence and presence of 0.4 mM PHA, respectively.

Finally, quantitative analysis of the NBRR product in the liquid phase was conducted after long-term electrolysis using HPLC and a double-chamber electrochemical cell. The chronoamperometric result of Cu-CTF/CP at −0.6 V is shown in Fig. 7. Fig. 8 shows the faradaic efficiency (FE) of CTF (without Cu) and Cu-CTF for the NBRR in 0.1 M PBS containing 5 mM NB at −0.6 V. The FE of Cu-CTF/CP and CTF/CP for AN production reached 65% and 26%, respectively. In addition, the FE for PHA production was 63% over CTF and 24% over Cu-CTF/CP. The CV results (Figs. 2–5) and this long-term experiment indicated that the NBRR from NB to PHA proceeds on the CTF/CP and further reduction of PHA to AN proceeds at Cu centers in Cu-CTF/CP. In contrast to the CV results, the author observed the AN formation by CTF/CP to some extent in the long-term electrolysis. Previous reports claimed that the disproportionation reaction of PHA to NSB and AN can occur easily [16–18]. Therefore, the author speculates that the disproportionation of PHA gradually proceeded during the long-term electrolysis, whereas no AN formation was observed in the short-term CV experiments.

110
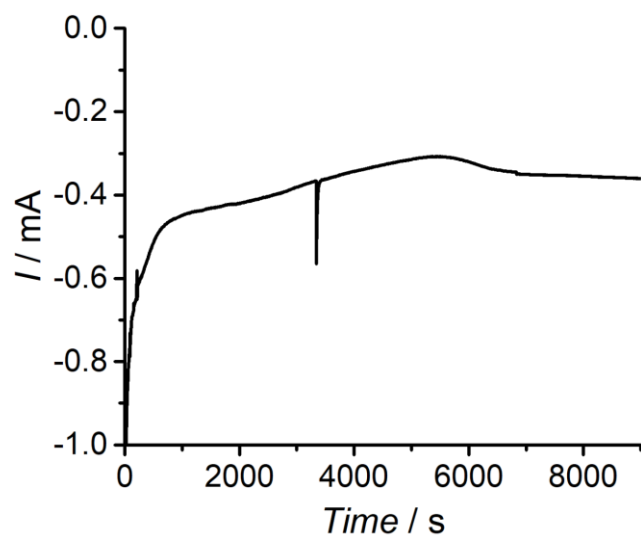
Fig. 7 Chronoamperometric results of Cu-CTF/CP at −0.6 V (vs. Ag/AgCl) in 0.1 M PBS + 5 mM NB.
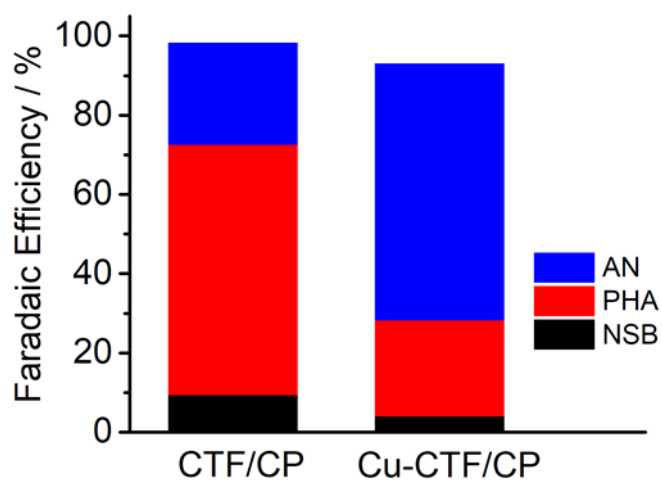
Fig. 8 Faradaic efficiency for the products of NBRR of CTF/CP and Cu-CTF/CP under a potentiostatic condition at −0.6 V (vs. Ag/AgCl) in 0.1 M PBS + 5 mM NB. Reaction time; 2.5 h.

Conclusions

In conclusion, the present work demonstrated that Cu-CTF/CP selectively catalyzes the generation of AN through the NBRR. In this reaction, the CTF/CP serves as active sites for the reduction of NB to PHA, and the Cu sites then reduce PHA to AN. This result revealed that desorption of reaction intermediates of NbRR from the electrocatalytic surface is suppressed by addition of single Cu center, which is expected to strongly adsorb those reaction intermediates. Additionally, this is the first demonstration of the functionality of the framework itself as a reaction center in electrochemical reactions with CTF-based materials. Various types of covalent organic frameworks are available, and because metals other than Cu can be doped into such frameworks, the development of cooperative electrocatalytic reactions over metal and frameworks can be expected as efficient electrocatalysts for various useful reactions, such as carbon dioxide and oxygen reduction reactions.

References

[1]   A. Agrawal, P. G. Tratnyek, *Environ. Sci. Technol.* **1995**, *30*, 153-160.

[2]   Y. Mu, H. Q. Yu, J. C. Zheng, S. J. Zhang, G. P. Sheng, *Chemosphere* **2004**, *54*, 789-794.

[3]   J. Dong, Y. S. Zhao, R. Zhao, R. Zhou, *J. Environ. Sci.* **2010**, *22*, 1741-1747.

[4]   X. F. Ling, J. S. Li, W. Zhu, Y. Y. Zhu, X. Y. Sun, J. Y. Shen, W. Q. Han, L. J. Wang, *Chemosphere* **2012**, *87*, 655-660.

[5]   Z. Z. Wei, J. Wang, S. J. Mao, D. F. Su, H. Y. Jin, Y. H. Wang, F. Xu, H. R. Li, Y. Wang, *Acs Cataly.* **2015**, *5*, 4783-4789.

[6]   R. M. Deshpande, A. N. Mahajan, M. M. Diwakar, P. S. Ozarde, R. V. Chaudhari, *J. Org. Chem.* **2004**, *69*, 4835-4838.

[7]   P. Sangeetha, P. Seetharamulu, K. Shanthi, S. Narayanan, K. S. R. Rao, *J. Mol. Catal. A: Chem.* **2007**, *273*, 244-249.

[8]   M. L. Kantam, T. Bandyopadhyay, A. Rahman, N. M. Reddy, B. M. Choudary, *J. Mol. Catal. A: Chem.* **1998**, *133*, 293-295.

[9]   D. Cantillo, M. M. Moghaddam, C. O. Kappe, *J. Org. Chem.* **2013**, *78*, 4530-4542.

[10]   Y. J. Gao, D. Ma, C. L. Wang, J. Guan, X. H. Bao, *Chem. Commun.* **2011**, *47*, 2432-2434.

[11]   P. F. Luo, K. L. Xu, R. Zhang, L. Huang, J. Wang, W. H. Xing, J. Huang, *Catal. Sci. Technol.* **2012**, *2*, 301-304.

[12]   T. Hirao, J. Shiori, N. Okahata, *Bull. Chem. Soc. Jpn.* **2004**, *77*, 1763-1764.

[13]   R. F. Nie, J. H. Wang, L. N. Wang, Y. Qin, P. Chen, Z. Y. Hou, *Carbon* **2012**, *50*, 586-596.

[14]   Y. Mu, R. A. Rozendal, K. Rabaey, J. Keller, *Environ. Sci. Technol.* **2009**, *43*, 8690-8695.

[15]   X. Sheng, B. Wouters, T. Breugelmans, A. Hubin, I. F. J. Vankelecom, P. P. Pescarmona, *ChemElectroChem* **2014**, *1*, 1198-1210.

[16] J. H. Jiang, R. S. Zhai, X. H. Bao, *J. Alloys Compd.* **2003**, *354*, 248-258.

[17] X. Sheng, B. Wouters, T. Breugelmans, A. Hubin, I. F. J. Vankelecom, P. P. Pescarmona, *Appl. Catal. B: Environ.* **2014**, *147*, 330-339.

[18] B. Wouters, X. Sheng, A. Boschin, T. Breugelmans, E. Ahlberg, I. F. J. Vankelecom, P. P. Pescarmona, A. Hubin, *Electrochim. Acta* **2013**, *111*, 405-410.

[19] Y. T. Sang, B. Y. Wang, Q. C. Wang, G. Zhao, P. Z. Guo, *Sci. Rep.* **2014**, *4*, 6321.

[20] A. J. Wang, H. Y. Cheng, B. Liang, N. Q. Ren, D. Cui, N. Lin, B. H. Kim, K. Rabaey, *Environ. Sci. Technol.* **2011**, *45*, 10186-10193.

[21] M. J. Bojdys, J. Jeromenok, A. Thomas, M. Antonietti, *Advanced Materials* **2010**, *22*, 2202-2205.

[22] P. Kuhn, A. Forget, D. S. Su, A. Thomas, M. Antonietti, *J. Am. Chem. Soc.* **2008**, *130*, 13333-13337.

[23] P. Kuhn, A. Thomas, M. Antonietti, *Macromolecules* **2009**, *42*, 319-326.

[24] R. Kamai, K. Kamiya, K. Hashimoto, S. Nakanishi, *Angew. Chem. Int. Ed.* **2016**, *55*, 13184-13188.

[25] K. Kamiya, R. Kamai, K. Hashimoto, S. Nakanishi, *Nat. Commun.* **2014**, *5*, 5040.

[26] S. Yamaguchi, K. Kamiya, K. Hashimoto, S. Nakanishi, *Chem. Commun.* **2017**, *53*, 10437-10440.

[27] T. Yoshioka, K. Iwase, S. Nakanishi, K. Hashimoto, K. Kamiya, *J. Phys. Chem. C* **2016**, *120*, 15729-15734.

[28] R. Kamai, S. Nakanishi, K. Hashimoto, K. Kamiya, *J. Electroanal. Chem.* **2017**, *800*, 54-59.

[29] M. Matsushita, H. Kuramitz, S. Tanaka, *Env. Sci. Technol.* **2005**, *39*, 3805-3810.

Chapter 4

Metal-modified covalent triazine frameworks as electrocatalysts for carbon dioxide reduction

In chapter 2 and 3, Cu modified CTF (Cu-CTF) and Cu modified S liked CTF (Cu-S-CTF) were developed as efficient electrocatalysts for oxygen reduction reaction and nitrobenzene reduction reaction in neutral solutions. In these studies, it is suggested that Cu centers with open coordination site (coordination number < 4) strongly adsorb reaction intermediates, and that this is essential for specific catalytic activity of those catalysts.

For electrochemical carbon dioxide reduction reaction (CO2RR), the adsorption energies of COOH*, which is one of the important reaction intermediates, is an important determining factor of catalytic activity. Considering that metal centers with lower coordination number show larger adsorption energy, it is expected that metal centers in metal modified CTFs possess larger adsorption energy than corresponding metal porphyrins (coordination number = 4). In this study, the author systematically measured CO2RR activity of M-CTFs (M: Co, Ni and Cu) and corresponding M-TPPs and compared CO2RR activity and adsorption energy of reaction intermediates of them from the view point of coordination structure of metal centers.
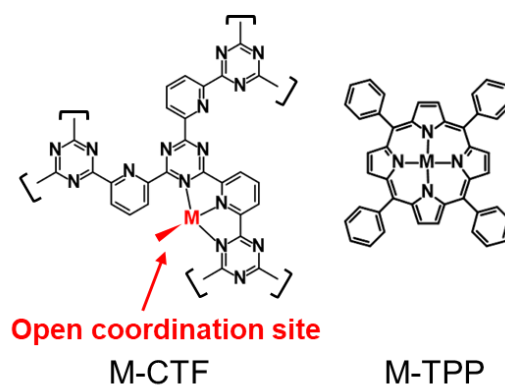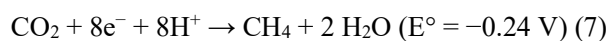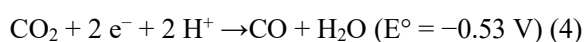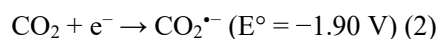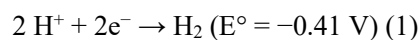

Figure. Schematic image of metal modified CTF and metal porphyrins

4-1

General introduction of carbon dioxide reduction reaction

Increasing the amount of carbon dioxide emission by fossil fuel consumption is a critical problem in our society. Electrochemical carbon dioxide reduction reaction (CO2RR) has attracted great attention as a next generation carbon fixation method. One of the biggest advantages of CO2RR is that various types of useful compounds such as hydrocarbons, alcohols and aldehydes can be produced by multi-electron transfer reaction under mild conditions, normal pressure and temperature [1,2]. Representative products which can be produced by CO2RR are shown below [3]:

$$2\,H^+ + 2e^- \rightarrow H_2\ (E° = -0.41\ V)\ (1)$$

$$CO_2 + e^- \rightarrow CO_2^{\bullet-}\ (E° = -1.90\ V)\ (2)$$

$$CO_2 + 2e^- + 2\,H^+ \rightarrow HCO_2H\ (E° = -0.61\ V)\ (3)$$

$$CO_2 + 2\,e^- + 2\,H^+ \rightarrow CO + H_2O\ (E° = -0.53\ V)\ (4)$$

$$CO_2 + 4e^- + 4H^+ \rightarrow HCHO + H_2O\ (E° = -0.48\ V)\ (5)$$

$$CO_2 + 6e^- + 6H^+ \rightarrow CH_3OH + H_2O\ (E° = -0.38\ V)\ (6)$$

$$CO_2 + 8e^- + 8H^+ \rightarrow CH_4 + 2\,H_2O\ (E° = -0.24\ V)\ (7)$$

(pH 7, vs. standard hydrogen electrode [SHE])

Various kinds of products can be generated during CO2RR as shown above (eq. 2–7) in the negative potential region. Generally, important elements for electrocatalysts for CO2RR are lower

over-potential and higher product selectivity. In addition, as hydrogen evolution reaction (HER, eq. (1)) occurs at same potential region as CO2RR, the reaction selectivity between CO2RR and HER is also important for efficient CO2RR catalysts. From this background of CO2RR, various types of materials have been utilized for CO2RR such as bulk metals [4–10], nanoparticles [11–13], alloys [14–15] and organometallic complexes [16–18] so far.

As for bulk CO2RR catalysts, the most notable material is Cu electrode. Cu electrode (and surface modified Cu electrodes) shows unique product selectivity. It is the only material which can generate hydrocarbons and alcohols such as CH_4, C_2H_4, CH_3OH and C_2H_5OH with high faradaic efficiency [4,5]. The specific reaction selectivity, crystal plane dependence and electrolyte dependence (such as pH and cation concentration) on the Cu electrodes was reported by Y. Hori and other researchers. One of those researches is shown in Table 1 [4]. As shown in Table 1, Cu electrode shows high faradaic efficiency of generation of hydrocarbons such as CH_4 (22.3%) and C_2H_4 (21.7%), whereas Fe and Ni electrode generate tiny amount of hydrocarbons. Because of such unique electrocatalytic property of Cu electrode, many researches have been conducted on clarifying the reaction mechanism of the formation of those hydrocarbons on Cu electrode [19–22]. Those researches suggest that surface Cu atoms on Cu electrode possess moderated adsorption strength of CO*, which is a key reaction intermediate for CO2RR. As those researches suggested that Cu(0) (metallic Cu) is an active species for CO2RR, one of the main approaches for improving product selectivity and activity (production rate) is modification of morphology of surface of Cu by using an electrodepositions of Cu ions or surface modification of Cu electrodes by reducing Cu oxides such as Cu_2O (this is called oxide derived Cu in some researches) [9,23] .
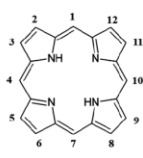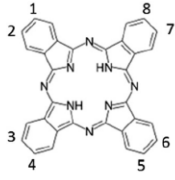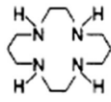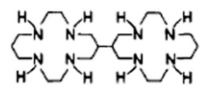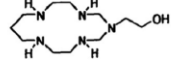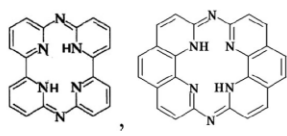
Table 1 Faradaic efficiencies of various products from Cu, Fe, and Ni electrodes[a]. Reprinted with permission from ref. [4]. Copyright 2002, American Chemical Society.

electrode	potential/V	Faradaic efficiencies/%									
		CH_4	C_2H_6	C_2H_4	MeOH	EtOH	n-PrOH	MeCHO	EtCHO	H_2	total
					Electrolyte: 0.1 M $KHCO_3$[b]						
Cu	−1.36	22.3	0.00	21.7	0.00	7.1	2.2	1.4	0.5	41.7	96.9
Fe	−1.38	1.1	0.4	0.1	0.1	tr.[c]	0.00	tr.	tr.	96.0	97.7
Ni	−1.49	1.1	0.3	0.2	0.5	tr.	tr.	0.1	tr.	100.3	102.5
					Electrolyte: 0.1 M KH_2PO_4 + 0.1 M K_2HPO_4 (pH 6.8)						
Cu	−1.24	15.6	0.00	4.1	0.00	0.3	0.00	0.00	0.00	73.0	93.0
Fe	−1.32	2.6	0.8	0.2	0.1	0.2	tr.	tr.	tr.	93.8	97.7
Ni	−1.14	1.5	0.5	0.1	0.2	0.1	tr.	0.1	tr.	89.7	92.1

[a] Potentials *vs* SHE. Temperature: 19 °C. Current density: 2.5 mA cm⁻². [b] pH is estimated at 9.0 at the electrode surface during the reactions. [c] tr. indicates a current efficiency between 0.01 and 0.05%.

As for CO2RR catalysts, organometallic complexes are also promising materials due to its high design flexibility. Various types of organometallic complexes such as bipyridine complexes, amine complexes and cyclams are developed as CO2RR catalysts as heterogeneous catalysts (adsorbed conductive substrates such as carbon nanoparticle or carbon felt electrode) and homogeneous catalysts [3,16–18,24]. For example, N. Sonoyama et al. systematically investigated the CO2RR activity on metal-tetraphenylporphyrins (M-TPPs) impregnated into gas diffusion electrode [18]. In this report, they reported that Co and Fe-TPP showed higher conversion efficiency on CO_2 to CO, and the current efficiency is 75% and 42%, respectively, whereas Cu and Zn-TPP show relatively lower current efficiency [18]. Many researchers have focused on Ru/Co/Fe/Ni organometallic complexes. Representative macrocyclic compounds developed to date are shown in Fig. 1. Notably, some of them show efficient catalytic activity due to the appropriate choice of organic ligands.

Major reaction products of those organometallic complexes are CO and HCOOH, which are two electron reduction products. Therefore, it might be one of the challenging issues to synthesize molecular catalysts which can further reduce two electron reduction products (CO or HCOOH) to CH_4 and C_2H_4 (8 and 12 electron reduction products, respectively).

Ligand core structure	Substitution on the ligand core structure	Fe/Co/Ni-complexes
(1) Porphyrin	1,4,7,10-H are substituted by 4-carboxyphenyl 1,4,7,10-H are substituted by 4-sulfophenyl 1,4,7,10-H are substituted by phenyl 1,4,7,10-H are substituted by $2'6'$-dihydroxylphenyl 1,4,7,10-H are substituted by $2'6'$-dimethoxyphenyl 1,4,7,10-H are substituted by 4-methoxyphenyl 1,4,7,10-H are substituted by p-ethynylphenyl 1,4,7-H are substituted by $C_6F_3H_2$, $C_6H_4CF_3$, and C_6F_5, respectively	Fe-$meso$-tetra(carboxyphenyl)porphine[83] Fe-tetraphenylporphine sulfonate[83] Fe–L;[32,33,55,84–86,97,98] Co–L;[55,89,90,95,97,98] Ni–L,[55,96] L = tetraphenylporphyrin (TPP) Fe–L;[86] Co–L,[91] L = 5,10,15,20-tetrakis-($2'6'$-dihydroxylphenyl)-porphyrin Fe-5,10,15,20-tetrakis($2'6'$-dimethoxyphenyl)-porphyrin[86] Co-5,10,15,20-tetrakis (4-methoxyphenyl)-porphyrin (CoTMeOPP)[133] Co-5,10,15,20-tetra(p-ethynylphenyl)-porphyrin[94] Co–L,[95] L = T3FPP, T3CF$_3$PP, and TF$_5$PP
(2) Phthalocyanine	Unsubstituted (1 or 2)H, (3 or 4)H, (5 or 6)H, and (7 or 8)H are substituted by "SO_3H" 1,2,3,4,5,6,7,8H are substituted by 8 of "$nCH_3CH_2CH_2$" (1 or 2)H, (3 or 4)H, (5 or 6)H, and (7 or 8)H are substituted by "NH_2"	Fe–L,[100] Co–L,[100–104,133] Ni–L,[100,102] L = phthalocyanine M-phthalocyanine tetrasulfonate; M = Fe, Co, Ni[99] Co-octabutoxyphthalocyanine[105] M-tetrakis aminophthalocyanine, M = Fe, Co, Ni[371] Naphthalocyanato cobalt(II)[133]
(3) Corrole	1,2,3 H are substituted by pentafluorophenyl 1,2,3 H are substituted by 2,6-dichlorophenyl	$(C_6H_5)_3PCo^{(III)}L$; $ClFe^{(IV)}L$, L = 5,10,15-tris(pentafluorophenyl)corrole[110] $ClFe^{(IV)}L$, L = 5,10,15-tris(2,6-dichlorophenyl)corrole[110] Hydrophobic vitamin B12[133]
(4) 1,4,8,11-Tetraazacyclotetradecane (cyclam)	Other (N–)H substituted cyclams Biscyclam 	Ni(cyclam)Cl$_2$[111–116,118,120–124,126] Ni–L,[119–121,123,136] L= (N–)H substituted cyclams [Ni$_2$(biscyclam)]$^{4+}$ (ref. 118) Ref. 119
(5) 14-Membered tetraazamacrocycles		Co,[125] Ni[125,127,128]
(6) Hexaazamacrocycle (ref. 109)	—	Ni,[108] Co[108,109]

Fig. 1 Fe/Co/Ni complexes and their tetradentate ligands for CO_2 electrochemical reduction catalysts. Reprinted with permission from ref. [24]. Copyright 2014, Royal Society of Chemistry.

References

[1]   M. Gattrell, N. Gupta, A. Co, *J. Electroanal. Chem.* **2006**, *594*, 1-19.

[2]   K. Tanaka, D. Ooyama, *Coord. Chem. Rev.* **2002**, *226*, 211-218.

[3]   J. Schneider, H. Jia, J. T. Muckerman, E. Fujita, *Chem. Soc. Rev.* **2012**, *41*, 2036-2051.

[4]   Y. Hori, I. Takahashi, O. Koga, N. Hoshi, *J. Phys. Chem. B* **2002**, *106*, 15-17.

[5]   Y. Hori, A. Murata, R. Takahashi, *J. Chem. Soc. Farad. Trans. 1: Phys. Chem. Cond. Phases* **1989**, *85*.

[6]   K. Hara, A. Kudo, T. Sakata, *J. Electroanal. Chem.* **1995**, *391*, 141-147.

[7]   M. Azuma, *J. Electrochem. Soc.* **1990**, *137*.

[8]   K. P. Kuhl, T. Hatsukade, E. R. Cave, D. N. Abram, J. Kibsgaard, T. F. Jaramillo, *J. Am. Chem. Soc.* **2014**, *136*, 14107-14113.

[9]   P. De Luna, R. Quintero-Bermudez, C.-T. Dinh, M. B. Ross, O. S. Bushuyev, P. Todorović, T. Regier, S. O. Kelley, P. Yang, E. H. Sargent, *Nat. Catal.* **2018**, *1*, 103-110.

[10]   D. D. Zhu, J. L. Liu, S. Z. Qiao, *Adv. Mater.* **2016**, *28*, 3423-3452.

[11]   D. Gao, H. Zhou, J. Wang, S. Miao, F. Yang, G. Wang, J. Wang, X. Bao, *J. Am. Chem. Soc.* **2015**, *137*, 4288-4291.

[12]   T. Shinagawa, G. O. Larrazábal, A. J. Martín, F. Krumeich, J. Pérez-Ramírez, *ACS Catal.* **2018**, *8*, 837-844.

[13]   H. Mistry, R. Reske, Z. Zeng, Z. J. Zhao, J. Greeley, P. Strasser, B. R. Cuenya, *J. Am. Chem. Soc.* **2014**, *136*, 16473-16476.

[14]   S. Rasul, D. H. Anjum, A. Jedidi, Y. Minenkov, L. Cavallo, K. Takanabe, *Angew. Chem. Int. Ed.* **2015**, *54*, 2146-2150.

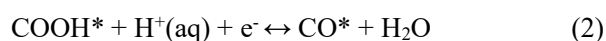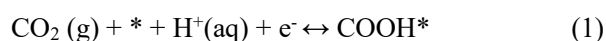[15]   D. Kim, J. Resasco, Y. Yu, A. M. Asiri, P. Yang, *Nat. Commun.* **2014**, *5*, 4948.

[16]   C. Costentin, S. Drouet, M. Robert, J. M. Saveant, *Science* **2012**, *338*, 90-94.

[17]   J. D. Froehlich, C. P. Kubiak, *Inorg. Chem.* **2012**, *51*, 3932-3934.

[18]   N. Sonoyama, M. Kirii, T. Sakata, *Electrochem. Commun.* **1999**, *1*, 213-216.

[19]   S. Hanselman, M. T. M. Koper, F. Calle-Vallejo, *ACS Energy Lett.* **2018**, *3*, 1062-1067.

[20]   A. A. Peterson, F. Abild-Pedersen, F. Studt, J. Rossmeisl, J. K. Nørskov, *Energy Environ. Sci.* **2010**, *3*.

[21]   H. Li, Y. Li, M. T. Koper, F. Calle-Vallejo, *J. Am. Chem. Soc.* **2014**, *136*, 15694-15701.

[22]   F. Calle-Vallejo, M. T. Koper, *Angew. Chem. Int. Ed.* **2013**, *52*, 7282-7285.

[23]   C. W. Li, J. Ciston, M. W. Kanan, *Nature* **2014**, *508*, 504-507.

[24]   J. Qiao, Y. Liu, F. Hong, J. Zhang, *Chem. Soc. Rev.* **2014**, *43*, 631-675.

4-2

Systematic investigation of electrochemical carbon dioxide reduction activity by metal-modified covalent triazine frameworks

Introduction

The electrochemical carbon dioxide reduction reaction (CO2RR) in aqueous media is a promising approach to closing the carbon cycle, and as such has attracted significant attention, as shown in Introduction of this thesis [1–2]. Especially, the reduction of CO_2 to CO summarized in the following equations is an important step in the CO2RR and represents the first two-electron reaction [3–6].

$$CO_2 (g) + * + H^+(aq) + e^- \leftrightarrow COOH* \qquad (1)$$

$$COOH* + H^+(aq) + e^- \leftrightarrow CO* + H_2O \qquad (2)$$

$$CO* \leftrightarrow CO (g) + * \qquad (3)$$

here, the asterisk represents a free adsorption site. Previous studies have shown that either reaction (1) or (3) can become the rate-determining step, depending on the relative magnitudes of the COOH* and CO* adsorption energies [4–6]. Importantly, there is a linear relationship (scaling relation) between the COOH and CO adsorption energies, such that these values do not change independently of one another [4–5]. For this reason, the adsorption energy of COOH* (or CO*) can serve as an indicator of

the CO generation activity, and a so-called volcano-type relationship has been established between the adsorption energy and the catalytic activity [4–5]. Therefore, developing a highly efficient CO generating electrocatalyst requires precise tuning of the adsorption energies of critical intermediate species.

There are two important factors determining the adsorption energies of intermediates on electrocatalysts. The first is the metal species in the catalyst i.e. transition metals at active sites having a greater number of d-electrons tend to lower the adsorption energy [7–9]. For this reason, the effects of metal species on the CO2RR have been systematically investigated using tetraphenylporphyrin (TPP) [3,10–12], which can serve as a platform to support various metals via coordination bonds. It is known that cobalt modified-TPP (Co-TPP) has an appropriate bond strength with COOH* and thus shows efficient CO2RR activity, whereas the catalytic activities of nickel (Ni) or copper (Cu) modified-TPP are low because the COOH* binding energy is insufficient [11,12]. The second critical factor is the coordination structure (or the coordination number) of the metal [13–17]. First principles calculations have demonstrated that a decrease in coordination number of bulk Pt or Cu leads to an increase in the CO* binding strength [4,14], thus affecting the CO2RR activity. Therefore, it may be possible to use the coordination number as a control parameter to improve the performance of metal species that have previously been thought to have no CO2RR activity.

In Chapter 2, the author newly synthesized covalent triazine framework (CTF), which is a kind of covalent organic framework with 1,3,5-triazine linker units, modified with Cu (Cu-CTF) as an efficient electrocatalysts for oxygen reduction reaction (ORR). In addition, the author demonstrated that Cu center in Cu-CTF possess open coordination site (unsaturated coordination structure), and that this coordination structure is essential for high ORR activity. Here, the author hypothesized that CTFs are promising platforms for metal species with coordination unsaturation. Chapter 2 and related previous works about CTF based electrocatalysts have shown that the adsorption energies of dioxygen

and nitrogen oxides on Cu-CTF are larger than those on Cu-TPP or bulk Cu, respectively [18]. This increase in the adsorption energy was attributed to the coordinatively unsaturated nature of the Cu atoms in the CTF. In the present work, the author synthesized CTFs modified with coordinatively unsaturated 3d metal atoms as electrocatalysts for CO2RR with the aim of eliciting the potential performance of metals that have, to date, been regarded as inactive.

Experimental

(1)   Synthesis procedure

・**Synthesis of M-CTFs**

Each metal modified CTF was prepared using essentially same method described in Chapter 2 in this thesis and a related previous work [18]. Briefly, 2,6-dicyanopyridine (64.5 mg, Koei Kagaku) and carbon nanoparticle (CP, 64.5 mg, Ketjen Black EC600JD, Lion Corp.) were mixed with $ZnCl_2$ (6.82 g, Wako) in a glass vacuum tube and then heated to 400 °C at 3.3 °C/min and held at that temperature for 40 h. The resulting powder was washed with deionized water, tetrahydrofuran (THF, Wako), HCl (1 M, Wako) and aqueous ammonia (1 M, Wako) and CTF hybridized with CP (CTF/CP) was obtained. The obtained CTF/CP was dispersed in a 10 mM aqueous solution of MCl_2 (M = Co, Ni or Cu) and stirred at 80 °C for 3 h. Subsequently, the product was collected by centrifugation and thoroughly washed with deionized water to remove any unbound metal salt, followed by drying at 60 °C in a vacuum oven for 1 day (M-CTF/CP).

・**Synthesis of M-TPPs (in this study, M-TPPs were loaded onto carbon particles)**

Here, the author takes Co-TPP electrode as an example to show the preparation procedure of M-TPP electrode. Firstly, Co-TPP (9.5mg) and CP (EC600JD, 90mg) were dispersed in 20mL DMF solvent using an ultrasonic bath, and then, the mixture was dried at 80 ℃ with a rotary evaporator (M-TPP/CP). The metal concentration of the mixture of M-TPP/CP is the same with that of the corresponding M-CTF/CP, which is determined by the X-ray photoelectron spectroscopy (XPS) and inductively coupled plasma atomic emission spectroscopy (ICP-AES).

(2)   Electrochemical characterization

Electrochemical measurements were performed using a Hokuto Denko Electrochemical Station (Model HZ-5000) in a two-compartment electrochemical cell (separated by a Nafion membrane) in conjunction with three electrodes. A Ag/AgCl electrode (with saturated KCl as the internal solution) and platinum wire were used as the reference and counter electrodes, respectively. Each working electrode was fabricated by dispersing 3 mg of the desired M-CTF/CP (or CTF/CP) and 28.5 μL Nafion (5 wt.%, Aldrich) in 300 μL ethanol using an ultrasonic bath to generate a catalyst ink. A 60 μL quantity of this ink was dropped onto a glassy carbon plate (2 cm^2), which was then left to dry in air at room temperature, to yield a catalyst layer with a loading of 0.3 mg cm^{-2}. The gaseous products that accumulated in the cathodic part of the reaction cell were analyzed by GC-MS (GCMS-QP 2010 Plus, Shimadzu, Japan), calibrated using CO and H$_2$ samples diluted with air to various concentrations. Products in liquid phase were analyzed on a Varian 500 MHz NMR spectrometer. A 0.5 mL electrolyte (0.1 M KHCO$_3$) after electrolysis was mixed with D$_2$O (0.1 mL) and dimethyl sulphoxide (32 μL) as internal standard.

(3)   Physical characterizations

XPS (Axis Ultra, Kratos Analytical Co.) spectra were obtained using monochromatic Al Kα X-rays at hν = 1486.6 eV. XAFS data were acquired by the transmission method using the hard X-ray BL01B01 beam line at the SPring-8 facility, Japan. Transmitted X-rays were detected using a double-crystal Si (111) monochromator. Surface inspection was carried out with a scanning electron microscope (SEM; JEOL, JSM-7600F.) and high-resolution transmission electron microscope (TEM; Hitachi, H-9000NAR.). XANES spectra and EXAFS were analysed using Athena, ARTEMIS and FEFF6L software. A powder X-ray diffraction (XRD) pattern was recorded on a PANalytical X'Pert PRO diffractometer with Cu Ka radiation. Metal content was determined by ICP-AES (Optima 8300,

PerkinElmer). The N$_2$ adsorption-desorption isotherm was obtained by a Micromeritics 3 Flex at 77K.

(4)　　DFT calculations

Density functional theory (DFT) calculations of the adsorption energies of intermediates on the M-CTF and M-TPP were performed using the OpenMX code [19,20]. The generalized gradient approximation of the Perdew−Burke−Ernzerhof model (GGA-PBE) was applied, and a kinetic energy cutoff of 120 Ryd was selected. The detailed structural parameters of the M-CTF can be found in related previous work [18] and Chapter 2. The structure of CTF frameworks without metals was first relaxed. Then, metal sites were doped in the framework and relaxed the metal configuration, while the frameworks were fixed. One COOH or CO molecules were adsorbed on one metal sites, and their configurations were relaxed to calculate the free energy diagram. To simplify the DFT calculations, a slab consisting of a single CTF layer was used as the model structure of M-CTFs in this study. A slab model was used with a 15 Å vacuum layer between the CTF layers. Zero-point energy and entropic corrections were applied based on reported values [11,21] to convert electronic energies into Gibbs free energies. In this work, the solvation energy was not applied and a −0.24 eV correction was added to CO to compensate for a limitation of the PBE model [11,22]. Reaction free energies were calculated using the computational hydrogen electrode (CHE) model, following the same method as described in previous reports [6,21,23]. Briefly, in this model, the chemical potential of a proton-electron pair in solution is equal to half that of a gas phase H$_2$ molecule at 0 V vs. RHE. Thus, the author utilized the following equation to apply the over-potential when calculating the free energy diagram.

$$G[H^+ + e^-] = 0.5\ G[H_2] - eU \qquad\qquad (4)$$

here, U is the applied over-potential and e is the elementary charge.

Results and discussion

The synthesis of CTF/CPs and metal modification to CTF/CPs by impregnation method with aqueous solutions of various divalent metal chlorides to obtain M(II)-CTF/CP (M = Co, Ni or Cu) were successfully achieved in the same manner as described in Chapter 2 and reported method [18,24,25]. The elemental analyses were conducted by semi-quantitative X-ray photoelectron spectroscopy (XPS) and inductively coupled plasma atomic emission spectroscopy (ICP-AES) (Table 1 and Table 2). The CTF layer was uniformly polymerized on CPs, which has been proven by N 1s XPS spectra and transmission electron microscopy (TEM) energy dispersive X-ray (EDX) mapping in previous reports [24] and results in Chapter 2. In addition, the SEM pictures for CTF/CP (Fig. 1) show that the particle size of 20–80 nm, which corresponded to the size of the CPs, also revealed that CTF was well mixed with CPs [18,24,25]. The powder XRD patterns for CTF/CP (Fig. 2) indicated that M-CTF/CPs synthesized in this study have amorphous structure, which is consistent with the reported CTF originated from 2,6-dicyanopyridine [26,27]. The high-resolution TEM images (Fig. 3) suggested that no metal or metal oxide nanoparticles (> 1nm) was formed on M-CTF/CP, which are consistent with the previous related works [24] and results in Chapter 2. The nitrogen adsorption– desorption isotherms indicate that CTF/CP and Ni-CTF/CP have a hierarchical pore system composed of micro and mesopores (see Fig. 4 for the detail).

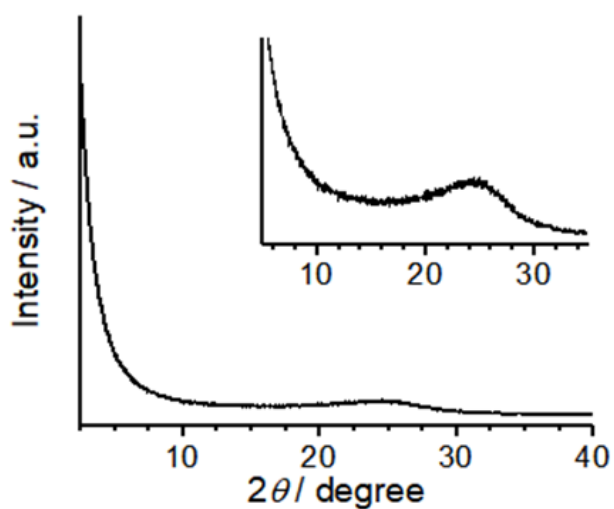**Table 1** XPS elemental analysis results (at. %).

	C	O	N	Metal
CTF	86.75	5.93	6.83	-
Ni-CTF/CP	88.29	3.95	7.06	0.14 (Ni)
Co-CTF/CP	89.47	3.09	6.70	0.17 (Co)
Cu-CTF/CP	88.20	3.60	6.74	0.55 (Cu)

Table 2 Metal concentration on M-CTF/CP derived from ICP-AES (at. %).
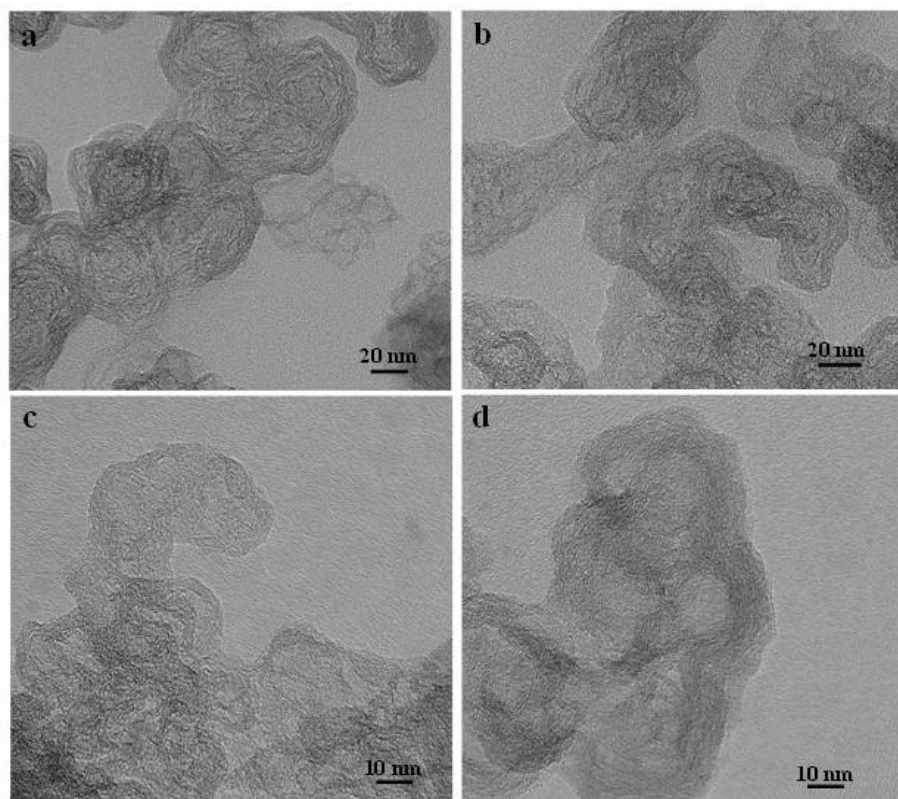
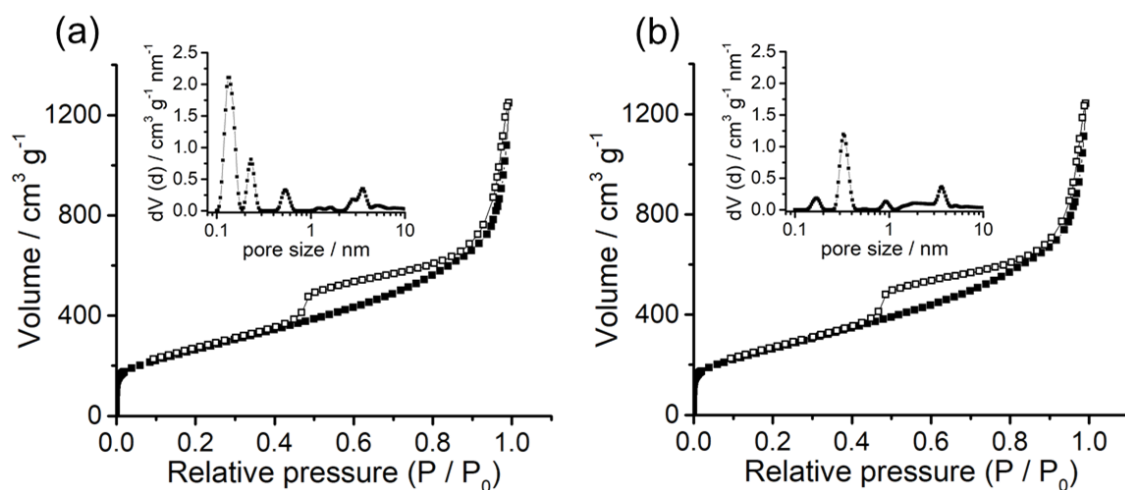|	Metal
Ni-CTF/CP	0.17 (Ni)
Co-CTF/CP	0.13 (Co)
Cu-CTF/CP	0.38 (Cu)
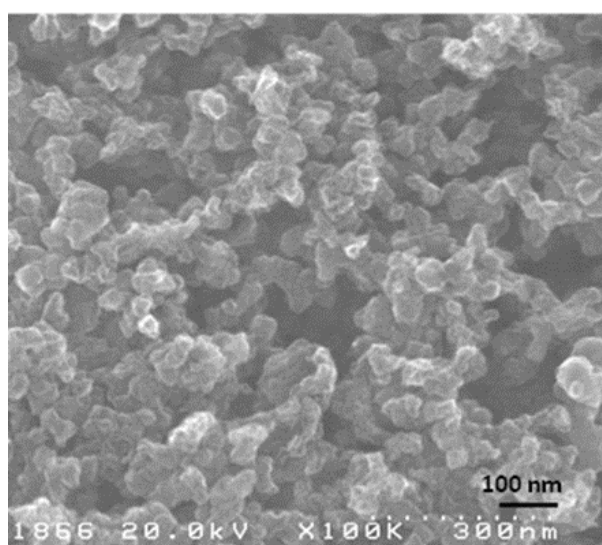
Fig. 1 Representative SEM image of CTF/CP

Fig. 2 The XRD pattern of CTF/CP. (inset) magnified one

Fig. 3 The TEM images of (a) CTF/CP, (b) Ni-CTF/CP, (c) Co-CTF/CP and (d) Cu-CTF/CP.


Fig. 4 N_2 adsorption-desorption isotherm for (a) CTF/CP and (b) Ni-CTF/CP. The insets show the pore size distributions calculated by nonlocal density functional theory (NL-DFT) method. BET surface area is 937.5 m^2/g and 933.4 m^2/g for CTF/CP and Ni-CTF/CP, respectively.

Electronic and structural characterizations of the metal sites in M-CTF/CP specimens were conducted using extended X-ray absorption fine structure (EXAFS) analyses. In Chapter 2, the author showed that the Cu atoms are in the form of Cu(II) and those possess unsaturated coordination structure. It is confirmed that Cu atoms have a lower first coordination number of 3.4 compared to the value of 4 in Cu-TPP by a related work of the author and co-workers [18]. The present study focused on the characterization of Ni-CTF/CP and Co-CTF/CP. Ni–K XANES spectra and Co-K XANES spectra were shown in Fig. 5a and Fig. 5b, respectively (the reference samples are also shown in those figures). Fig. 5a shows the Ni-K XANES spectra for Ni-CTF/CP and the reference samples. The XANES absorption edge corresponding to 1s -> 4p transitions [28] for Ni-CTF/CP located at 8333 eV, which is consistent with that for NiO and Ni(II)-TPP. These results indicated that the Ni(II) valence state was dominant in Ni-CTF/CP. Similarly, Fig. 5b indicated that the Co(II) valence state was dominant in Co-CTF.

The author also acquired EXAFS data to assess the molecular structure of the Ni-CTF (Fig. 6a). The EXAFS results before and after Fourier transformation of M-CTF/CPs (M: Co, Ni) and corresponding M-TPPs as reference are shown in Fig. 7. Ni-CTF shows one strong peak at 1.7 Å, whereas no strong peak corresponds to Ni–Ni bond and Ni–O–Ni bonds were not observed [29,30]. In chapter 2, the author demonstrated that no Cu species were found on CPs that were treated with $CuCl_2$ solutions. In this study, the author also found that no Co and Ni species were observed on CPs treated with MCl_2 solutions, indicating that metal species were anchored on CTFs (Fig. 8). In addition, the TEM results showed that no NiO nanoparticle was formed. Thus, the first coordination sphere (the peak at 1.7 Å) was composed of N atoms of CTF. The curve fitting for EXAFS spectra were performed for Ni-CTF/CP (detail see Table 3 and its captions). The coordination number of N atoms in the first coordination sphere of Ni-CTF/CP is 3.4. These data indicate that the Ni atoms in the Ni-CTF/CP were individually isolated and had an unsaturated first coordination sphere in the pores of the CTF, identical

result is also obtained for Co-CTF/CP (Fig. 6b). The schematic illustration of those M-CTF is shown in Fig. 9.
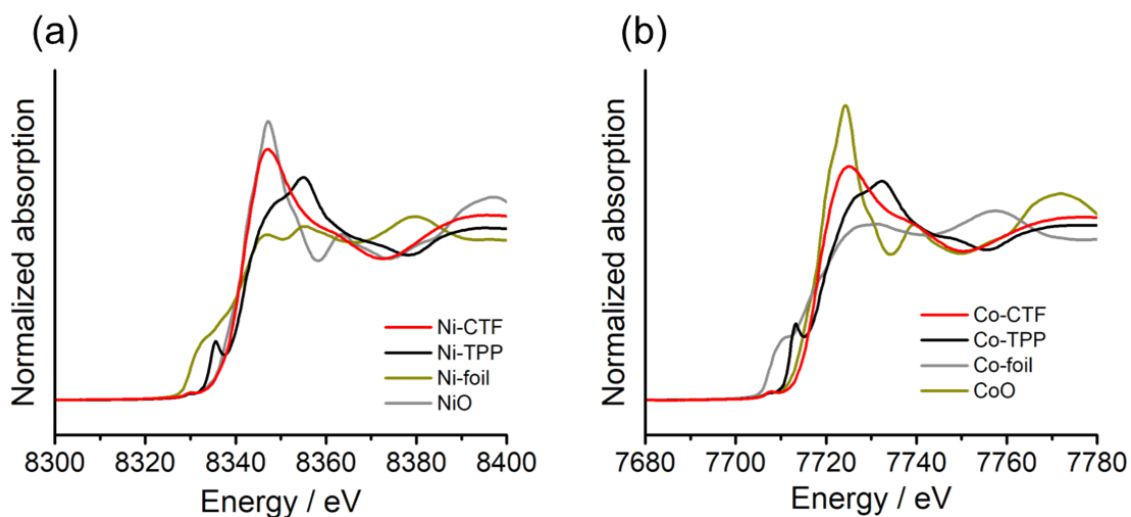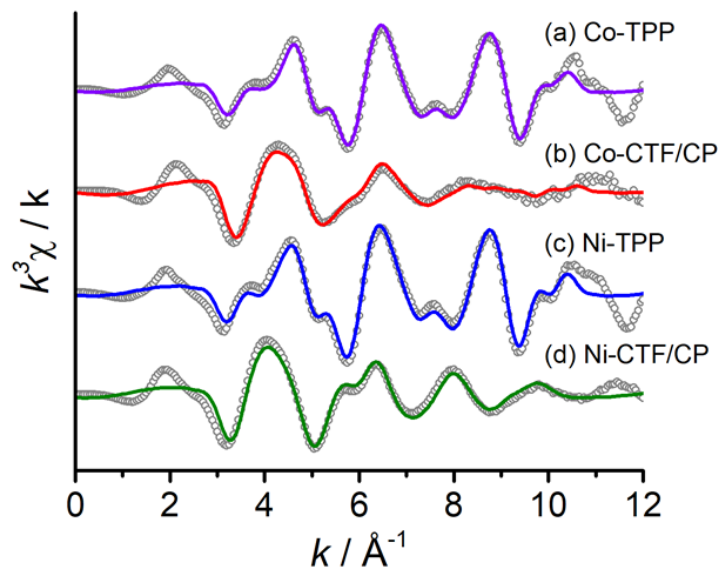

Fig. 5 The Ni-K XANES spectra for Ni-CTF/CP, Ni metal, NiO and Ni(II)-TPP and (b) The Co-K XANES spectra for Co-CTF/CP, Co metal, CoO and Co(II)-TPP.
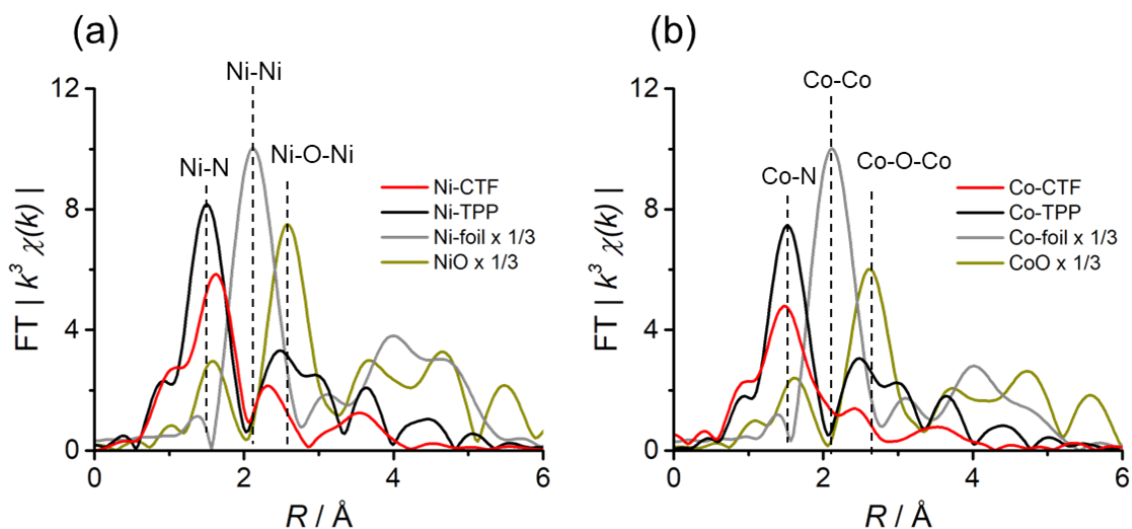

Fig. 6 The k^3-weighted Fourier transform EXAFS spectra (a) at the Ni K-edge of Ni-CTF/CP (red), Ni-TPP (black), Ni foil (gray) and NiO (dark yellow), and (b) at the Co K-edge for Co-CTF/CP (red), Co-TPP (black), Co-foil (gray) and CoO (dark yellow).

Fig. 7 k^3-weighted EXAFS oscillations (gray dots) and Inverse Fourier Transform of FT-EXAFS (solid colored lines) in Fig. 6 for (a) Co-TPP, (b) Co-CTF/CP, (c) Ni-TPP and (d) Ni-CTF/CP. k: 3–10.5 Å^{-1}, R: 1–6.
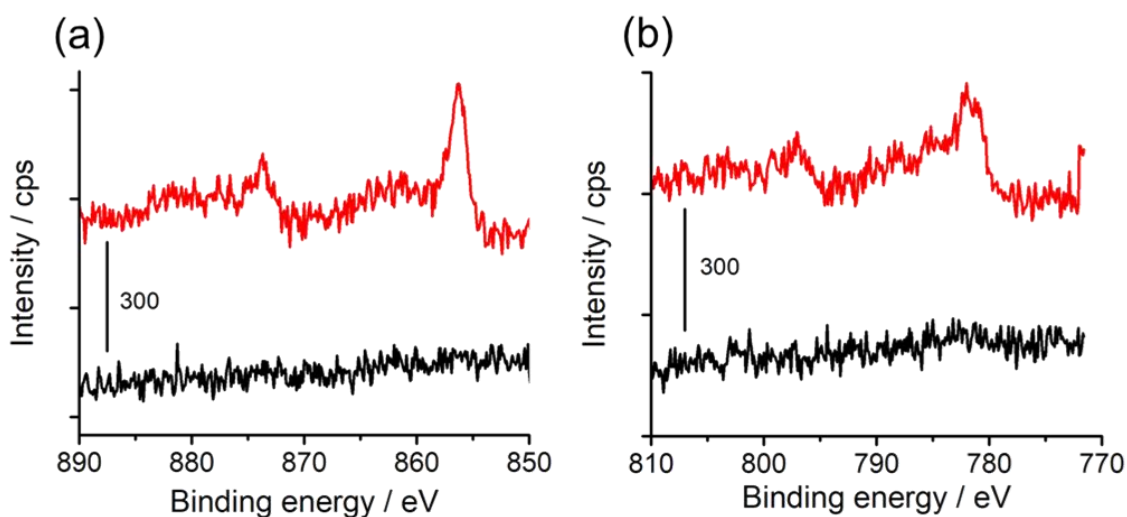
Fig. 8 (a) Ni-2p XPS spectra for Ni-CTF/CP (red) and CP treated with NiCl$_2$ solution (black). (b) Co-2p XPS spectra for Co-CTF/CP (red) and CP treated with CoCl$_2$ solution (black)

.

Table 3 R: atomic distance (Å), CN: coordination number, s^2: Debye–Waller factor, S_0^2: amplitude reduction factor. Curve fitting for the EXAFS spectra was conducted by using ARTEMIS software [31]. *a*: value from a previous related work of the author and co-workers [18].

	Bond type	CN	R	s^2 ($\times 10^{-3}$, Å)	S_0^2
Co-TPP	Co-N	4	1.95 ± 0.02	3.0 ± 1.6	0.99
Co-CTF	Co-N	3.2	2.00 ± 0.10	7.0 ± 4.2	0.99
Ni-TPP	Ni-N	4	1.94 ± 0.03	3.1 ± 2.1	1.08
Ni-CTF	Ni-N	3.4	2.08 ± 0.05	5.7 ± 1.5	1.08
Cu-TPP^a	Cu-N	4	1.99 ± 0.02	4.1 ± 4.0	1.03
Cu-CTF^a	Cu-N	3.4	2.01 ± 0.01	7.2 ± 2.1	1.03
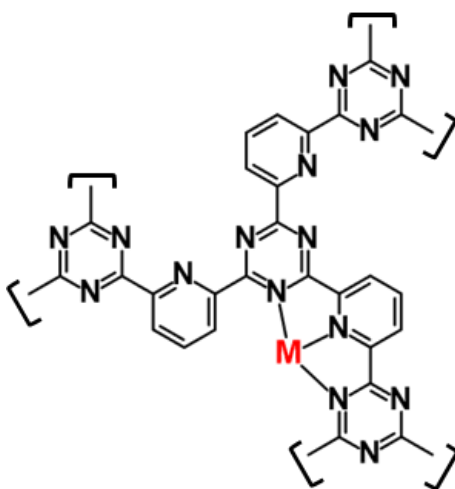
Fig. 9 An illustration showing the metal sites (M) in metal modified CTF (M-CTF) (weakly adsorbed species in electrolyte, anion species such as OH$^-$ and water molecule, and ethanol molecule used for the preparation of electrodes are not shown for clarity).

Because the data confirmed that the metal centers in the M-CTF/CP had lower coordination numbers than those in the corresponding M-TPP, the author next evaluated and compared the CO2RR activities of these samples. Changes in current density (j) at different potentials (U) were examined using M-CTF/CP electrodes in Ar-saturated phosphate buffer solutions (PBS, pH 6.8) and CO_2-saturated $KHCO_3$ solutions (pH 6.8). As shown in Fig. 10b, the cathodic current produced by the Ni-CTF/CP was significantly increased when CO_2 was present in the electrolyte. The onset potential for the reduction reaction in CO_2-saturated solutions was −0.48 V versus RHE, whereas a current attributed solely to the hydrogen evolution reaction (HER) was observed from −0.72 V vs. RHE in the absence of CO_2. In contrast, little or no increase in the reduction current in the presence of CO_2 was observed when using the Co-CTF/CP, Cu-CTF/CP or bare CTF/CP (Fig. 10a, c and d, respectively). The reduction peak of metal centers was not observed for M-CTF/CP in the absence of CO_2. This is likely because these peaks were overlapped with the HER current.
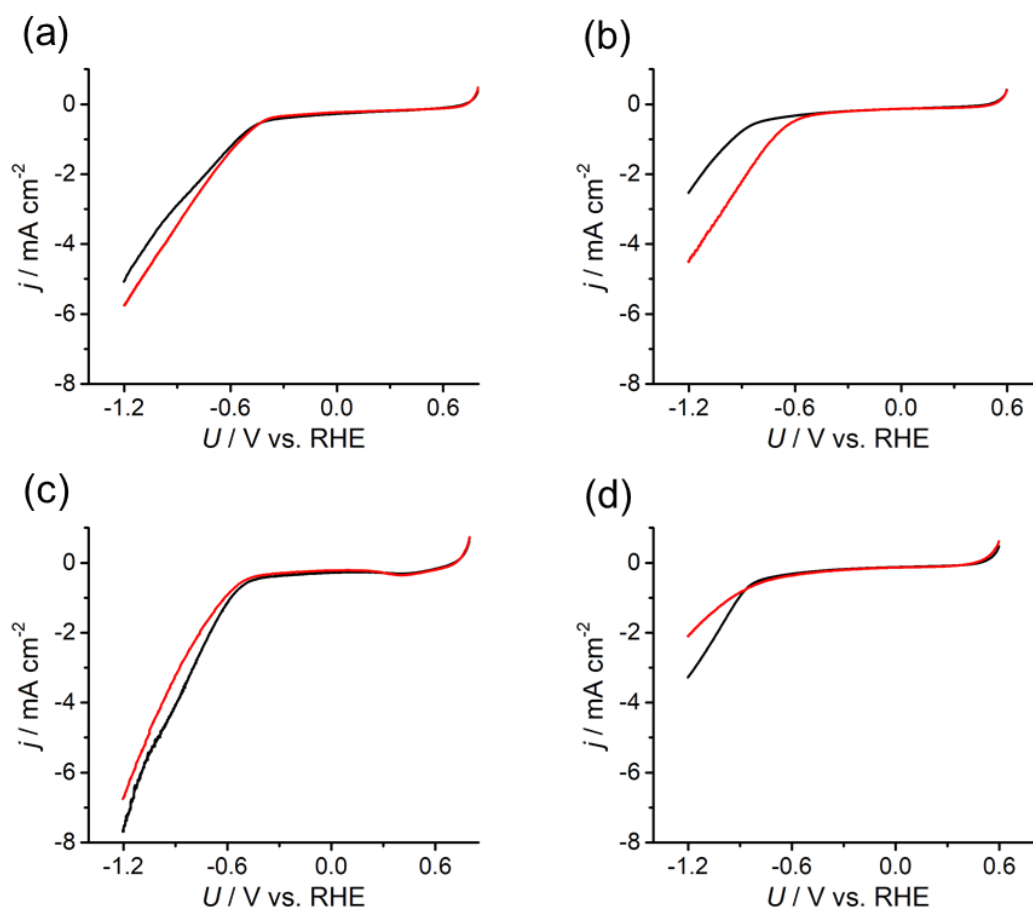
Fig. 10 Current density (j) versus potential (U) curves obtained from (a) Co-CTF/CP, (b) Ni-CTF/CP, (c) Cu-CTF/CP, and (d) CTF/CP in a phosphate buffer (saturated with Ar, black line) and a $KHCO_3$ electrolyte (saturated with CO_2, red line).

CVs alone cannot provide conclusive evidence for CO_2 reduction because the different electrolytes (PBS and $KHCO_3$ solutions) were used for the comparison. Thus, subsequently, the author quantitatively analysed the CO_2 reduction products in the gas phase using gas chromatography-mass spectrometry (GC-MS). A representative GC-MS chart is shown in Fig. 11. The effects of potential on the faradaic efficiency (FE) of the CO generation reaction using M-CTF/CPs in neutral solutions are summarized in Fig. 12. At the appropriate potential, the main product of the electrolysis in the presence of CO_2 when employing either Ni-CTF/CP or Co-CTF/CP was CO, whereas almost no CO evolution

was observed with the Cu-CTF/CP or bare CTF/CP throughout the entire experimental potential region. In particular, the Ni-CTF/CP exhibited CO formation with a FE exceeding 90% over the range of -0.8 to -0.9 V. It should be noted that the extent of CO evolution by the bare CTF/CP was almost negligible, indicating that the Ni/Co sites in the CTF served as the catalytic centers. In contrast, the FE of Cu-CTF/CP was similar with that of bare CTF/CP, meaning that the FE of Cu-CTF/CP was affected by the CO2RR activity of CTF frameworks to some extent. GC-MS and nuclear magnetic resonance (NMR, Fig. 13) data showed that H_2 was the other major product in all cases, along with trace amounts of methane (<0.5%). Note that only H_2 was observed in the absence of CO_2, indicating that the CO was generated not from the degradation of CTF/CP but from CO2RR (Fig. 11). The partial current density values (Fig. 14) during the CO generation using Ni-CTF/CP and Co-CTF/CP (3–4 A g^{-1}) were equivalent to those reported for a carbon-supported Au catalyst and metal-modified nitrogen-doped carbon catalysts [23,32–35]. The Tafel plots of M-CTF are shown in Fig. 15. The slope of Tafel plots for Ni-CTF/CP and Co-CTF/CP is 164 mV dec^{-1} and 204 mV dec^{-1}, respectively. In contrast, the Tafel slopes for Cu-CTF/CP (345 mV dec^{-1}) and CTF/CP (322 mV dec^{-1}) were much larger than that of Ni-CTF/CP and Co-CTF/CP, implying the inefficiency of Cu-CTF/CP and CTF/CP for CO_2 electrochemical reduction. The electrocatalytic stability of Ni-CTF/CP was evaluated at -0.65 V (vs. RHE) for 3 h in CO_2 saturated $KHCO_3$ electrolyte. As Fig. 16 shows, the FE for CO displayed almost negligible change, while the reduction current exhibited mildly decreased. As the stability for CO2RR catalysts developed in this study is not enough for the real application, further experiments to improve the stability by choosing the appropriate framework should be conducted.
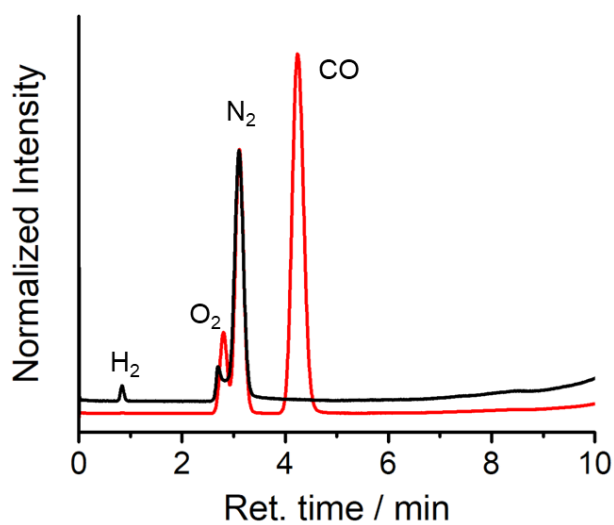
Fig. 11 A representative GC-MS result of Ni-CTF/CP catalyst at −0.9V vs RHE after 3C of electrons flow. Red line; Ni-CTF/CP in KHCO$_3$ solution under CO$_2$, Black line; Ni-CTF/CP in phosphate buffer solutions under Ar.
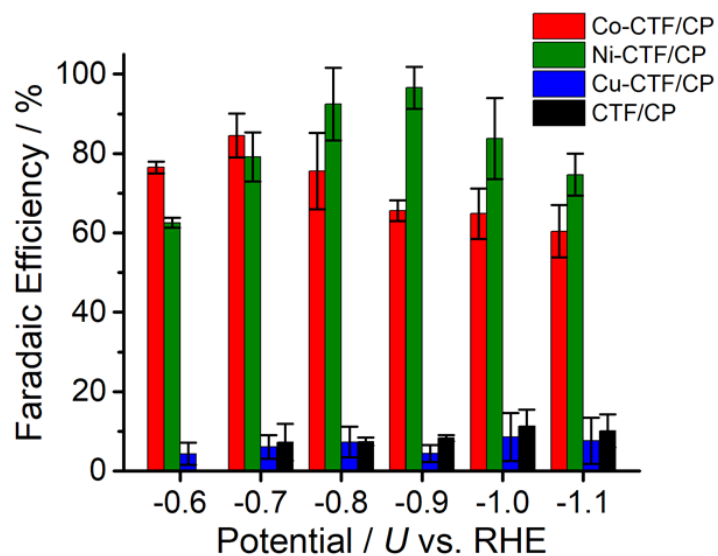
Fig. 12 Effect of potential on the faradic efficiency values during the CO2RR to generate CO using Co-CTF/CP (red), Ni-CTF/CP (green), Cu-CTF/CP (blue) and CTF/CP (black) in a KHCO$_3$ electrolyte (saturated with CO$_2$) at pH 6.8. The error bar represents the standard deviation from three experimental trial.
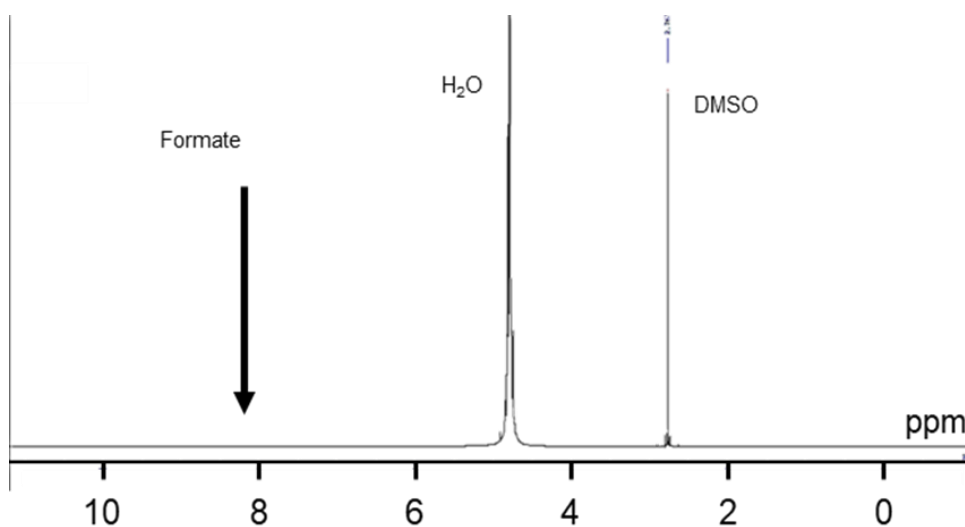
Fig. 13 NMR result of Ni-CTF/CP catalyst at −0.8V vs RHE for 1h. DMSO was added as internal standard.
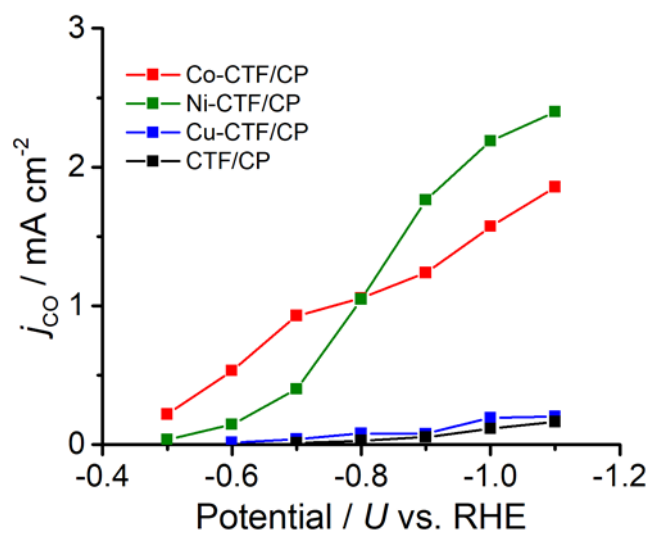
Fig. 14 Partial current density values during the CO generation reaction using Co-CTF/CP (red), Ni-CTF/CP (green), Cu-CTF/CP (blue) and CTF/CP (black).
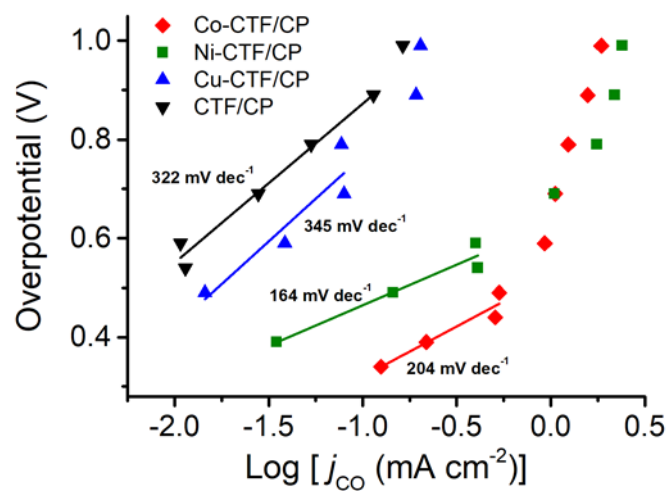
Fig. 15 Tafel plots at different over-potentials as a function with the CO partial current density on M-CTF/CP and CTF/CP catalysts.
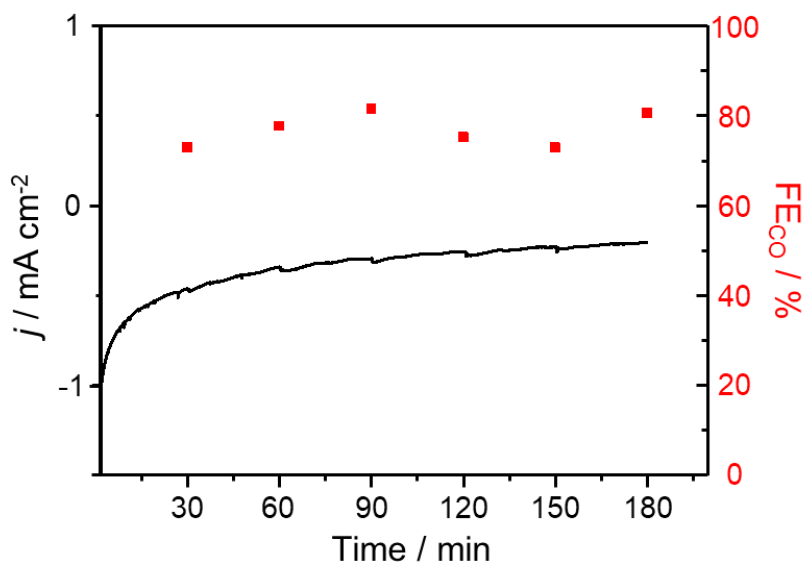
Fig. 16 Chronoamperometric and FE of CO results for the Ni-CTF/CP catalyst in CO_2-saturated $KHCO_3$ (0.1 M) solution at −0.65 V vs RHE for 3h.

For comparison purposes, the CO_2 reduction activities of M-TPP/CP were also tested. In the present work, the M-TPP samples were adsorbed on carbon nanoparticles prior to electrochemical measurements. An increase in the cathodic current from -0.5 V was observed when using Co-TPP/CP in the presence of CO_2, whereas the Ni- and Cu-TPP/CP showed no such increase (Fig. 17). The FE and partial current density values of the CO generation using M-TPP/CP are shown in Fig. 18a and b, respectively. The partial current density values in association with Co, Ni and Cu-TPP/CP were 1.1, 0.02 and 0.10 mA cm^{-2} at -0.9 V vs. RHE, respectively. The major product resulting from the use of Ni- and Cu-TPP was H_2 at all potentials. Therefore, only Co-TPP exhibited effective CO2RR activity among these three TPPs, a result that is consistent with previous studies [11,12].

Fig. 17 Current density (j) versus potential (U) curves obtained from (a) Ni-TPP/CP, (b) Co-TPP/CP, and (c) Cu-TPP/CP in a phosphate buffer (saturated with Ar, black line) or a KHCO$_3$ electrolyte (saturated with CO_2, red line).

Fig. 18 (a) Faradaic efficiency values and (b) partial current densities during CO generation for Co, Ni and Cu-TPP/CP. The error bar represents the standard deviation from three experimental trial.

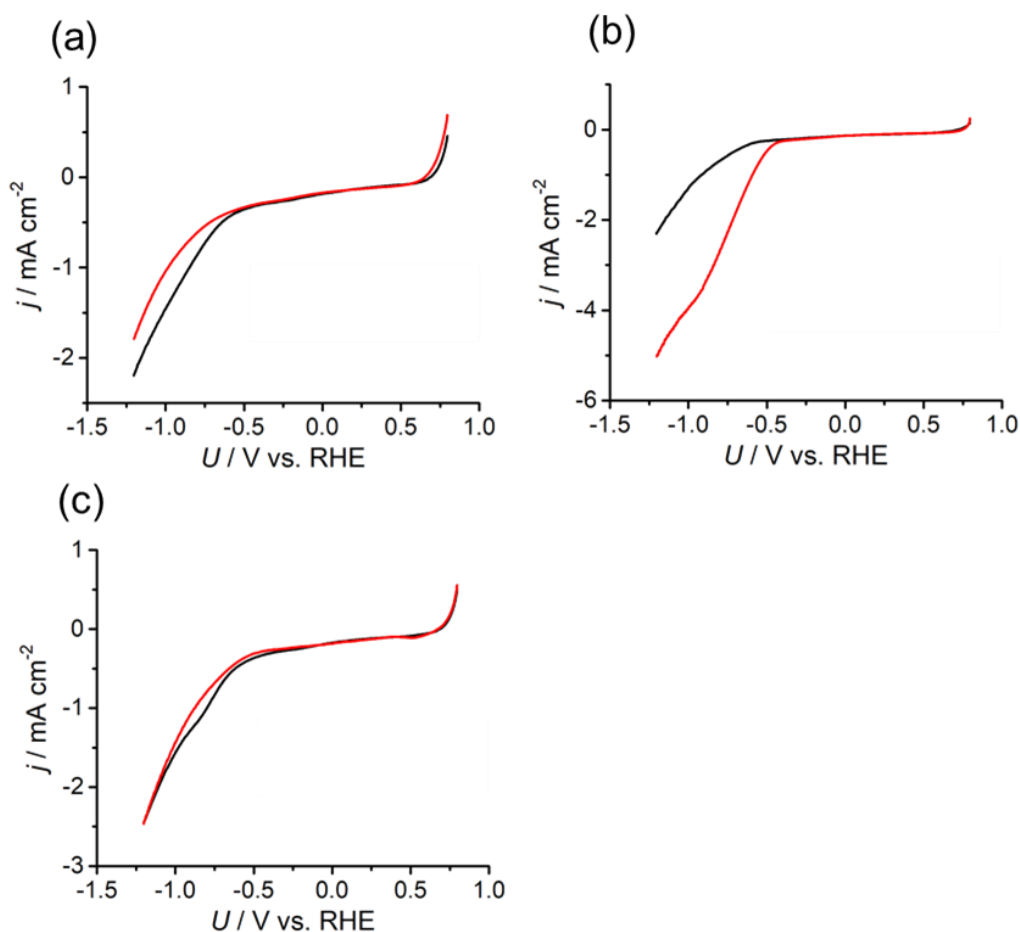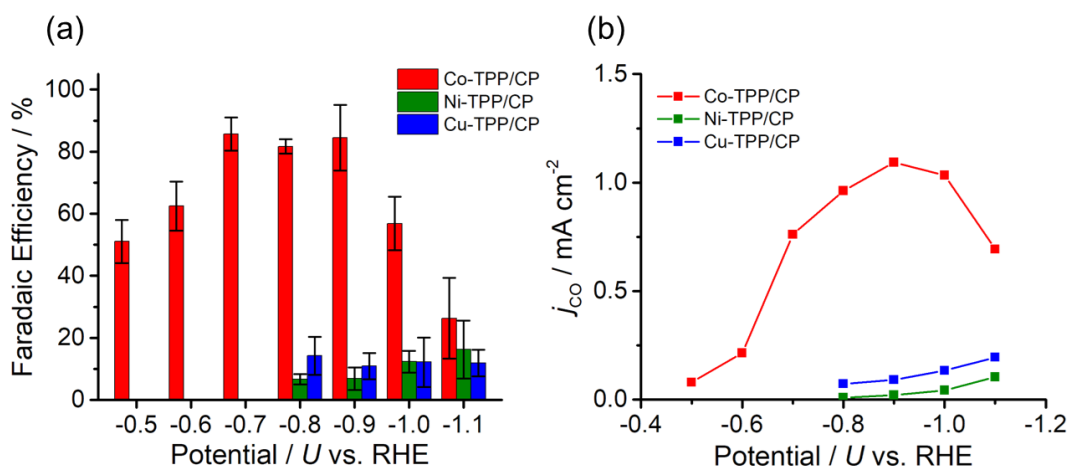The origin of the differences in the activities during CO_2 reduction to CO of the M-CTF and M-TPP were subsequently examined, employing DFT calculations. After structural optimization of M-CTF, the 3-coordination metal site was the most stable, as represented in Fig. 19 (for detail, see the Experimental section). Thus, the DFT results also revealed that the low coordination metal sites were stabilized by the CTF frameworks, which is basically consistent with the EXFAS results. Fig. 20 and Table 4 shows the free energy diagrams for the electrochemical reduction of CO_2 to CO on M-CTF and M-TPP at 0 V and −0.87 V vs. RHE, based on the computational hydrogen electrode model [6,21,23,36]. Notably, an increase in the number of d-electrons of the transition metal representing the active sites increased the Gibbs free energy change (ΔG) value associated with the formation of COOH* and CO* in the case of both the CTFs and TPPs (although the energy change was in the order of Co < Ni < Cu). These data are consistent with results reported for work with M-porphyrins in association with the CO2RR and also the HER and oxygen reduction reaction [7–9,11]. The rate determining step when using these materials is evidently the first reduction reaction: the formation of COOH* (reaction (1)). The free energy barrier of this step depends on the applied potential [6,21,23],

142

and so the author calculated the CO_2 limiting potential (U_L (CO_2)) for each catalyst, defined as the potential at which all elementary steps become exergonic, as summarized in Table 5. The $U_L(CO_2)$ obtained with the Co-TPP was approximately -0.6 V vs. RHE, whereas the values for the Cu-TPP and Ni-TPP were much more negative (<-2.0 V). Therefore, a low energy barrier to the formation of COOH* apparently resulted in the high CO_2 reduction activity exhibited by the Co-TPP. In addition, the U_L (CO_2) values of the CTFs were smaller than those of the corresponding TPP. In particular, the overall reaction pathway on the Ni-CTF becomes exergonic at -0.87 V vs. RHE (Fig. 20a), which essentially coincides with the potential range at which CO formation was observed on the same material. In contrast, the U_L (CO_2) of the Cu-CTF (-1.2 V) was 0.33 V more negative, and so the formation of COOH* is still endothermic at -0.87 V on the latter.
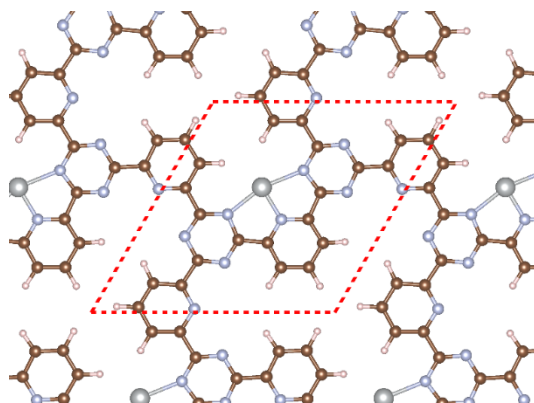
Fig. 19 Optimized structures of metal-CTF (Ni-CTF) for the DFT calculation (brown: C, pink: H, blue: N, gray: Ni). The red dashed line shows the unit cell. Almost the same structure was obtained for Cu- and Co-CTF. Red dashed line represents the unit cell. The detail structural parameters were shown in a previous related work report by the author and co-workers about CTF based electrocatalysts [18].
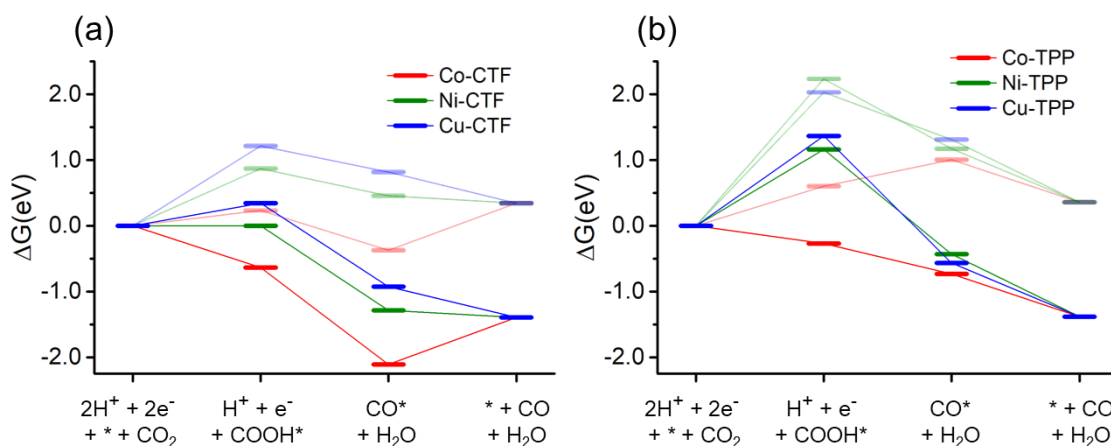
Fig. 20 Free energy diagrams for CO_2 reduction to CO on Co (red), Ni (green) and Cu (blue)-modified (a) CTF, and (b) TPP at 0 V (pale lines) and 0.87 V (dark lines).

Table 4 Calculated values for free energy diagrams in Fig. 20 (@ −0.87V).

	CTF / eV			TPP / eV		
	Co	Ni	Cu	Co	Ni	Cu
Step 1	-0.63584	0.000259	0.35071	-0.2668	1.162001	1.366827
Step 2	-2.11152	-1.28383	-0.92238	-0.73393	-0.4277	-0.56717
Step 3	-1.39497	-1.39497	-1.39497	-1.38032	-1.38032	-1.38032

Table 5 $U_L(CO_2)$ values for M-CTF and M-TPP specimens: the potentials at which all elementary steps become exergonic (*: The reaction (3) on Co-CTF is endothermic).

$U_L(CO_2)$ / eV	CTF	TPP
Co	-0.23*	-0.60
Ni	-0.87	-2.03
Cu	-1.22	-2.24

144

In this study, further reaction mechanism investigation by DFT calculation was conducted. First, adsorption behaviour of substrate (CO_2 molecule in this study) was investigated. In previous reports, it is suggested that adsorption of CO_2 molecule is favourable after one electron reduction of the metal center of active sites in some catalysts such as Co-porphyrin or Ni-cyclams [37,38]. The reaction scheme of formation of CO_2 adduct after one electron transfer is shown below:

$$[\text{M-catalysts}] + e^- \rightarrow [\text{M-catalysts}]^{-1} \qquad (4)$$

$$[\text{M-catalysts}]^{-1} + CO_2 \rightarrow [\text{M-catalysts} - CO_2]^- \qquad (5)$$
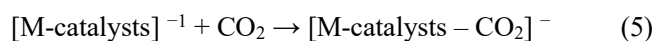
In this reaction scheme (equation (4) and (5)), one electron transfer from electrodes to metal centers (M) of catalysts (i.e. M-TPP or M-CTF) occurs at the initial steps, followed by adsorption of CO_2 molecule, then negatively charged CO_2 (namely, CO_2^-) adduct is formed [37]. Therefore, in this study, adsorption behaviour of CO_2 molecule and CO_2^- on M-TPPs and M-CTFs was systematically investigated by DFT calculations.

First, the CO_2 and CO_2^- formation on M-TPP is discussed. Table 6 shows the bond length between M in M-TPP or M-CTF and C atom in CO_2 (M-C), C-O bond length of adsorbed CO_2 molecule (C-O) and bond angle of CO_2 molecule (angle of O-C-O). Calculated M-C values are 3.33 Å, 3.29 Å and 3.26 Å for Co-TPP, Ni-TPP and Cu-TPP, respectively. Additionally, the bond angle of O-C-O of CO_2 molecule on M-TPPs is close to the original value of free CO_2 molecule (180º). These results indicate that neutral CO_2 molecule adduct on those M-TPPs is unstable, and that interaction between neutral CO_2 molecules and M-TPP is weak. For CO_2^- adduct on M-TPPs (Table 7), the result of CO_2^- species on Ni-TPP is essentially same as the result of neutral CO_2 molecule. On the other hand, M-C value of CO_2^- on Co-TPP is 2.29 Å, which is shorter value than that of neutral CO_2 molecule on Co-TPP. A bond angle of O-C-O is 146º, which is much smaller value than that of neutral CO_2

145

molecule. These results indicate that Co-TPP can form CO_2^- species on Co center. Additionally, CO_2^- is formed at η^1-C form as shown in Fig. 21. This result is essentially same as previous reports [25,38]. These results show that Co-TPP can proceed CO2RR through the formation of CO_2^- species, COOH* and CO* on Co center, whereas Ni-TPP and Cu-TPP cannot stabilize any CO2RR intermediates including CO_2^-. CO_2^- adduct on Cu-TPP was not calculated since Cu-TPP does not show redox activity of Cu [39,40].

For M-CTF case, based on the similar interpretation on CO_2 adsorption on M-TPPs, DFT calculation results show that Co-CTF and Ni-CTF can adsorb and interact with neutral CO_2 molecule, whereas Cu-CTF shows no interaction with it, judging from M-C bond length and bond angle of adsorbed CO_2 molecule. Notably, CO_2^- species are stabilized on all M-CTFs investigated in this study. The optimized structure of CO_2^- adduct on Ni-CTF is shown in Fig. 22. CO_2^- species are stabilized on η^1-C form for Co-TPP (similar structure to Fig. 21), whereas it is stabilized on η^2-side-on form on Ni-CTFs (Fig. 22). CO_2^- adduct on Co-CTF and Cu-CTF is similar structure to Ni-CTF. Especially for Ni-CTF case, considering that CO_2^- species is not stabilized on Ni of Ni-TPP, it is suggested that lower steric hindrance derived from lower coordination number of Ni in Ni-CTF is essential for η^2-side-on form of CO_2^- adduct and strong interaction between CO_2^- species and Ni in Ni-CTF.

Table 6 DFT calculation result of CO_2 adsorption on metal centers of M-TPP and M-CTFs. M-C distance represents the bond length of metal centers and adsorbing C atoms in CO_2 molecules, and C-O distance represents the bond length between C and O atoms of CO_2 molecule. O-C-O angle represents the bond angle of CO_2 molecules.

	M-C (Å)	C-O (Å)	C-O (Å)	Ave. of C-O (Å)	O-C-O (º)
Co-TPP	3.33	1.19	1.18	1.19	179.4
Ni-TPP	3.29	1.19	1.19	1.19	177.6
Cu-TPP	3.26	1.19	1.19	1.19	179.4
Co-CTF	1.88	1.22	1.28	1.25	144.4
Ni-CTF	1.88	1.21	1.28	1.25	145.4
Cu-CTF	3.29	1.18	1.19	1.19	179.4
Free CO_2		1.18	1.18	1.18	180.0

Table 7 DFT calculation results on formation of CO_2^- species on metal centers of M-TPP and M-CTFs. M-C distance represents the bond length of metal centers and adsorbing C atoms in CO_2^- species, and C-O distance represents the bond length between C and O atoms of CO_2^- species. O-C-O angle represents the bond angle of CO_2^- species. ([a]: Cu-TPP doesn't show redox couple of Cu but porphyrin rings [39,40], therefore CO_2^- adsorption on Cu-TPP was not calculated)

	M-C (Å)	C-O (Å)	C-O (Å)	Ave. of C-O (Å)	O-C-O (º)
Co-TPP	2.29	1.22	1.22	1.22	146.0
Ni-TPP	2.98	1.19	1.19	1.19	172.3
Cu-TPP[a]					
Co-CTF	1.85	1.23	1.29	1.26	139.7
Ni-CTF	1.87	1.22	1.27	1.25	142.7
Cu-CTF	2.02	1.24	1.24	1.25	140.3
Ni-cyclam	2.01	1.31	1.30	1.30	123.8
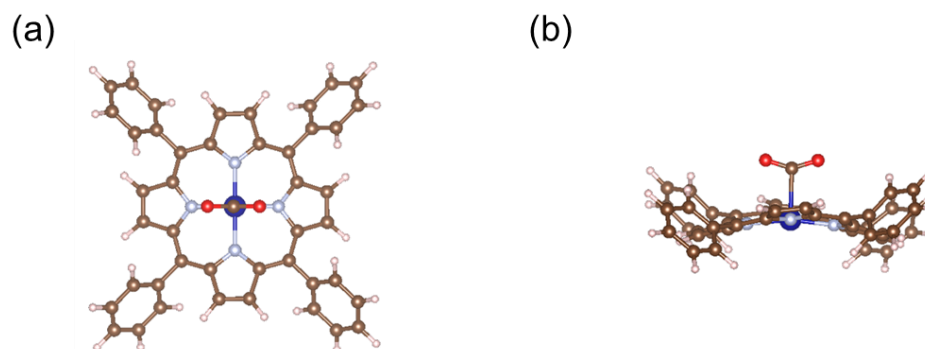
Fig. 21 Optimized structure of CO_2^- adduct on Co-TPP. (a) top view and (b) side view.
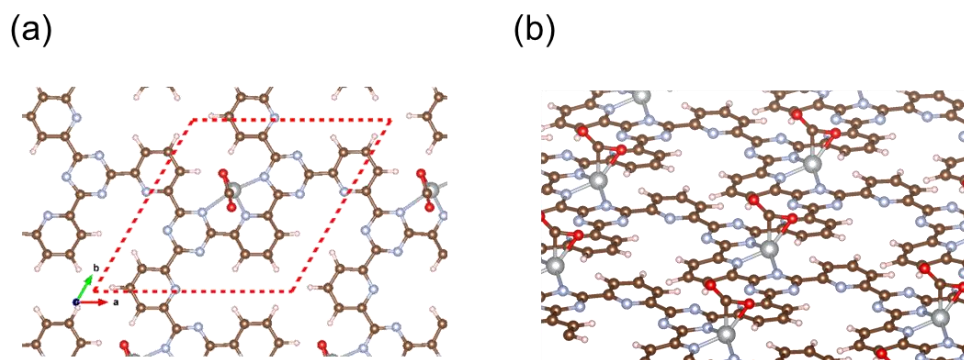
Fig. 22 Optimized structure of CO_2^- adduct on Ni-CTF. (a) top view and (b) slating view. CO2$^-$ species is stabilized at η^2-side-on form on Ni in Ni-CTF.

d orbital configuration from ligand field theory (LTF) supports the above mentioned DFT calculation results of CO2RR on M-TPP and M-CTF as discussed in chapter 2. Fig. 23a and b show the d-electron configuration of Co(I) and Ni(I)-TPP which are described by following Fig. 18 in section 2 in chapter 2. Previous reports suggested that electron π back donation from metal centers to CO_2 molecule and HOMO of metal center is important to CO_2 coordination to metal centers [41–44]. For Co(I)-TPP, the HOMO orbital is directed to z axis of the metal center, which is accessible for CO_2

molecules (Fig. 23a and c). Therefore, CO_2 molecule is expected to adsorb on Co(I)-TPP at η^1-C form as described in a previous report [37]. However, for Ni(I)-TPP, the HOMO orbital is occupied by ligand (TPP ligand, as shown in Fig. 23b and c). This is the possible reason why Ni(I)-TPP cannot adsorb CO_2 molecule and showed very poor CO2RR activity in this study. For Ni(I)-CTF, the HOMO orbital is not occupied by CTF because Ni-CTF possess an open coordination site as suggested by EXAFS result (Table 3 and Fig. 23e). Therefore, the author speculates that Ni centers in Ni-CTF can interact with CO_2 molecule as shown in Fig. 23d. The HOMO orbital shape of Ni(I)-CTF and π^* orbital of CO_2 molecule is well consistent with the DFT calculation result which shows that optimized structure of CO_2^- species on Ni(I)-CTF is η^2-side-on form (Fig. 23d).

CO2RR mechanism for Ni-cyclam [45,46], which is known to be active for CO generation by CO2RR as a homogeneous catalyst, was also investigated (detail calculated results are listed in Table 7) by DFT calculation. It is reported that CO_2 adduct after first one electron transfer from electrodes to Ni-cyclam is favourable [45]. Therefore, in this thesis, CO_2^- adduct on Ni-cyclam is also investigated. The bond length of Ni-C is 2.01 Å which is an essentially same value as the previous reports [45], and O-C-O bond angle is 123.8º, which is smaller value than previous reports (142.9º, [45]) as shown in Table 7 and Fig. 24. These results strongly indicate that Ni-cyclam can adsorb and interact with CO_2^-. Previous results indicated that hydrogen bond between H atom on N atom in cyclam ligand and O atom in CO_2 molecule may play an important role for stabilization of CO_2^- species on Ni center [45,46]. The bond length of O atoms in CO_2^- and H atom on N in cyclam ligand is 2.09 Å and 2.61 Å in this study, which is consistent with the value of previous reports (about 2.4 Å and 2.6 Å) [45]. The bond length is enough to form hydrogen bonding. Fig. 25 shows the free energy diagrams for the electrochemical reduction of CO_2 to CO on Ni-cyclam. This result shows that reaction intermediates of CO2RR are stable on Ni-cyclam and Ni-cyclam possesses CO2RR activity for CO production as reported previously [46]. Above mentioned DFT calculation results suggest that lower

steric hindrance of CTF ligand or more accessible d orbitals are essential for efficient CO2RR activity on Ni-CTF/CP. Additionally, modulation of detail structure of metal centers such as coordination number or hydrogen bonding ability of framework to CO2RR intermediates by appropriate choice of framework possibly increase the CO2RR activity for Co, Ni, Cu modified CTF (and COF) based catalysts. The author expects that Cu-based catalysts with a further low-coordination number (less than 3) exhibit efficient CO2RR activity.

Fig. 23 Representative d-electron configuration of (a) Co(I)-TPP, (b) Ni(I)-TPP and (d) Ni(I)-CTF and Ni(I)-CTF with CO_2 molecule [41–44]. Schematic illustration of coordination structure of (c) M-TPP and (e) M-CTF (metal-N3 with open coordination site).

Fig. 24 (a) Molecular structure of Ni-cyclam and optimized structure of CO_2^- adduct on Ni-cyclam from (b) top view and (c) side view. CO_2^- species is stabilized at η^1-C on Ni in Ni-cyclam.
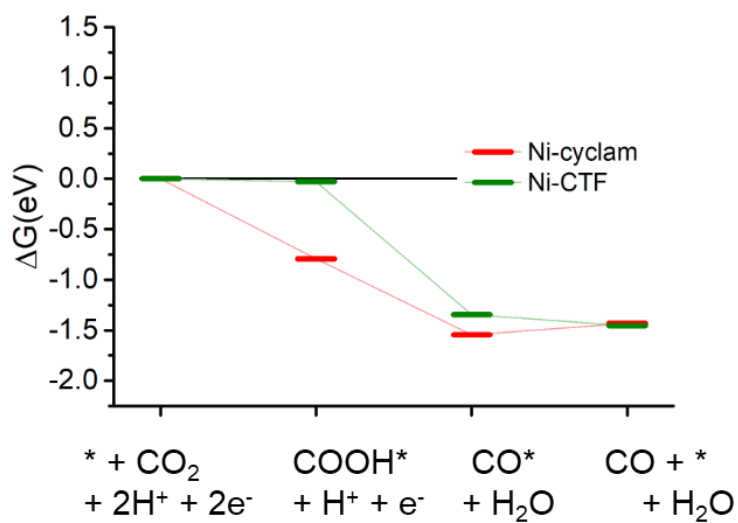

Fig. 25 Free energy diagram of the CO2RR on Ni-CTF (green, replotted from Fig. 20) and Ni-cyclam (red). $U = -0.9$ V. * denote the adsorption site on each catalyst.

The partial current densities during CO generation are plotted against ΔG (COOH*) in Fig. 26, clearly indicating that the low ΔG (COOH*) is important for high CO2RR activity, and also showing that the Ni active sites appear quite high on the plot of CO2RR activity upon changing the ligand from TPP to CTF. That is, by transitioning the ligand from TPP to CTF, a lower ΔG (COOH*) was obtained such that Ni became the optimal metal species. In the case of the Co-CTF/CP, the release of CO (reaction (3)), which is independent of the applied potential, was an endothermic reaction. As mentioned in the Introduction, the rate-determining step for CO2RR, which depends on the adsorption energy of CO and COOH, is the reaction (1) or the reaction (3). However, the existence of the scaling relationship of them does not allow us to independently control these two adsorption energies [4,5,47]. Therefore, on the basis of the DFT calculations, there should be the volcano-type relation accompanied with the single peak which locates between Co-CTF and Co-TPP in Fig. 26. The rate-determining step can be evaluated by the position in the volcano plot against the peak. Co-CTF has lower ΔG (COOH*) than the optimal value (the peak of the volcano plot), resulting that the rate-determining step was the reaction (3) (CO desorption). Thus, in contrast to Cu-based catalysts, Co based catalysts with a further low-coordination number, which bind CO more strongly, should show poor CO2RR activity. In contrast, the rate-determining step of the other catalysts in the higher ΔG (COOH*) side was the reaction (1) (CO_2 activation). To complete the wide range of volcano-type curve, the investigation of CO2RR activity of catalysts with different metal species and coordination numbers should be conducted.

At this point, the author can explain the origin of the lower ΔG (COOH) values exhibited by the M-CTF/CP compared to those for the corresponding M-TPP/CP. The EXAFS results demonstrate that the metal atoms in the CTF have unsaturated coordination structures (that is, low coordination numbers, as shown in Fig. 9), compared with the metals in the porphyrin-like ligands. Calle-Vallejo and co-authors have used first principles calculations to show that metal sites with lower coordination

values have higher adsorption energies because they possess numerous accessible d-orbitals as well as low steric hindrance [13,15,16]. Therefore, metal atoms in CTF with low coordination numbers can more strongly bind small molecules than those in N4 macrocycles, resulting in a low free energy barrier to the first reaction step (COOH* formation) as well as initial first CO_2 molecule or CO_2^- species adsorption.
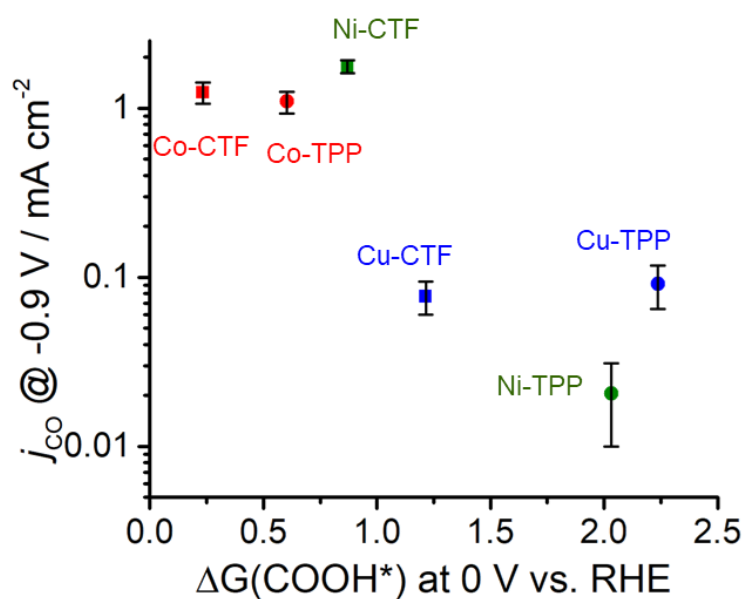
Fig. 26 Relationship between ΔG (COOH*) at 0 V and j_{co} at −0.9 V. The error bar represents the standard deviation from three experimental trial.

Conclusions

In the present work, the author developed a novel route to precisely tune the adsorption energies of critical intermediate species for efficient CO2RR through the modulation of the coordination number of active centers. The Ni and Co-CTF effectively reduced CO_2 to CO, whereas, among the M-TPP, only the Co-TPP showed any activity. DFT calculations demonstrated that the free energy barrier of the first reduction step, the formation of adsorbed COOH, was decreased by changing the ligands from TPP to CTF. The lower coordination metal sites were stabilized on the CTF due to their rigid framework, allowing COOH* species to be absorbed at these low coordination sites. Consequently, the Ni based catalyst obtained using CTF rather than TPP ligands was situated at a higher position on the volcano-like CO2RR activity plot. Thus, the present work provides a new avenue to design efficient catalysts for CO2RR.

References

[1]   C. Costentin, M. Robert, J. M. Saveant, *Chem. Soc. Rev.* **2013**, *42*, 2423-2436.

[2]   J. Qiao, Y. Liu, F. Hong, J. Zhang, *Chem. Soc. Rev.* **2014**, *43*, 631-675.

[3]   S. Lin, C. S. Diercks, Y. B. Zhang, N. Kornienko, E. M. Nichols, Y. Zhao, A. R. Paris, D. Kim, P. Yang, O. M. Yaghi, C. J. Chang, *Science* **2015**, *349*, 1208-1213.

[4]   K. P. Kuhl, T. Hatsukade, E. R. Cave, D. N. Abram, J. Kibsgaard, T. F. Jaramillo, *J. Am. Chem. Soc.* **2014**, *136*, 14107-14113.

[5]   A. A. Peterson, J. K. Nørskov, *J. Phys. Chem. Lett.* **2012**, *3*, 251-258.

[6]   K. Chan, C. Tsai, H. A. Hansen, J. K. Nørskov, *ChemCatChem* **2014**, *6*, 1899-1905.

[7]   F. Calle-Vallejo, N. G. Inoglu, H.-Y. Su, J. I. Martínez, I. C. Man, M. T. M. Koper, J. R. Kitchin, J. Rossmeisl, *Chem. Sci.* **2013**, *4*.

[8]   F. Calle-Vallejo, J. I. Martinez, J. M. Garcia-Lastra, J. Rossmeisl, M. T. Koper, *Phys. Rev. Lett.* **2012**, *108*, 116103.

[9]   F. Calle-Vallejo, J. I. Martinez, J. Rossmeisl, *Phys. Chem. Chem. Phys.* **2011**, *13*, 15639-15643.

[10]   C. Costentin, M. Robert, J. M. Saveant, *Acc. Chem. Res.* **2015**, *48*, 2996-3006.

[11]   M.-J. Cheng, Y. Kwon, M. Head-Gordon, A. T. Bell, *J. Phys. Chem. C* **2015**, *119*, 21345-21352.

[12]   N. Sonoyama, M. Kirii, T. Sakata, *Electrochem. Commun.* **1999**, *1*, 213-216.

[13]   H. Li, Y. Li, M. T. Koper, F. Calle-Vallejo, *J. Am. Chem. Soc.* **2014**, *136*, 15694-15701.

[14]   Z. Zhao, Z. Chen, X. Zhang, G. Lu, *J. Phys. Chem. C* **2016**, *120*, 28125-28130.

[15]   F. Calle-Vallejo, J. I. Martinez, J. M. Garcia-Lastra, P. Sautet, D. Loffreda, *Angew. Chem. Int. Ed.* **2014**, *53*, 8316-8319.

[16] F. Calle-Vallejo, D. Loffreda, M. T. Koper, P. Sautet, *Nat. Chem.* **2015**, *7*, 403-410.

[17] X. Ma, H. Xin, *Phys. Rev. Lett.* **2017**, *118*, 036101.

[18] T. Yoshioka, K. Iwase, S. Nakanishi, K. Hashimoto, K. Kamiya, *J. Phys. Chem. C* **2016**, *120*, 15729-15734.

[19] T. Ozaki, *Phys. Rev. B* **2003**, *67*.

[20] T. Ozaki, H. Kino, *Phys. Rev. B* **2004**, *69*.

[21] H. Mistry, R. Reske, Z. Zeng, Z. J. Zhao, J. Greeley, P. Strasser, B. R. Cuenya, *J. Am. Chem. Soc.* **2014**, *136*, 16473-16476.

[22] F. Calle-Vallejo, M. T. Koper, *Angew. Chem. Int. Ed.* **2013**, *52*, 7282-7285.

[23] W. Zhu, Y. J. Zhang, H. Zhang, H. Lv, Q. Li, R. Michalsky, A. A. Peterson, S. Sun, *J. Am. Chem. Soc.* **2014**, *136*, 16132-16135.

[24] K. Kamiya, R. Kamai, K. Hashimoto, S. Nakanishi, *Nat. Commun.* **2014**, *5*, 5040.

[25] R. Kamai, K. Kamiya, K. Hashimoto, S. Nakanishi, *Angew. Chem. Int. Ed.* **2016**, *55*, 13184-13188.

[26] P. Kuhn, M. Antonietti, A. Thomas, *Angew. Chem. Int. Ed.* **2008**, *47*, 3450-3453.

[27] R. Palkovits, M. Antonietti, P. Kuhn, A. Thomas, F. Schuth, *Angew. Chem. Int. Ed.* **2009**, *48*, 6909-6912.

[28] G. Kwag, E. Park, S. Kim, *Bull. Korean Chem. Soc.* **2004**, *25*, 298-300.

[29] A. K. Agegnehu, C.-J. Pan, J. Rick, J.-F. Lee, W.-N. Su, B.-J. Hwang, *J. Mater. Chem.* **2012**, *22*.

[30] A. Anspoks, A. Kuzmin, *J. Non-Cryst. Solids* **2011**, *357*, 2604-2610.

[31] B. Ravel, M. Newville, *J. Synchrotron Radiat.* **2005**, *12*, 537-541.

[32] W. Zhu, R. Michalsky, O. Metin, H. Lv, S. Guo, C. J. Wright, X. Sun, A. A. Peterson, S. Sun, *J. Am. Chem. Soc.* **2013**, *135*, 16833-16836.

[33]   A. S. Varela, N. Ranjbar Sahraie, J. Steinberg, W. Ju, H. S. Oh, P. Strasser, *Angew. Chem. Int. Ed.* **2015**, *54*, 10758-10762.

[34]   H. Nishihara, T. Hirota, K. Matsuura, M. Ohwada, N. Hoshino, T. Akutagawa, T. Higuchi, H. Jinnai, Y. Koseki, H. Kasai, Y. Matsuo, J. Maruyama, Y. Hayasaka, H. Konaka, Y. Yamada, S. Yamaguchi, K. Kamiya, T. Kamimura, H. Nobukuni, F. Tani, *Nat. Commun.* **2017**, *8*, 109.

[35]   P. Su, K. Iwase, S. Nakanishi, K. Hashimoto, K. Kamiya, *Small* **2016**, *12*, 6083-6089.

[36]   J. K. Nørskov, J. Rossmeisl, A. Logadottir, L. Lindqvist, J. R. Kitchin, T. Bligaard, H. Jónsson, *J. Phys. Chem. B* **2004**, *108*, 17886-17892.

[37]   J. Shen, M. J. Kolb, A. J. Göttle, M. T. M. Koper, *J. Phys. Chem. C* **2016**, *120*, 15714-15721.

[38]   J. Shen, R. Kortlever, R. Kas, Y. Y. Birdja, O. Diaz-Morales, Y. Kwon, I. Ledezma-Yanez, K. J. Schouten, G. Mul, M. T. Koper, *Nat. Commun.* **2015**, *6*, 8177.

[39]   A. Antipas, D. Dolphin, M. Gouterman, E. C. Johnson, *J. Am. Chem. Soc.* **1978**, *100*, 7705-7709.

[40]   A. Wolberg, J. Manassen, *J. Am. Chem. Soc.* **1970**, *92*, 2982-2991.

[41]   S. Sakaki, *J. Am. Chem. Soc.* **1992**, *114*, 2055-2062.

[42]   S. Sakaki, K. Kitaura, K. Morokuma, *Inorg. Chem.* **1982**, *21*, 760-765.

[43]   S. Sakaki, T. Aizawa, N. Koga, K. Morokuma, K. Ohkubo, *Inorg. Chem.* **1989**, *28*, 103-109.

[44]   S. Sakaki, *Bull. Chem. Soc. Jap.* **2015**, *88*, 889-938.

[45]   J. Song, E. L. Klein, F. Neese, S. Ye, *Inorg. Chem.* **2014**, *53*, 7500-7507.

[46]   J. D. Froehlich, C. P. Kubiak, *Inorg. Chem.* **2012**, *51*, 3932-3934.

[47]   H. A. Hansen, J. B. Varley, A. A. Peterson, J. K. Norskov, *J. Phys. Chem. Lett.* **2013**, *4*, 388-392.

Chapter 5

Conclusion and perspective

Conclusion

Adsorption energy (ΔE_{ads}) of reaction intermediates is one of the important factors which determine the reaction activity and selectivity on various electrochemical reactions. Especially, coordination structure of metal center is one of the essential determining factors of ΔE_{ads} on reaction intermediates for metal containing electrocatalysts. On the basis of these background, in this thesis, the author attempted to synthesize electrocatalysts with high activity or selectivity by modulation of coordination structure of metal centers with covalent organic framework (COF). In this thesis, the author developed covalent triazine frameworks (CTFs), which is a kind of COF and possess 1,3,5-triazine unit as a linker, modified with first transition metal (M-CTF) as electrocatalysts for oxygen reduction reaction (ORR), nitrobenzene reduction reaction (NBRR) and carbon dioxide reduction reaction (CO2RR).

In chapter 2, the author successfully synthesized Cu modified CTF (Cu-CTF) with singly isolated Cu center. In this chapter, it is demonstrated that Cu-CTF can function as a non-noble metal catalyst for ORR. Notably, ORR onset potential of synthesized Cu-CTF is 810 mV vs. RHE (pH 7), which is the highest value at neutral pH among synthetic Cu-based molecular catalysts reported so far. For Cu-CTF, it is revealed that Cu center possesses open coordination site, lower coordination number compared with Cu porphyrin (coordination number = 4), which is hardly achieved by conventional organometallic complex based electrocatalysts. First principle density functional theory (DFT) calculation revealed that O_2 molecules and ORR intermediates are adsorbed on open coordination site of Cu-CTF. Importantly, on the basis of ligand field theory (LFT) and proposed ORR mechanism of

Cu containing enzymes in previous reports, it is proposed that open coordination site is essential for Cu based molecular catalysts to catalyze ORR. Thus, it is suggested that inflexible framework structure of CTF might be essential to construct unsaturated coordination structure with open coordination site which is known to be active for ORR, stronger adsorption of O_2 molecule and ORR intermediates, and high ORR activity.

In this chapter, further enhancement of ORR activity of Cu-CTF was attempted. Since ORR is mediated by Cu(I) species, a positive shift of the Cu(II/I) potential is required to increase the ORR onset potential. On the basis of HSAB theory, Cu ions coordinated to S show higher Cu(II/I). However, auto-reduction of Cu(II) to Cu(I) in Cu complexes simultaneously occurs due to high redox potentials of Cu, resulting in formation of a closed tetrahedral configuration in conventional Cu-S complexes. Cu centers with tetrahedral configuration are known to be inactive for ORR because of lack of O_2 adsorption site. To mitigate this problem, the author synthesized a Cu-modified S-linked CTF (Cu-S-CTF) as an electrocatalyst for ORR in neutral solutions. It is revealed that Cu center in Cu-S-CTF exists as Cu(I), and that Cu center takes a distorted three-coordinated structure with accessible coordination sites for O_2. This suppression of spontaneous formation of the tetrahedral configuration with formation of Cu(I) is supposed to be derived from inflexibility of S-CTF. ORR onset potential of Cu-S-CTF was 880 mV vs. RHE at pH 7, which is higher than that of Cu-CTF by 70 mV. This is the first example of an ORR electrocatalyst containing Cu sites with both high redox potential and oxygen-binding ability. This work confirmed that regulation of the coordination structure of Cu by a rigid framework structure is an effective method to solve a trade-off relationship between the high redox potential and the oxygen-binding ability of Cu for Cu-based ORR catalysts. It should be noted that this concept can be expanded to other electrochemical reaction, such as CO2RR and nitrate reduction reaction.

In chapter 3, the electrocatalytic activity of nitrobenzene reduction to aniline in neutral

aqueous solutions on Cu-CTF synthesized in chapter 2 was evaluated. In this chapter, it is revealed that Cu-CTF can catalyze selective electrochemical reduction of nitrobenzene to aniline in neutral aqueous solutions with a faradaic efficiency reaching up to 65% at −0.6 V versus Ag/AgCl. Electrochemical characterization indicated that the organic framework part of Cu-CTF reduced nitrobenzene to phenylhydroxylamine, followed by the reduction of phenylhydroxylamine to aniline at single Cu sites. The detail electrochemical characterization by addition of the reaction intermediates of nitrobenzene reduction such as nitrosobenzene and phenylhydroxylamine confirmed that those reaction intermediates desorption from the surface of the catalyst was suppressed by addition of the single Cu center. This work suggests that both of functionalization of framework and coordination structure regulation of metal center can change reaction selectivity of the metal-modified COF-loaded catalysts.

In chapter 4, CO2RR activity of M-CTFs (M: Co, Ni, Cu) was systematically investigated. For CO2RR, adsorbed COOH* and CO* (* represents the active site of the catalysts) are suggested as important reaction intermediates. Thus, in this work, the author attempted to use coordination number as a control parameter to tune ΔE_{ads} of CO2RR intermediates. For CO2RR activity, Co-CTF and Ni-CTF effectively reduced CO_2 to CO. Specifically, the faradaic efficiency of the Ni-CTF during CO formation reached over 90% at −0.9 V versus RHE. The performance of Ni-CTF is much higher than that of the corresponding metal-porphyrin (using tetraphenylporphyrin; TPP). DFT calculations demonstrated that CO_2 molecule (substrate) and the intermediate species (adsorbed COOH*) were stabilized on the open coordination site of Ni modified in the CTF due to the low-coordination structure of metal centers (lower steric hindrance and more accessible d orbitals of this support). This work suggests that precise control of coordination structure of metal center is quite important to tune the CO2RR activity.

In the series of these researches, the author demonstrated that metal center in M-COFs

(CTFs) can possess unsaturated coordination structure with open coordination site (lower coordination number than 4 in metal-N4 macrocyclic compounds). This means that coordination structure of metal centers modified in COFs can be controlled by COF framework structure. Especially, DFT calculation results and d orbital configuration from LFT suggest that metal centers in M-CTFs strongly adsorb reaction intermediates due to low steric hindrance of ligand (CTFs) and more accessible d orbitals. However, in general, the metal centers with open coordination site is inherently unstable because of its high surface energy and reactivity. Therefore, aggregation of metal atoms or ligand reorganization easily occur to stabilize such metal centers. Thus, it is suggested that COFs, which possess cross-linked and rigid framework structure, might be new platforms to regulate the coordination structure and catalytic activity as intended by sophisticated choice of framework structure.

Perspective

In this thesis, the author demonstrated that M-COFs show specific catalytic activity and selectivity due to the existence of open coordination site on metal centers. Various types of COFs were synthesized so far. Thus, the author suggests (1) regulation of the coordination structure (coordinating atoms and geometric structure) by sophisticated choice of framework, and (2) controlling the reaction field by COFs to develop COF based electrocatalysts as described below.

First, as demonstrated in chapter 2, changing coordinating atoms and regulation of coordination structure of metal centers by COF framework structure are promising approaches for further improvement of catalytic activity since various types of COFs were synthesized so far. Fig. 1 shows representative COFs (and CTFs) with various kinds of framework structure and function groups. Those COFs with different pore structure and different function groups can be synthesized by an appropriate choice of precursors (monomers) and synthesis method [1–7]. The coordination structure of metal centers is expected to be controlled by those framework structure. For example, Co modified COF with bipyridine moiety was developed as an electrocatalyst for water oxidation in neutral solutions [8]. As shown in this thesis and metal modified COF based electrocatalysts in previous reports, various metal modified COFs can function as efficient electrocatalysts with specific catalytic activity and selectivity by tuning coordination structure and adsorption energy of reaction intermediates. Additionally, hydrogen bonding between reaction intermediates and function groups of COFs might be effective to stabilize reaction intermediates as suggested in chapter 4. Thus, addition of function groups such as SO_3H and OH, which possess hydrogen bonding ability, in framework can be a promising approach.

Second, construction of multi-nuclear active sites is also promising approach to achieve lower over-potential and promote multi-electron transfer reaction. For example, multi-copper oxidases,

which catalyze ORR, and manganese clusters, which catalyze oxygen evolution reactions, are well known enzymes which contains multi-nuclear active centers in their structure. It is well known that these multi-nuclear active centers are essential to realize an efficient multi-electron transfer reaction. If we can introduce metal ions in the crystalized micropores of COFs with high concentration, it is expected that multi-nuclear active centers are constructed in the pores of COFs (schematic illustrations are shown in Fig. 2). Such multi-nuclear centers are achieved only by specific natural enzymes and organometallic complexes. If the multi-nuclear active centers can be constructed efficiently in the pores of COFs, further development of the COF based electrocatalysts would be achieved. It is also expected that reaction electron number would increase by multi-nuclear active centers since electrons are transferred simultaneously from multiple metal active centers. In this thesis, the CO_2 reduction product by M-CTFs is CO, which is two-electron reduction product. Thus, if the multi-active center containing COFs are applied to CO_2 reduction electrocatalysts, more reduced product such as methane, eight-electron reduction product, and methanol, 6-electron reduction product, might be generated.

In addition, controlling the reaction field of active centers by COFs might be effective approach to enhance the catalytic activity and reaction selectivity since transport rate of ions or substrates in solution phase is expected to be controlled by introducing specific function groups to the COFs. Especially, modulation of proton transfer rate and hydrophilicity and/or hydrophobicity (reaction field) of catalytic centers would be promising approaches to enhance catalytic activity and selectivity for metal particles or bulk metals hybridized with COFs. For example, Y. Katayama et al. reported that the local ion supply to the metal electrodes can change the electrocatalytic activity [9]. As H^+ or OH^- transfer rate should be an important factor which determines the electrocatalytic activity since many electrocatalytic reactions proceed with transfer of these species. On the basis of these backgrounds, it is expected that modification of function groups of COFs hybridized with metal electrodes or metal nanoparticles can change the reaction selectivity of them (schematic illustration is

shown in Fig. 3). As function group of side chains of COFs can be controlled by appropriated choice of monomers or post modification process, product selectivity control by modulation of proton transfer rate or the diffusion rate of substrate to catalytic centers would be achieved. As this strategy, control of reaction activity and selectivity by regulation of reaction field, is adopted by natural enzymes, electrocatalysts composed of COFs can be one of the promising materials to show higher activity by mimicking the structure and the mechanism of enzymes.
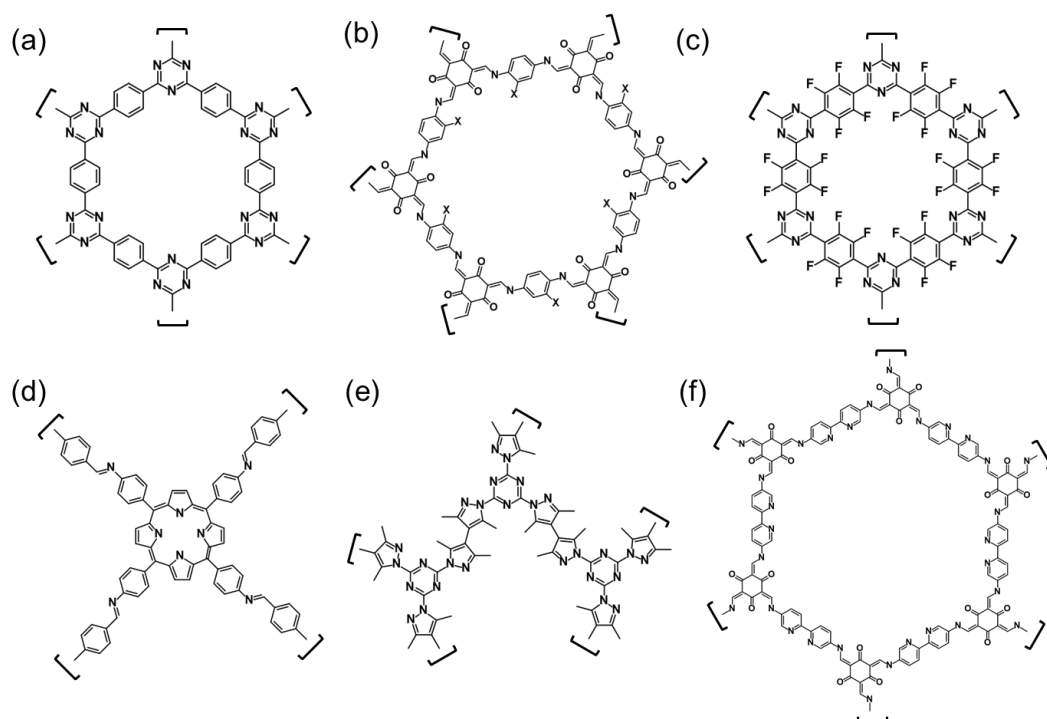
Fig. 1 Representative structure of COFs synthesized so far from (a) ref. [1], (b) ref. [2,3], (c) ref. [4], (d) ref. [5], (d) ref. [6], (f) ref. [7,8].
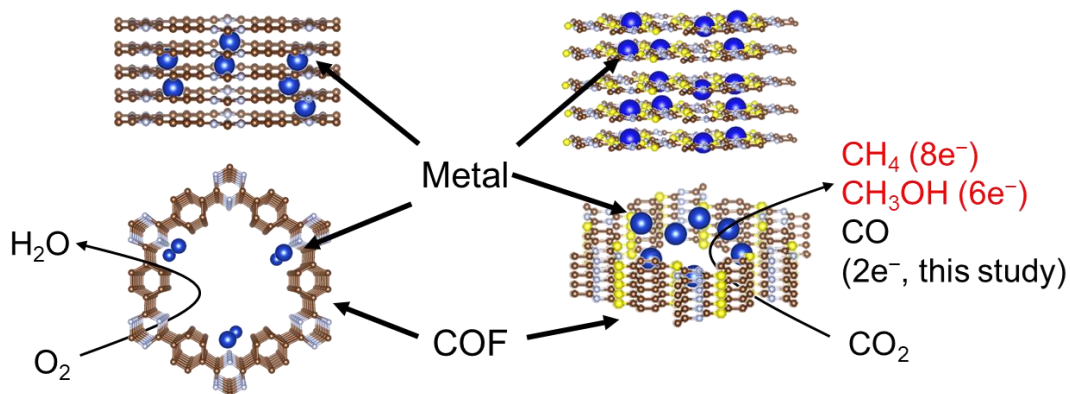
Fig. 2 Schematic illustration of metal modified COF electrocatalysts with multi nuclear active centers.
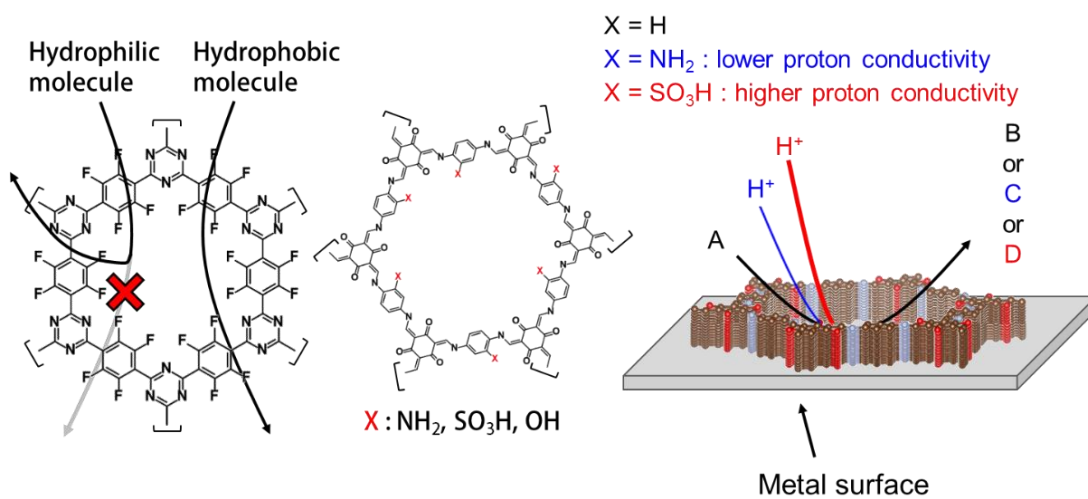
Fig. 3 Schematic illustration of COF modified metal (electrode or particle) electrocatalysts.

References

[1]   P. Kuhn, A. Thomas, M. Antonietti, *Macromolecules* **2009**, *42*, 319-326.

[2]   J. L. Segura, M. J. Mancheno, F. Zamora, *Chem. Soc. Rev.* **2016**, *45*, 5635-5671.

[3]   Y. Peng, Z. Hu, Y. Gao, D. Yuan, Z. Kang, Y. Qian, N. Yan, D. Zhao, *ChemSusChem* **2015**, *8*, 3208-3212.

[4]   Y. Zhao, K. X. Yao, B. Teng, T. Zhang, Y. Han, *Energy Environ. Sci.* **2013**, *6*.

[5]   S. Lin, C. S. Diercks, Y. B. Zhang, N. Kornienko, E. M. Nichols, Y. Zhao, A. R. Paris, D. Kim, P. Yang, O. M. Yaghi, C. J. Chang, *Science* **2015**, *349*, 1208-1213.

[6]   J. Liu, K. K. Yee, K. K. Lo, K. Y. Zhang, W. P. To, C. M. Che, Z. Xu, *J. Am. Chem. Soc.* **2014**, *136*, 2818-2824.

[7]   D. B. Shinde, H. B. Aiyappa, M. Bhadra, B. P. Biswal, P. Wadge, S. Kandambeth, B. Garai, T. Kundu, S. Kurungot, R. Banerjee, *J. Mater. Chem. A* **2016**, *4*, 2682-2690.

[8]   H. B. Aiyappa, J. Thote, D. B. Shinde, R. Banerjee, S. Kurungot, *Chem. Mater.* **2016**, *28*, 4375-4379.

[9]   Y. Katayama, T. Okanishi, H. Muroyama, T. Matsui, K. Eguchi, *J. Phys. Chem. C* **2015**, *119*, 9134-9141.

List of publications

[1] **K. Iwase**, T. Yoshioka, S. Nakanishi, K. Hashimoto, K. Kamiya.

"Copper-Modified Covalent Triazine Frameworks as Non-Noble-Metal Electrocatalysts for Oxygen Reduction" *Angew. Chem. Int. Ed.*, **2015**, 54, 11068.

[2] **K. Iwase,** N. Fujinami, K. Hashimoto, K. Kamiya, S. Nakanishi.

"Cooperative Electrocatalytic Reduction of Nitrobenzene to Aniline in Aqueous Solution by Copper Modified Covalent Triazine Framework" *Chem. Lett.*, **2018**, 47, 304.

[3] **K. Iwase,** K. Kamiya, M. Miyayama, K. Hashimoto, S. Nakanishi.

"Sulfur-Linked Covalent Triazine Frameworks doped with Coordinatively-Unsaturated Cu(I) as Electrocatalysts for Oxygen Reduction" *ChemElectroChem,* 2018, **5**, 805.

[4] P. Su[†], **K. Iwase**[†], T. Harada, K. Kamiya and S. Nakanishi. (†: equally contributed)

"Covalent triazine framework modified with coordinatively-unsaturated Co or Ni atoms for CO_2 electrochemical reduction" *Chem. Sci*., **2018**, 9, 3941.

[5] **K. Iwase**, K. Kamiya, M. Miyayama, K. Hashimoto, S. Nakanishi.,

"Systematic Investigation of Adsorption Energy of Oxygen Reduction Reaction Intermediates on Metal-modified Covalent Organic Framework"

in preparation.

Other Publications

[6] T. Yoshioka, **K. Iwase**, S. Nakanishi, K. Hashimoto, K. Kamiya.

"Electrocatalytic reduction of nitrate to nitrous oxide by a copper-modified covalent triazine framework" *J. Phys. Chem. C*, **2016**, 120, 15729.

[7] P. Su, **K. Iwase**, S. Nakanishi, K. Hashimoto, K. Kamiya.

"Nickel-Nitrogen-Modified Graphene: An Efficient Electrocatalyst for the Reduction of Carbon Dioxide to Carbon Monoxide" *Small*, **2016**, 12, 6083.

[8] K. Kamiya, T. Tatebe, S. Yamamura, **K. Iwase**, T. Harada, S. Nakanishi.

"Selective Reduction of Nitrate by the Local Cell Catalyst Composed of Metal-Doped Covalent Triazine Frameworks" *ACS Catal.*, **2018**, 8, 2693.

Acknowledgements

September 2018

Kazuyuki Iwase